学位論文

Photostable Luminescent Radicals: (3,5-Dihalo-4-pyridyl)bis(2,4,6-trichlorophenyl)methyl Radicals and Their Gold Complexes

（ 光安定な発光性ラジカル：(3,5-ジハロ-4-ピリジル)ビス(2,4,6-トリクロロフェニル)メチルラジカル及びそれらの金錯体 ）

平成２７年１２月　博士（理学）申請

東京大学大学院理学系研究科

化学専攻

服部　陽平

Abstract

This thesis describes development of photostable luminescent radicals: (3,5-dihalo-4-pyridyl)bis(2,4,6-trichlorophenyl)methyl radicals and their gold complexes.

Chapter 1: I describe why luminescent radicals attract much interest recently. Spin-multiplicity is an important factor to control the optical properties of luminescent materials, thus luminescent radicals with unique spin-doublet state are interesting. However, to design stable luminescent radicals is not easy and the number of known examples is few. Especially, stability under photoirradiation has not been reported. Thus the aim of my Ph.D. course study to develop photostable luminescent radicals is meaningful. As background knowledge of the design concepts and optical properties of the luminescent radicals shown in the thesis, characteristic molecular orbitals of a rare luminescent radical, tris(1,3,5-trichlorophenyl)methyl radical (TTM) are explained.

Chapter 2: I prepared the first photostable luminescent radical: 3,5-dichloro-4-pyridyl)bis(2,4,6-trichlorophenyl)methyl radical (PyBTM). Introduction of a nitrogen atom into a TTM skeleton enhanced the photostability up to 115 times in solution. The fundamental properties of PyBTM, such as protonation on the nitrogen atom, and emission in rigid solvent (77K) and polymer (room temperature) were investigated.

Chapter 3: Effects of halogen atoms on the pyridine ring of PyBTM were examined. (3,5-Dibromo-4-pyridyl)bis(2,4,6-trichlorophenyl)methyl radical (Br_2PyBTM) and (3,5-difluoro-4-pyridyl)bis(2,4,6-trichlorophenyl)methyl radical (F_2PyBTM) were prepared. I revealed that Br_2PyBTM showed higher photostability than that of PyBTM, and F_2PyBTM displayed greater fluorescence quantum yield than that of PyBTM.

Chapter 4: I aimed to enhance the luminescent properties of the stable luminescent radical, PyBTM through its coordination to gold(I). A prepared gold(I) complex, $[Au^{I}(PyBTM)PPh_3]BF_4$ became the first luminescent metal complex with a coordinated luminescent photostable radical. $[Au^{I}(PyBTM)PPh_3]BF_4$ displayed both enhanced photostability and increased fluorescence quantum yield.

Chapter 5: Combining the two approaches established in Chapters 3 and 4, *i.e.* coordination to gold(I) and replacement of halogen atoms (from Cl to F), a new gold(I) complex with stable luminescent radical, $[Au^{I}(F_2PyBTM)PPh_3]BF_4$ was synthesized. I revealed that $[Au^{I}(F_2PyBTM)PPh_3]BF_4$ was a luminescent radical with the highest fluorescence quantum yield in the thesis.

Chapter 6: Concluding remarks of the work are stated.

Contents

Chapter 1

General Introduction

1-1 Spin multiplicity and luminescence

Luminescent molecules have been developed for extensive applications such as electroluminescent (EL) devices,[1] chemical sensors,[2] and fluorescent probes.[3] While, most of known luminescent molecules are of closed-shell nature in the ground state, open-shell luminescent molecules have attracted much interest recently.

Spin multiplicity is an important factor for understanding photophysical processes. A closed-shell molecule has a singlet ground state (S_0), singlet excited states, and triplet excited states. Upon photon absorption, a molecule in a singlet ground state yields singlet excited states. When a molecule is fluorescent, fluorescence (spin-allowed luminescence) is emitted usually from the lowest singlet excited state (S_1), because transition from higher singlet excited states to S_1 is usually very fast (Kasha's rule). In a closed-shell molecule, the lowest triplet excited state (T_1) is lower in energy than the lowest singlet excited state (S_1). Phosphorescence (spin-forbidden luminescence) can be emitted from the T_1 state produced via the S_1 state by intersystem crossing. This intersystem crossing can be an annihilation path for fluorescence (Figure 1-1-1).

Annihilation via the triplet excited state can be a problem that is more important in electroluminescence than in photoluminescence. In EL devices such as organic light-emitting diode (OLED), statistic formation of excited states occurs. In usual fluorescent molecules, S_1 state of 25% and T_1 state of 75% are formed upon electron-hole pair recombination, thus the upper limit of internal quantum efficiency of fluorescence is only 25%. To avoid the problem of the low maximum internal quantum efficiency, phosphorescent molecules, in which at most 100% of excited states can emit via T_1 were developed for EL devices. However efficient phosphorescent materials often contain expensive rare metals such as iridium. Another method is to utilize delayed fluorescence. The energy level of the T_1 state has to be high enough in order that thermally activated transition can reach the S_1 state (Figure 1-1-2).

On the other hand, an open-shell molecule can have a non-singlet ground state. A (mono)radical has a doublet ground state (D_0) and a biradical can have a triplet ground state (T_0). In these cases, doublet-doublet fluorescence and triplet-triplet fluorescence are possibly observed respectively. The order of the energy levels of the excited states of open-shell molecules is rather complicated compared to those of close-shell molecules. In certain cases, the lowest excited state has the same spin multiplicity as the ground state does, and fluorescence is not disturbed by the other spin multiplicity states. Radicals are expected to be possible candidates as luminescent materials for EL devices.[4]

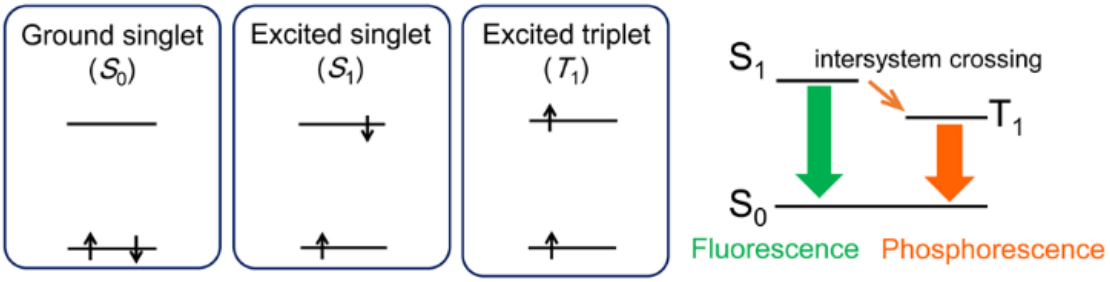

Figure 1-1-1. Ground and excited states of closed-shell molecules and simple Jablonski diagram. There are non-radiative internal conversion from S_1 to S_0 and that from T_1 to S_0, which are not shown in the diagram.

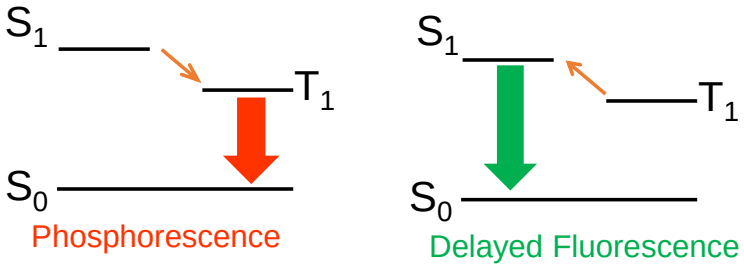

Figure 1-1-2. Scheme of phosphorescence and thermally activated delayed fluorescence of closed-shell emitter used in EL devices. Maximum internal quantum efficiency is 100% because of $S_1 \rightarrow T_1$ process in the scheme of phosphorescence, and $T_1 \rightarrow S_1$ process in the scheme of delayed fluorescence.

1-2 Radicals toward luminescent materials

Reactivity of radicals is the first problem to be overcome, when we attempt to treat the materials in ambient conditions. Especially, small organic radicals are very reactive as seen in organic radical reactions such as chain reactions.[5] Origin of reactivity of a radical is its unpaired electron. Singly occupied molecular orbital (SOMO), the orbital of the unpaired electron is usually higher in energy than HOMO of another closed-shell molecule and lower in energy than LUMO of other closed-shell molecule. Because of that, radicals easily react with the other molecules to form a new covalent bond.

In order to stabilize radicals, π-conjugation and steric protection are effective methods.[6] Both conjugations with electron rich π-orbital and electron deficient π-orbital are thought to stabilize a radical. When the SOMO conjugates with an unoccupied orbital, a bonding orbital and an antibonding orbital are formed, then the energy of the unpaired electron is lowered (Figure 1-2-1). When the SOMO conjugates with an orbital of paired electrons, the former is stabilized and the latter is destabilized, and the total energy of three electrons are lowered. Delocalization of spin on plural atoms is also attributable to lower reactivity to make bonds to other atoms. Steric repulsion makes reactions with other molecules structurally difficult. Bulky groups can protect radicals on heavy atoms, which hardly make conjugation.[7]

By combining π-conjugation and steric protection, some radicals are stabilized in air at room temperature. Many nitroxyl radicals such as (2,2,6,6-tetramethylpiperidin-1-yl)oxyl (TEMPO) derivatives are commercially available. Such examples are shown in Figure 1-2-2. Stable radicals show interesting functions attributable to the unpaired electrons, such as redox, magnetic, and conducting properties. They were employed as oxidation catalysts,[8] rechargeable battery electrode,[9] molecular memory,[10] photovoltaic material[11] and fundamental building blocks for functional molecular materials.[12]

There are not so many studies focusing on optical properties of radicals. Especially in the field of luminescence, radicals are often seen as quenching molecules rather than luminescent molecules. Their reactivity, redox activity and promotion of intersystem crossing are thought as the reason of quenching luminescence of other materials; however there is no reason that radicals themselves are non-luminescent.

Since there are few numbers of research aiming to produce luminescent radicals, how radicals can acquire luminescent properties has not been well investigated so far. It seems that rigid structure such as expanded π-conjugation can help luminescence.[13] As rare examples of fluorescent radicals, perchlorotriphenylmethyl radical (PTM)[14] and tris(1,3,5-trichlorophenyl)methyl radical (TTM)[15] are reported (Figure 1-2-3). In these

radicals, six ortho-chlorine atoms protect radical centers from reaction, such as dimerization (Figure 1-2-4).[6,15]

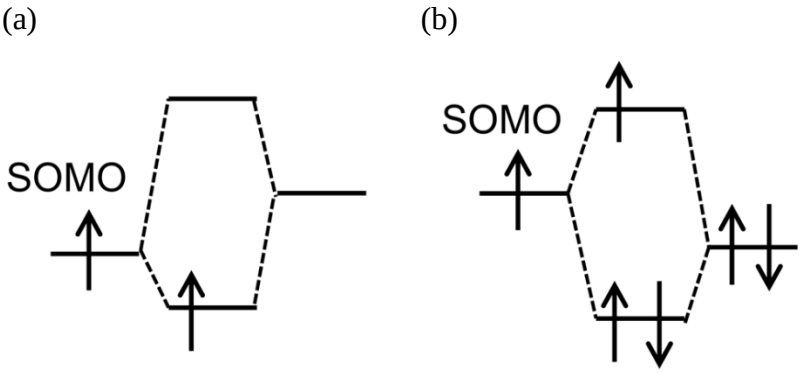

Figure 1-2-1. Stabilization of the total energy of electrons by conjugation of an unpaired electron with (a) an unoccupied orbital and (b) an occupied orbital.

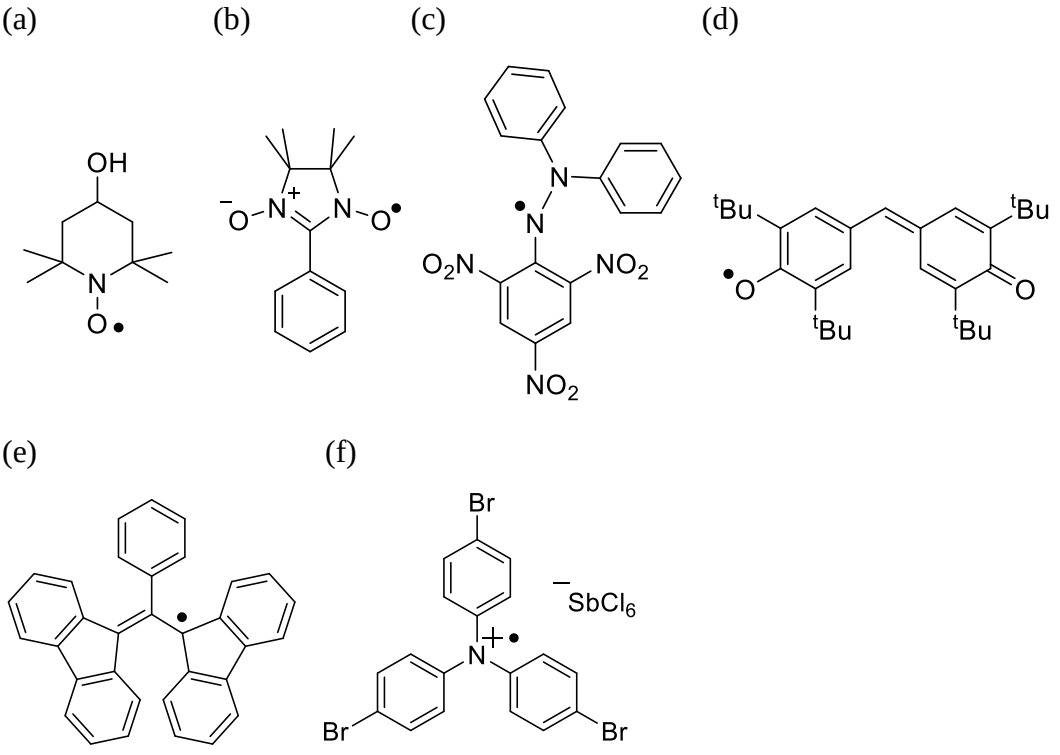

Figure 1-2-2. Examples of commercially available radicals; (a) 4-hydroxy-TEMPO, (b) 2-(4-nitrophenyl)-4,4,5,5-tetramethylimidazoline-3-oxide-1-oxyl radical (one of nitronyl nitroxide radicals), (c) 2,2-diphenyl-1-picrylhydrazyl (DPPH) radical, (d) galvinoxyl radical, (e) 1,3-bisdiphenylene-2-phenylallyl (BDPA) radical, and (f) tris(4-bromophenyl)ammoniumyl hexachloroantimonate (aminium salt).

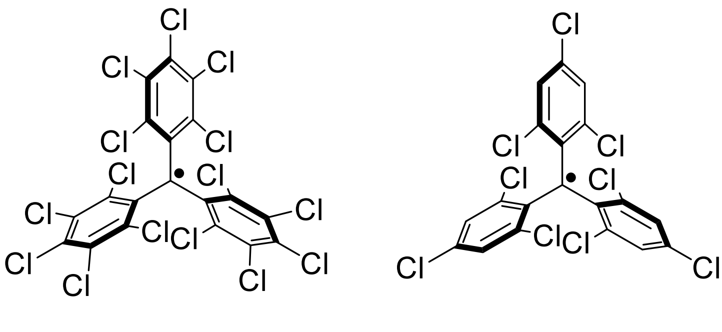

Figure 1-2-3. Chemical structures of PTM and TTM radicals.

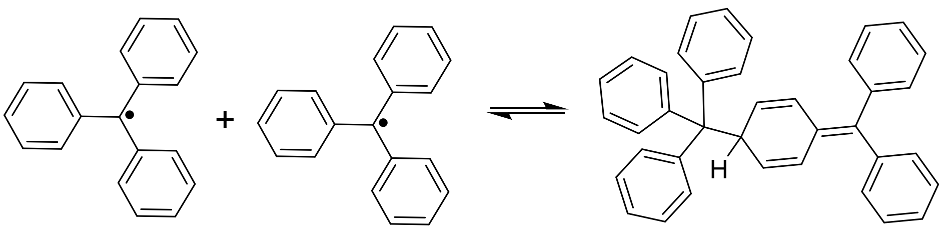

Figure 1-2-4. Dimerization of triphenylmethyl radical.

1-3 Polychlorotriphenylmethyl radicals as representative luminescent radicals

Fluorescence quantum yields of PTM and TTM are low (~2%), but a few derivatives which show high quantum yields have already been reported. Juliá et al. reported that carbazole-bound TTM with donor-acceptor character demonstrates efficient red-light fluorescence (λ_{em} = 628 nm, ϕ = 0.64 in cyclohexane).[16] The first OLED using monoradical as an emitter has recently been reported utilizing this radical.[17] Lambert et al. revealed the intramolecular charge transfer (ICT) process and the fluorescence (λ_{em} = 763 nm, ϕ = 0.38 at maximum in cyclohexane) of triarylamine-PTM radicals upon photoexcitation (Figure 1-3-1).[18]

However, the PTM and TTM radicals have serious problems as luminescent materials. They decompose upon photoirradiation, and photoluminescent for only short time. They undergo efficient photolysis reactions such as cyclization to yield non-fluorescent molecules (Figure 1-3-2). The quantum yield of cyclized product formation from PTM was measured at 0.3 ± 0.1.[19] So far, no improvement of photostability in PTM and TTM derivatives has been reported.

(a) (b)

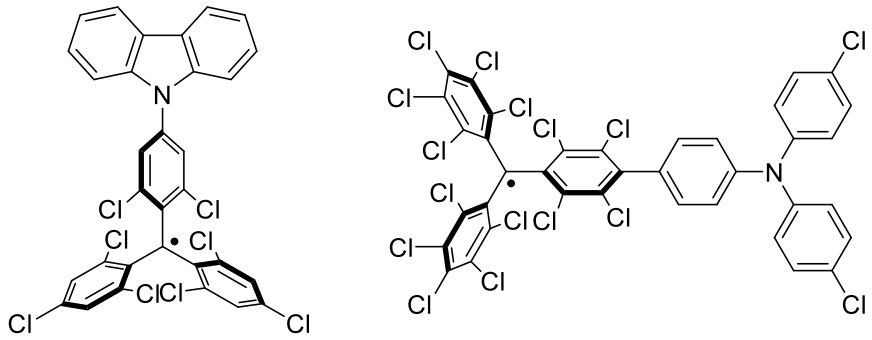

Figure 1-3-1. Chemical structures of (a) carbazole-bound TTM radical[16a] and (b) triarylamine-bound PTM radical.[18a]

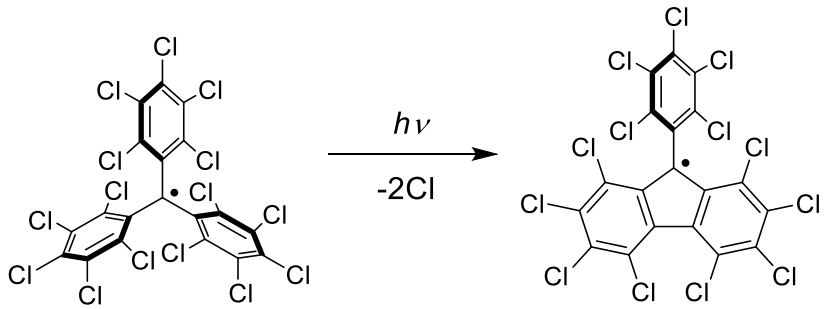

Figure 1-3-2. Photochemical cyclization reaction of PTM radical.

1-4 The aim of this work

In this study I added some modification to TTM to improve the luminescent properties.

The low stability in the excited state is a critical problem to be overcome for luminescent radicals. The first aim of this study is to stabilize luminescent radicals under photoirradiation. As the lifetime under photoirradiation becomes longer, possibility of application of the luminescent radical increases.

Quantum efficiency is also very important in luminescent materials. Enhancing luminescence without making donor-acceptor unit discriminate this work from the previous reports, which showed high quantum yield only in nonpolar solvent. Another purpose of this work is to increase photoluminescence quantum yield of luminescent radicals.

The first aim was achieved by introduction of a nitrogen atom into the TTM skeleton. In Chapter 2, I describe photophysical and photochemical properties of a newly prepared stable radical, (3,5-dichloro-4-pyridyl)bis(2,4,6-trichlorophenyl)methyl radical (PyBTM), which was much more photostable than TTM. The photostability was further enhanced by introduction of bromine atoms instead of two chlorine atoms on the pyridine ring (Br_2PyBTM, Chapter 3), and coordination to gold(I) ([Au^I(PyBTM)PPh_3]X, Chapter 4).

Although PyBTM displayed low quantum efficiency similarly to TTM in solution, I found that these radicals showed high quantum yields in low temperature glasses or polymer at room temperature (Chapter 2). The photoluminescence quantum yield in solution was enhanced by introduction of fluorine atoms instead of two chlorine atoms on the pyridine ring (F_2PyBTM, Chapter 3), and coordination to gold(I) ([Au^I(PyBTM)PPh_3]X, Chapter 4). The highest quantum yield in solution in my Ph.D. studies was achieved by combining F_2PyBTM and [Au^I(PyBTM)PPh_3]X. [Au^I(F_2PyBTM)PPh_3]BF_4 displayed the quantum yield of 20%, which is 10 times that of PyBTM (Chapter 5).

1-5 Molecular orbitals of TTM radical

To explain the meaning of modification of the TTM radical, DFT calculated molecular orbitals of TTM are shown (Figure 1-5-1, detailed methods are included in Chapter 2-2). Because TTM is a radical, orbitals were calculated using unrestricted DFT methods, and energies of α-spin and β-spin orbitals are non-degenerated. Since there is not decided nomenclature for frontier orbitals of open-shell molecules, terms; α-SOMO, β-SOMO, α-NLUMO, β-NLUMO, α-NHOMO and β-NHOMO are used in this thesis for convenience. The energy difference between α-SOMO and β-SOMO is mainly interpreted as on-site Coulomb repulsion. Both α-SOMO and β-SOMO are centered on the methyl carbon, and delocalized onto the aromatic rings.

Considering excitation of electrons, there are α-spin electron transitions and β-spin electron transitions. In the case of the TTM radical, the β-spin electron transition forms the lowest excited state. All the doublet excited states are thought to follow Kasha's rule because the photophysical processes are spin-allowed in nature, and relax to the lowest excited state in short time ($< 10^{-11}$ s, exceptions of Kasha's rule can occur when S_2-S_1 gap is large.[20]). Rearrangement of spins in the excited states (from α-spin-centered excited states to β-spin-centered excited states) is not considered in the emission process of conventional closed-shell fluorescent molecules (Figure 1-5-2).

Concerning spin multiplicity, the lowest excited state of TTM is an excited doublet state. Excited quartets can be generated by intersystem crossing, but they are higher in energy (Figure 1-5-3). Thus only fluorescence from the lowest excited doublet state to the ground doublet state is shown. This fluorescence can be interpreted by this simple mechanism and the wavelength is longer (TTM derivatives show red emission (> 600 nm)[16c]) than those of the other small fluorescent molecules. Thus fluorescence of modified TTM will be suitable for application to future EL devices or near IR emitters.

In modified TTM radicals shown in this thesis, the lowest excited state is thought to play the most important role in the stability and efficiency. As a result, in Chapters 2 and 4, introduction of a nitrogen atom and coordination to gold lowers the energy levels of β-SOMO. In the Chapter 3, change of halogen atoms on pyridine ring affects the energy levels of β-NHOMO (Figure 1-5-4).

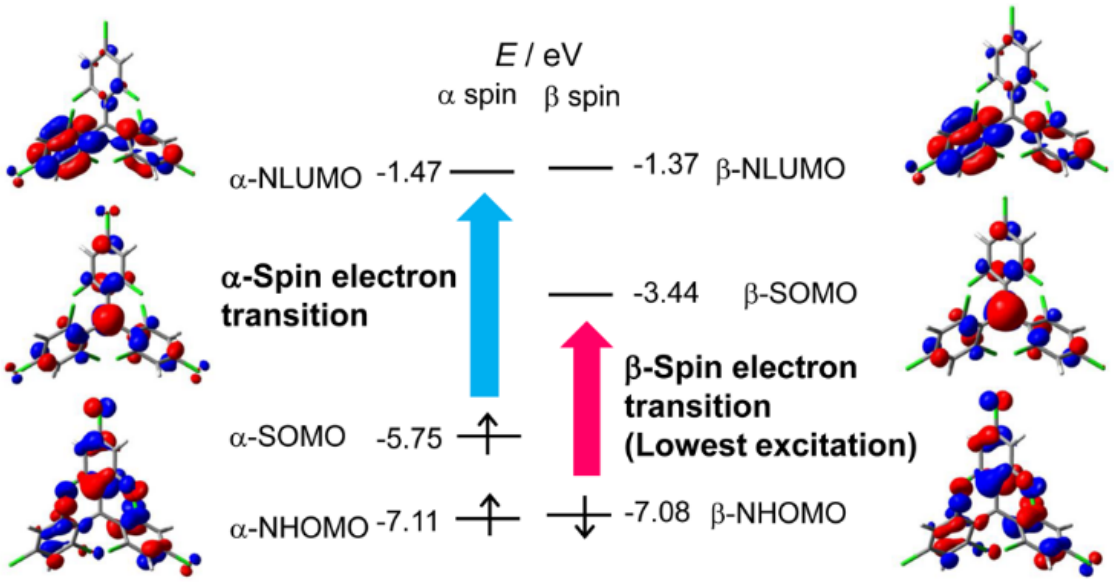

Figure 1-5-1. Frontier orbitals of TTM calculated using DFT methods (UB3LYP/6-31G(d))

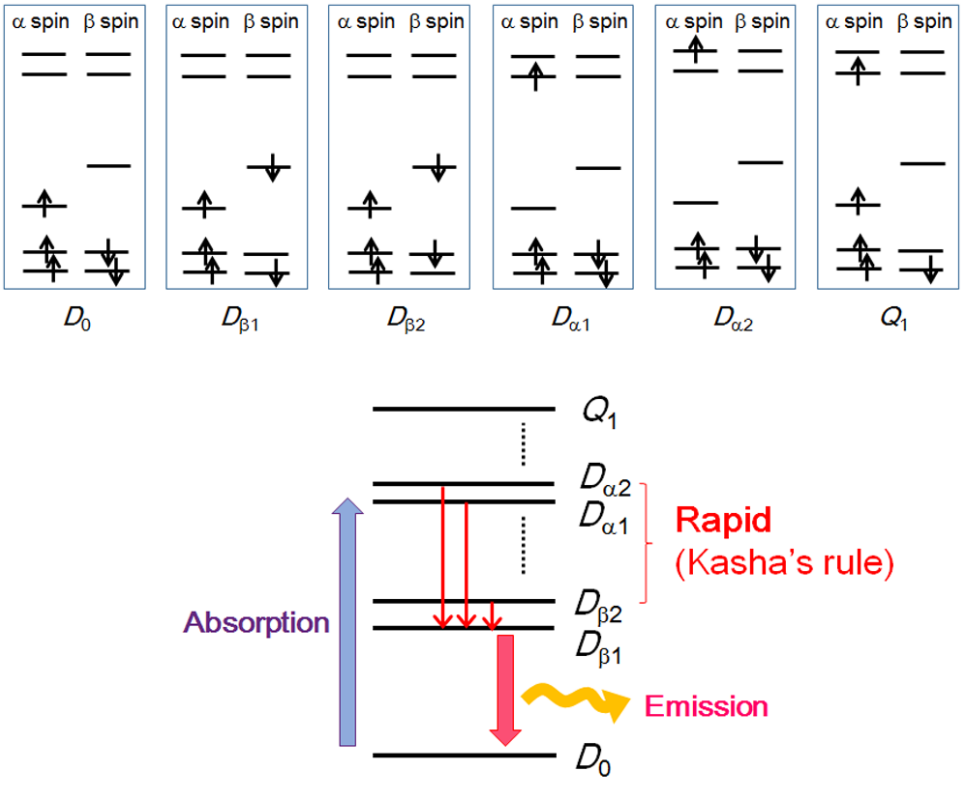

Figure 1-5-2. Jablonski diagram of TTM radical. The lowest β-spin-centered excited state ($D_{\beta 1}$) is the lowest doublet excited state (D_1) state and transition from the lowest α-spin-centered excited state ($D_{\alpha 1}$) to $D_{\beta 1}$ is rapid by Kasha's rule.

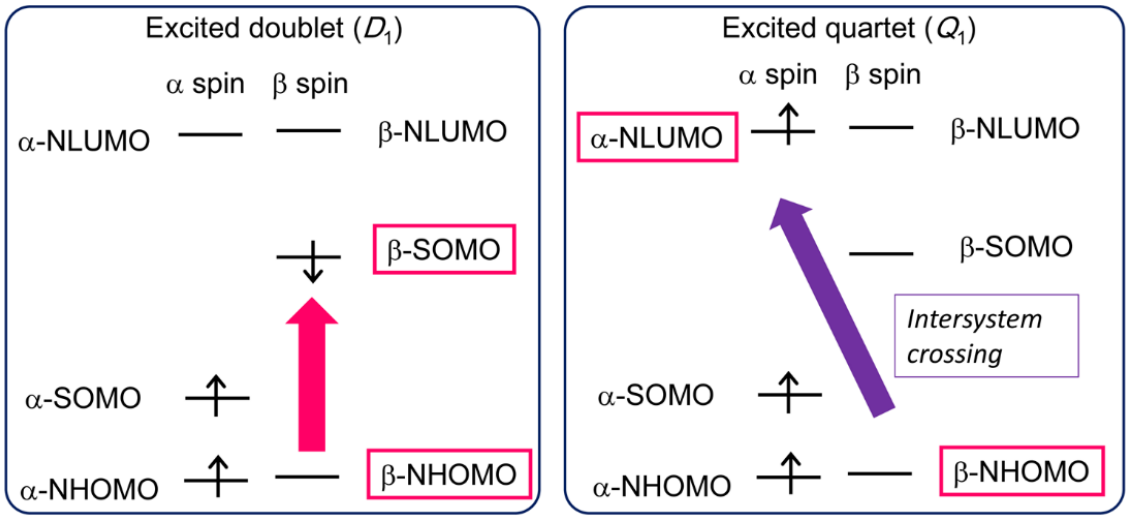

Figure 1-5-3. Comparison of the lowest excited doublet (D_1) state and the lowest quartet (Q_1) excited state of TTM radical. Since the energy level of α-NLUMO is much higher than that of β-SOMO, the energy of D_1 is lower than that of Q_1.

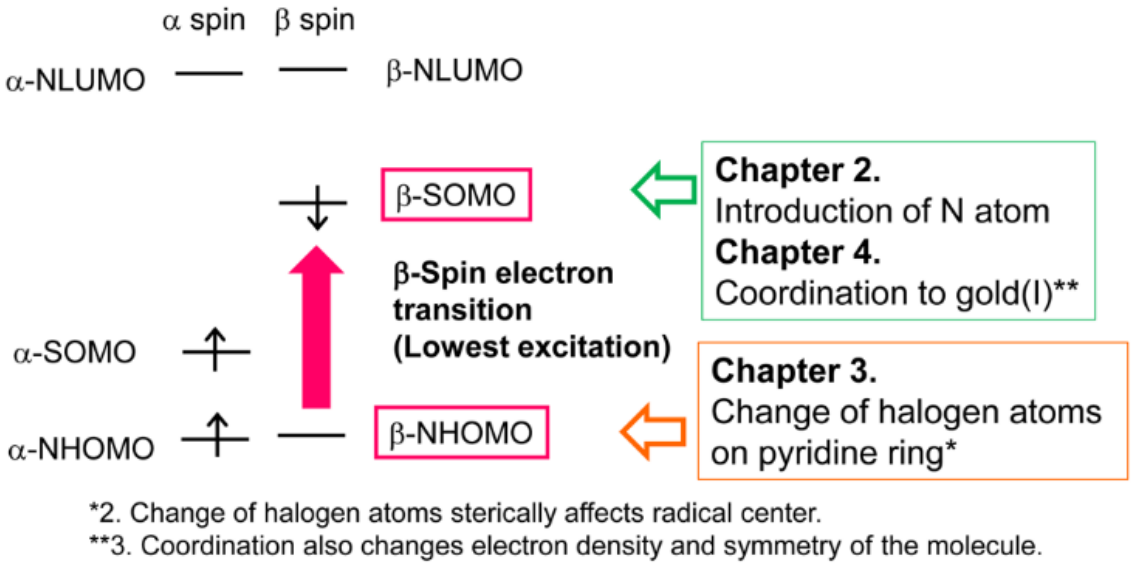

Figure 1-5-4. Frontier orbitals focused in this thesis.

1-6 Molecular design and structures in this study

In this thesis, I modified three moieties on the TTM skeleton. In Chapter 2, I modified the para-position of the trichlorobenzene ring of TTM, where the C−Cl moiety was substituted to N atom, yielding PyBTM (Figure 1-6). This modification is expected to give a pronounce effect on properties of the radical, because there is much difference between benzene and pyridine in organic chemistry. Lowering energy of the β-SOMO orbital affects optical properties. Especially, photostability is dramatically improved as shown in the results. Protonation allowed by introduction of the nitrogen atom reversibly switches the properties of PyBTM.

Second moiety modified was halogen atoms on the pyridine ring (Chapter 3). The β-NHOMO orbitals are slightly delocalized on these atoms, which affects the optical properties through the lowest excited states. Bromine atoms are larger than chlorine atoms, and fluorine atoms are smaller than chlorine atoms. Smaller atoms can allow more suitable configuration for efficient luminescence, and larger atoms can sterically prevent some chemical reactions.

Thirdly, introduction of the nitrogen atom enabled coordination to metal cations. Gold(I) was employed in Chapter 4 to yield a luminescent complex with a coordinated luminescent radical, because gold(I) can form a strong coordination bond and is used in many efficient luminescent complexes. Coordination gives a positive charge on the molecule and lowers the energies of molecular orbitals such as β-SOMO. The photostability is expected to be further enhanced from PyBTM. The electronic state of the pyridine ring, which coordinates to gold(I), is clearly distinguished from the two benzene rings; thus 3-fold symmetry is broken.

Modification in Chapter 5 is combination of introduction of fluorine (or bromine) atoms and coordination to gold(I). Modification on different parts is expected to act independently to the properties of the complex. In the results, multiplier effect is shown in the fluorescence lifetime and enhancement of the fluorescence quantum yield.

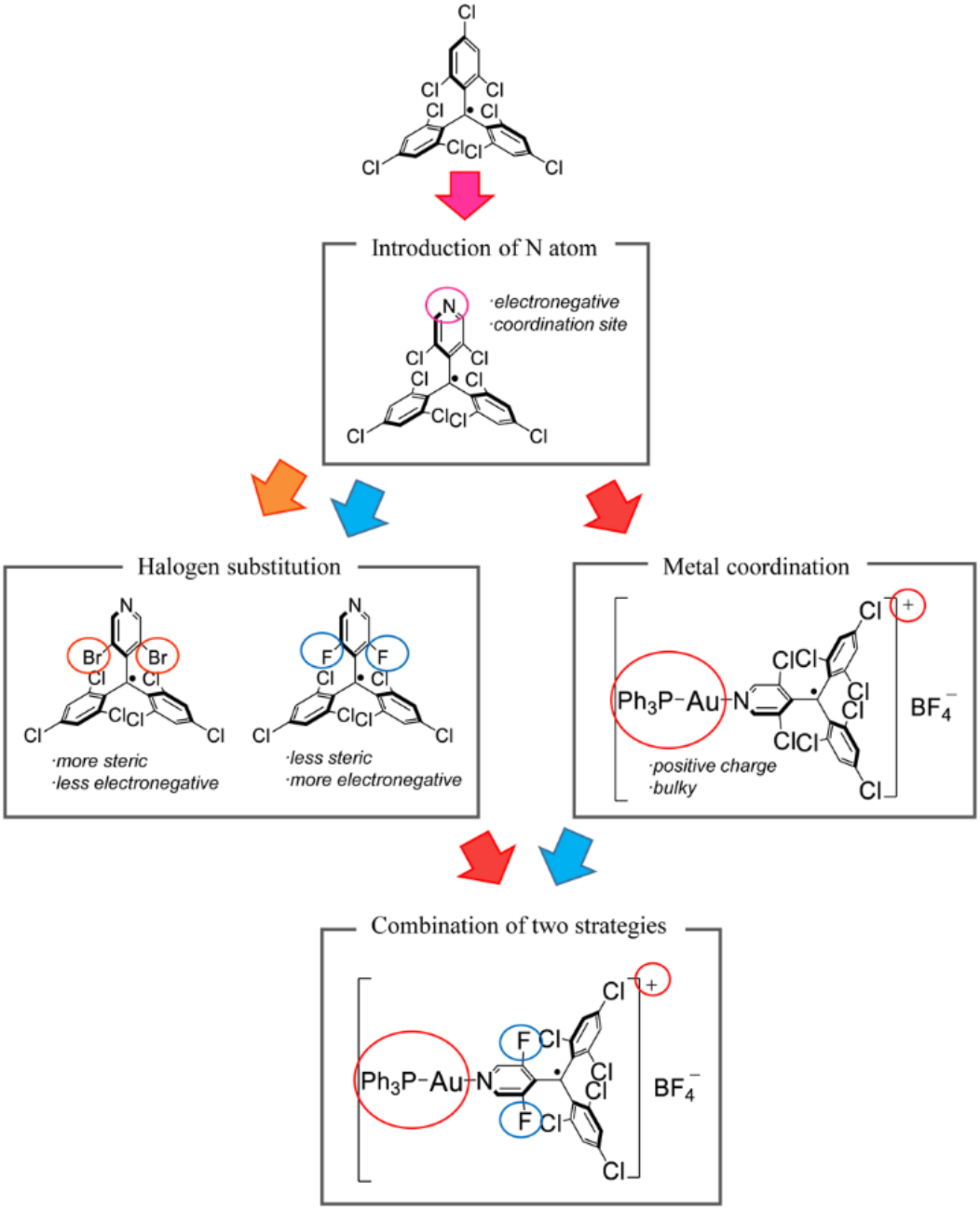

Figure 1-6. Molecular design and structures in this study.

1-7 References

[1] a) Y. Sun, N. C. Giebink, H. Kanno, B. Ma, M. E. Thompson, S. R. Forrest, *Nature* **2006**, *440*, 908 – 912; b) H. Uoyama, K. Goushi, K. Shizu, H. Nomura, C. Adachi, *Nature* **2012**, *492*, 234 –238.

[2] a) N. Boens, V. Leen, W. Dehaen, *Chem. Soc. Rev.* **2012**, *41*, 1130 – 1172; b) L. Prodi, F. Bolletta, M. Montalti, N. Zaccheroni, *Coord. Chem. Rev.* **2000**, *205*, 59 – 83; c) J. F. Callan, A. P. de Silva, D. C. Magri, *Tetrahedron* **2005**, *61*, 8551 – 8588; d) X. Chen, Y. Zhou, X. Peng, J. Yoon, *Chem. Soc. Rev.* **2010**, *39*, 2120 – 2135.

[3] a) P. Jiang, Z. Guo, *Coord. Chem. Rev.* **2004**, *248*, 205 – 229; b) J. S. Kim, D. T. Quang, *Chem. Rev.* **2007**, *107*, 3780 – 3799.

[4] H. Namai, H. Ikeda, Y. Hoshi, N. Kato, Y. Morishita, K. Mizuno, *J. Am. Chem. Soc.* **2007**, *129*, 9032 – 9036.

[5] a) D. P. Curran, *Synthesis* **1988**, *6*, 417 – 439; b) D. P. Curran, *Synthesis* **1988**, *7*, 489 – 513.

[6] J. Veciana, I. Ratera in *Stable Radicals: Fundamentals and Applied Aspects of Odd-Electron Compounds* (Ed.: R. G. Hicks), John Wiley & Sons, Ltd, New York, **2010**.

[7] a) A. Sekiguchi, T. Fukawa, M. Nakamoto, V. Y. Lee, M. Ichinohe, *J. Am. Chem. Soc.* **2002**, *124*, 9865 – 9869; b) V. Y. Lee, A. Sekiguchi, *Acc. Chem. Res.* **2007**, *40*, 410 – 419.

[8] Adam, W.; Saha-Möller, C. R.; Ganeshpure, P. R. *Chem. Rev.* **2001**, *101*, 3499 – 3548.

[9] Nakahara, K.; Oyaizu, K.; Nishide, H. *Chem. Lett.* **2011**, *40*, 222 – 227.

[10] Yonekuta, Y.; Susuki, K; Oyaizu, K.; Honda, K.; Nishide, H. *J. Am. Chem. Soc.* **2007**, *129*, 14128 – 14129.

[11] Lv, X.; Mao, J.; Liu, Y.; Huang, Y.; Ma, Y.; Yu, A.; Yin, S.; Chen, Y. *Macromolecules*, **2008**, *41*, 501 – 503.

[12] Retera, I.; Veciana, J. *Chem. Soc. Rev.* **2012**, *41*, 303 – 349.

[13] (a) R. Beaulac, G. Bussière, C. Reber, C. Lescop, D. Luneau, *New J. Chem.* **2003**, *27*, 1200 – 1206; (b) A. Lannes, M. Intissar, Y. Suffren, C. Reber, D. Luneau, *Inorg. Chem.* **2014**, *53*, 9548 – 9560; (c) E. V. Tretyakov, V. F. Plyusnin, A. O. Suvorova, S. V. Larionov, S. A. Popov, O. V. Antonova, E. M. Zueva, D. V. Stass, A. S. Bogomyakov, G. V. Romanenko, V. I. Ovcharenko, *J. Lumin.* **2014**, *148*, 33 – 38; (d) Q. Peng, H. Ma, Y. Chen, C. He, A. Obolda, F. Li, arXiv:1406.5285[physics.chem-ph].

[14] M. Ballester, J. Riera, J. Casteñer, C. Badia, J. M. Monsó, *J. Am. Chem. Soc.* **1971**, *93*, 2215 – 2225.

[15] O. Armet, J. Veciana, C. Rovira, J. Riera, J. Casteñer, E. Molins, J. Rius, C.

Miravitlles, S. Olivella, J. Brichfeus, *J. Phys. Chem.* **1987**, *91*, 5608 – 5616.
[16] a) V. Gamero, D. Velasco, S. Latorre, F. López-Calahorra, E. Brillas, L. Juliá, *Tetrahedron lett.* **2006**, *47*, 2305 – 2309; b) D. Velasco, S. Castellanos, M. López, F. López-Calahorra, E. Brillas, L. Juliá, *J. Org. Chem.* **2007**, *72*, 7523 – 7532; c) S. Castellanos, D. Velasco, F. López-Calahorra, E. Brillas and L. Juliá, *J. Org. Chem.* **2008**, *73*, 3759–3767; d) L. Fajalí, R. Papoular, M. Reig, E. Brillas, J. L. Jorda, O. Vallocorba, J. Rius, D. Velasco, L. Juliá, *J. Org. Chem.* **2014**, *79*, 1771 – 1777.
[17] Q. Peng, A. Obolda, M. Zhang and F. Li, *Angew. Chem., Int. Ed.* **2015**, *54*, 7091 – 7095.
[18] a) A. Heckmann, S. Dümmler, J. Pauli, M. Margraf, J. Köhler, D. Stich, C. Lambert, I. Fischer, U. Resch-Genger, *J. Phys. Chem. C* **2009**, *113*, 20958 – 20966; b) A. Heckmann, C. Lambert, M. Goebel, R. Wortmann, *Angew. Chem. Int. Ed.* **2004**, *43*, 5851 – 5856; c) A. Heckmann, C. Lambert, *J. Am. Chem. Soc.* **2007**, *129*, 5515 – 5527;
[19] a) M. A. Fox, E. Gaillard, C.-C. Chen, *J. Am. Chem. Soc.* **1987**, *109*, 7088 – 7094; b) S. R. Ruberu, M. A. Fox, *J. Phys. Chem.* **1993**, *97*, 143 – 149.
[20] V. Chynwat, H. A. Frank, *Chem. Phys.* **1995**, *194*, 237 – 244.

Chapter 2

Luminescence and Stability of an Open-Shell (3,5-Dichloro-4-pyridyl)bis(2,4,6-trichlorophenyl)methyl Radical

2-1 Introduction

As I mentioned in Chapter 1, so far, the luminescence of organic radicals has been little investigated because of small numbers of the examples and instability under some conditions such as under photoirradiation; TTM decomposed even under room light. An establishment of the method for improving the photostability will expand the scope of luminescent organic radicals as functional luminescent materials. An interplay between luminescence and unique properties of radicals (spin multiplicity, magnetism, redox activities, etc.) is expected to find new applications.

I have prepared a novel luminescent stable radical, (3,5-dichloro-4-pyridyl)bis(2,4,6-trichlorophenyl)methyl radical[1] (PyBTM, Figure 2-1-1) with a unique molecular design concept. A pyridine ring was introduced into the TTM skeleton. The substitution is expected to lower the energies of the frontier orbitals on the TTM skeleton owing to the greater effective nuclear charge (electronegativity) of the nitrogen atom than that of the carbon atom. Especially, the lower β-SOMO decreases the energy of the lowest excited state, thus leading to a lower reactivity under photoirradiation. In this chapter, the electronic structure, optical characteristics, and stability of PyBTM are discussed.

The nitrogen atom on the pyridyl group allows for not only enhancing the stability, but also coordination to proton, Lewis acid, or metal cations by its lone pair. Here I show a reversible proton-response, which tunes the electronic and optical properties of PyBTM.

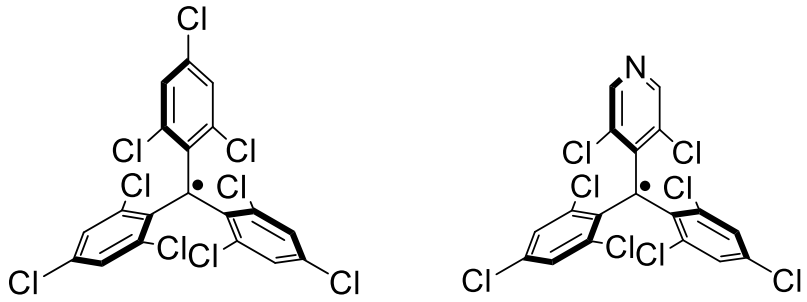

TTM **PyBTM**

Figure 2-1-1. Structures of TTM and PyBTM radicals.

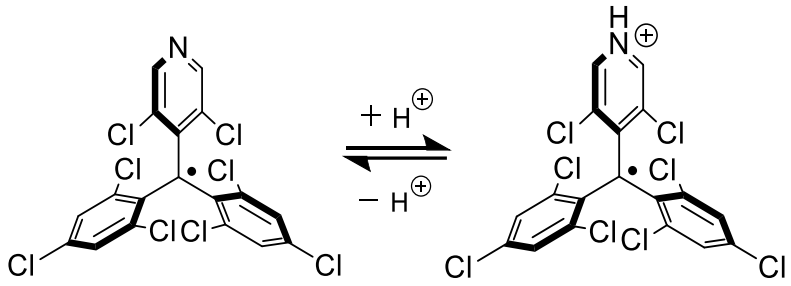

PyBTM **[*NH*-PyBTM]$^+$**

Figure 2-1-2. Protonation equilibrium of PyBTM.

2-2 Experimental section

Materials

TTM was prepared according to literature protocol.[2] 3,5-Dichloro-4-pyridine carboxaldehyde, ^{t}BuOK in THF (1 M solution), and 4-hydroxy-TEMPO were purchased from Sigma-Aldrich Co.LLC., 1,3,5-trichlorobenzene was from Wako Pure Chemical Industries, Ltd., trifluoromethanesulfonic acid was from Tokyo Chemical Industry Co., Ltd.

Synthesis of (3,5-dichloro-4-pyridyl)bis(2,4,6-trichlorophenyl)methane (*αH*-PyBTM)

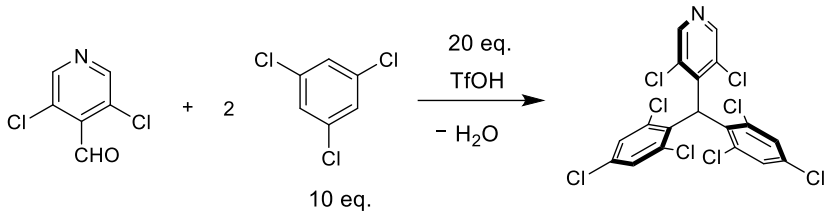

*α*H-PyBTM was synthesized by superacid-catalyzed condensation of pyridine carboxaldehyde with arenes.[3] Under a nitrogen atmosphere, 3,5-dichloro-4-pyridine carboxaldehyde (1.76 g, 10.0 mmol, 1 eq.) and 1,3,5-trichlorobenzene (18.14 g, 100 mmol, 10 eq.) were heated to 180 °C. Trifluoromethanesulfonic acid (30.0 g, 200 mmol, 20 eq.) was added dropwise, and the reaction mixture was stirred for 10 hours at 180 °C. The reaction mixture was cooled to r.t., dissolved in dichloromethane, and added to ice water. The mixture was neutralized to pH 7 using $NaHCO_3$ aq, extracted with dichloromethane (3 × 100 mL), washed with $NaHCO_3$ aq two times, and dried by Na_2SO_4. The organic layer was purified by SiO_2 column chromatography (dichloromethane : hexane = 1:1), evaporated and solidified by cooling at 243 K, and dried in vacuo to afford *α*H-PyBTM (3.43 g, 6.56 mmol, 66%) as a white solid. **^{1}H NMR** (400 MHz, $CDCl_3$): δ 8.48 (s, 1H), 8.36 (s, 1H), 7.39 (d, J = 2.4 Hz, 1H), 7.38 (d, J = 2.2 Hz, 1H), 7.27 (d, J = 2.2 Hz, 1H), 7.24 (d, J = 2.2 Hz, 1H), 6.69 (s, 1H). **Elem. Anal.** Calcd for $C_{18}H_7NCl_8$: C 41.51, H 1.35, N 2.69. Found, C 41.47, H 1.62, N 2.40.

Synthesis of (3,5-dichloro-4-pyridyl)bis(2,4,6-trichlorophenyl)methyl radical (PyBTM)

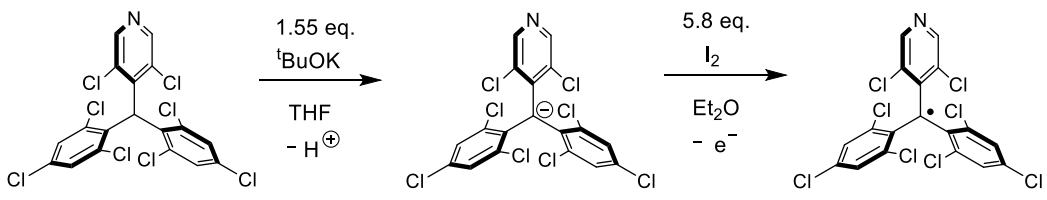

Under a nitrogen atmosphere, α*H*-PyBTM (234 mg, 0.45 mmol) was dissolved in dry THF (17 mL). ^{t}BuOK in THF (1M solution, 0.7 mL, 1.55 eq.) was added dropwise and the color of the solution changed to red. The reaction mixture was stirred overnight in the dark. I_2 (664 mg, 2.61 mmol, 5.8 eq.) in dry diethyl ether (60 mL) was added dropwise and stirred for 2.25 h.[4] Remaining I_2 was reduced by washing with 10 % $Na_2S_2O_3$ aq 3 times, water layer was extracted with diethyl ether, and the combined organic layer was dried with $MgSO_4$. The red solution was filtered, evaporated, purified by Al_2O_3 column chromatography (diethyl ether : hexane = 1:4) and dried in vacuo to afford PyBTM (218 mg, 0.42 mmol, 93%) as a red solid. **IR** (KBr) 3095 (w), 2922 (w), 1554 (s), 1525 (s), 1383 (s), 1371 (s), 1294 (m), 1208 (m), 1182 (m), 1140 (m), 1099 (w), 1083 (w), 926 (w), 890 (w), 863 (m), 821 (s), 801 (s), 730 (w), 671 (w), 565 (w), 544 (w) **HRMS** (negative ion mode ESI-TOF) m/z: $[M]^-$ Calcd for $C_{18}H_6NCl_8$ 519.7949; Found 519.7924. **Elem. Anal.** Calcd for $C_{18}H_6NCl_8$: C 41.59, H 1.16, N 2.69. Found, C 41.63, H 1.29, N 2.39. **ESR** Spin concentration of PyBTM in toluene (9.7×10^{-5} M) was estimated by comparing the value of twice-integration of the signal intensity with that of the reference sample (4-hydroxy-TEMPO in toluene; 9.9×10^{-5} M). The existence of S = 1/2 spin on one PyBTM molecule was confirmed.

X-ray structural analysis

Diffraction data for X-ray analysis were collected with an AFC10 diffractometer coupled with a Rigaku Saturn CCD system equipped with a rotating-anode X-ray generator producing graphite-monochromated MoKα radiation (λ = 0.7107 Å). Lorentz polarization and numerical absorption corrections were performed with the program *Crystal Clear 1.3.6.* Structures were solved by the direct method using SIR 92 software[5] and refined against F2 using SHELXL-97.[6] *Crystal Structure 4.0* software was used to prepare the material for publication for the crystals of PyBTM and [*NH*-PyBTM]·H_2O·BF_4. H atoms of pyridinium and water in the crystal of [*NH*-PyBTM]·H_2O·BF_4 were refined, while the other H atoms were constructed. The crystallographic data are listed in Tables 2-3 and 2-8. CCDC 1006484 and 1006485 contain the supplementary crystallographic data of this paper. These data can be obtained free of charge from The Cambridge Crystallographic Data Centre via www.ccdc.cam.ac.uk/data_request/cif.

Instruments

^{1}H NMR spectra were recorded using a JEOL AL400. The reported chemical shifts of the solvent residual peaks were used for calibration of the ^{1}H NMR spectra in $CDCl_3$

(δ 7.26). ESI–TOF mass spectra were recorded using an LCT Micromass spectrometer. ESR spectra were recorded with a JEOL JES-RE2X spectrometer with X-band microwave. 4-Hydroxy-TEMPO was used as a spin concentration standard. Deoxygenated sample solutions were charged in a 5mmϕ sample tube. Magnetic field was calibrated with the Mn^{2+}/MgO standard. UV-vis absorption spectra were recorded with a JASCO V-570 spectrometer. Steady-state emission spectra were measured with a HITACHI F-4500 spectrometer. Sample solutions were bubbled with argon before measurement. Absolute photoluminescence quantum yields were measured with a Hamamatsu Photonics C9920-02G. Fluorescence lifetime measurements were performed using a Hamamatsu Photonics Quantaurus-Tau C11367-02. Temperature dependence of fluorescence and UV-vis spectra were measured with a temperature controller (UNISOKU USP-203A and OXFORD INSTRUMENTS Optistat DN, respectively). Electrochemical measurements were recorded with an ALS 650DT electrochemical analyzer (BAS. Co., Ltd.). The working electrode was a 0.3 mm o.d. glassy carbon electrode; a platinum wire served as auxiliary electrode, and the reference electrode was an Ag^+/Ag electrode (a silver wire immersed in 0.1 M Bu_4NClO_4/0.01 M $AgClO_4$/CH_3CN). Ferrocene was used as an internal standard for calibrating potentials. The solutions were deoxygenated with pure argon prior to the electrochemical measurements.

Evaluation of stability of PyBTM and TTM under UV light

A solution (ca. 1×10^{-5} M, 2 mL) in 1-cm-optical-path-length quartz cells was bubbled with argon, sealed, and set at a HITACHI F-4500 spectrometer. Intensity of luminescence at 570 nm was observed exciting at 370 nm light (excitation slit was 5.0 nm, and shutter control was off). Radiation flux of a Xe lamp in the fluorometer was measured using a photon counter (8230E, ADC Corporation). A typical value for this condition was ~70 μW. Logarithm of fluorescence intensity versus time was plotted and a slope of approximate line was estimated to be a rate of photolysis.

Evaluation of pK_a value of $PyBTMH^+$

In an acetonitrile solution, pK_a of $PyBTMH^+$ was evaluated using a method and references developed by Leito et al..[7] PyBTM solution was titrated with three reference bases, 3-nitroaniline: acid dissociation constant of conjugate acid pK_a = 7.68, 2-chloropyridine: pK_a = 6.79, and 4-nitroaniline: pK_a = 6.22. From UV−Vis absorption spectral simulation of each titration experiment adding trifluoromethanesulfonic acid as a proton source, concentration of each species was decided and ΔpK_a (pK_a(PyBTM) −

pK_a(reference base)) was calculated using equation ΔpK_a = [PyBTMH$^+$][B] / [BH$^+$][PyBTM]; where B is the reference base. The ΔpK_a values were calculated to be pK_a(3-nitroaniline) − 0.67 ± 0.05, pK_a(2-chloropyridine) + 0.06 ± 0.05, pK_a(4-nitroaniline) + 0.72 ± 0.05 respectively, and pK_a of PyBTMH$^+$ was decided to be 6.9. This value (pK_a = 6.9) was much smaller than that of PyH$^+$ (conjugated acid of pyridine, pK_a = 12.53). PyBTM is therefore more than five orders of magnitude weaker than pyridine in its basicity, because of the presence of the electron-withdrawing chlorine atoms.

Computational details

DFT calculations were executed using the Gaussian09 program package.[8] The geometries of the compounds were optimized without symmetry constraints using the crystal structure coordinate as the starting structure. Calculations were performed using the unrestricted Becke three-parameter hybrid functional with Lee–Yang–Parr correlation functional (B3LYP)[9] or M06 functional[10] with the 6-31G(d) basis set. Cartesian coordinates of all the optimized geometries are listed in the supporting information. Frequency calculations were carried out to ensure that the optimized geometries were minima on the potential energy surface, in which no imaginary frequencies were observed in any of the compounds. TDDFT calculations were performed using UB3LYP to calculate the first 15 doublet transitions.

2-3 Single crystal X-ray diffraction

Red single crystals of PyBTM were obtained by diffusing water (the lower layer) into an acetonitrile solution of PyBTM (the upper layer). Single crystal X-ray diffraction studies revealed the molecular structure of PyBTM in the crystalline state (Figure 2-3, Table 2-3, CCDC 1006484). The methyl carbon C1 is sp^2 hybridized: C1 and the three carbons bonded to C1 (C4, C10, and C16) lie in one plane (with angles of C4C10C13 = 117.5(4)°, C4C13C16 = 121.0(4)°, and C10C13C16 = 121.5(4)°, a total of 360°). The three aryl groups adopt a propeller-like conformation because of the steric repulsion between the chlorine atoms in the ortho positions. The C4C10C16 plane was defined as the reference plane, and the dihedral angles between the aryl group planes and the reference plane were measured. The angles, which were found to be 49.3° (3,5-dichloropyridyl), 49.5° (2,4,6-trichlorophenyl including C10), and 42.6° (2,4,6-trichlorophenyl including C16) are similar to other triarylmethyl radicals containing six chlorine atoms in the ortho positions.[2] The C1 atom is shielded sterically by six chlorine atoms, at which appreciable spin density is located.

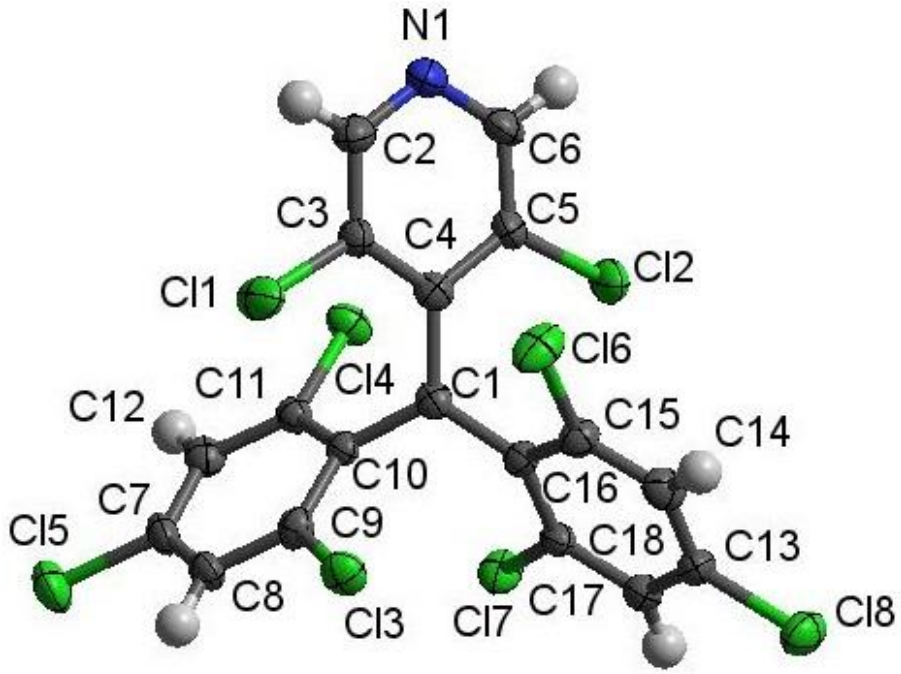

Figure 2-3. Molecular structure of crystalline PyBTM with thermal ellipsoids at the 50% probability level.

Table 2-3. Crystallographic data of PyBTM

	PyBTM
Empirical formula	C_{18} H_6 Cl_8 N
Fw / g mol^{-1}	519.88
Crystal system	monoclinic
Space group	$P2_1/c$
Crystal size / mm	0.3×0.1×0.1
Temperature / K	113(2)
a / Å	8.115(5)
b / Å	15.950(9)
c / Å	15.725(9)
α / º	90
β / º	89.415(10)
γ / º	90
V / Å^3	2035.1 (19)
Z	4
ρ_{calced} / g cm^{-3}	1.697
λ / Å	0.7107
μ / mm^{-1}	1.110
Reflections collected	14504
Independent reflections	4405
Parameters	244
R_{int}	0.0588
[a]*R*1	0.0608
[b]*wR*2	0.1701
[c]GoF	1.096
CCDC No.	1006484

[a]$R_1 = \Sigma||F^o|-|F^c||/\Sigma|F^o|$ ($I>2\sigma(I)$). [b]$wR_2 = [\Sigma(w(F^{o2}-F^{c2})^2/\Sigma w(F^{o2})^2]^{1/2}$ ($I>2\sigma(I)$). [c]GoF = $[\Sigma(w(F^{o2}-F^{c2})^2/\Sigma(N^r-N^p)^2]$

2-4 ESR spectroscopy

An ESR spectrum of PyBTM in dichloromethane was recorded at 175 K to examine the spin density distribution (Figure 2-4-1). The g value (2.004) was close to those of TTM radical (2.0034)[2] and of a free electron (g_e = 2.0023). The spectrum showed hyperfine coupling with ^{1}H, ^{14}N, and ^{13}C atoms, and was fitted by computer simulation with hyperfine coupling constants: 0.115, 0.115, 2.75, 1.27, and 1.27 mT for, the N, H, α-^{13}C, ipso-^{13}C, and ortho-^{13}C atoms, respectively. These values were similar to those of related compounds[2,4] and to the DFT-calculated values (Table 2-4). The results indicate that the spin density is distributed on the central C1 atom and also on the phenyl and pyridyl moieties. A non-negligible spin density exists on the nitrogen atom of the pyridyl moiety. This spin density distribution was reproduced by the DFT calculation, in which the density extended onto the phenyl and pyridyl moieties (Figure 2-4-2). PyBTM radical is therefore stabilized by delocalization of the SOMO as well as by steric hindrance around the C1 atom.

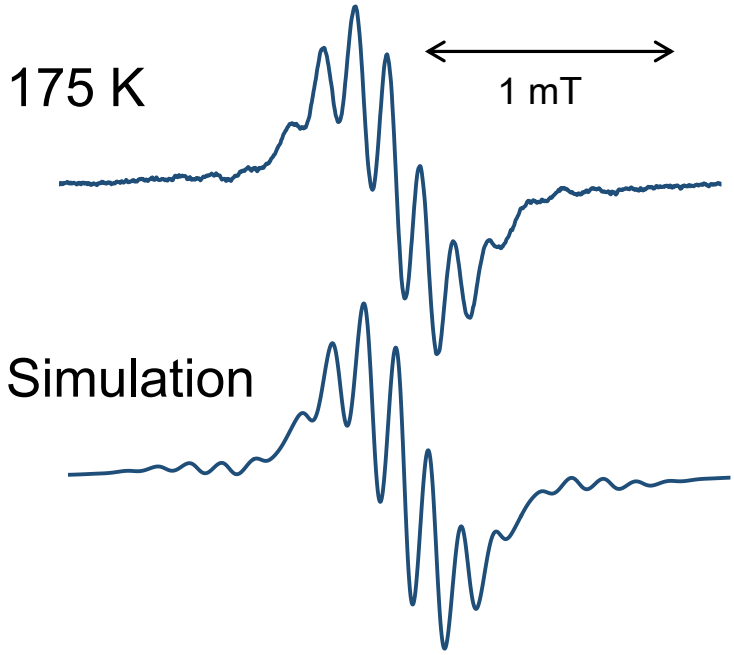

Figure 2-4-1. ESR spectrum of PyBTM in dichloromethane solution at 175 K (top) and computer simulation (bottom).

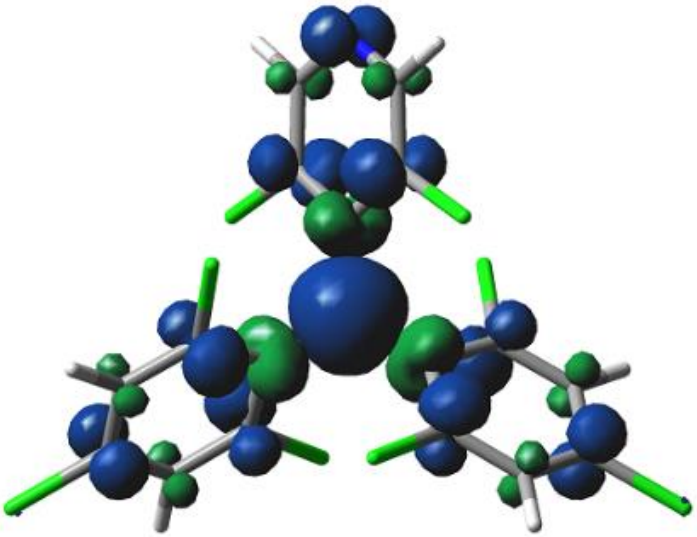

Figure 2-4-2. Spin density distribution calculated using DFT (UB3LYP/6-31G(d)) with isovalue at 0.003.

Table 2-4. Hyperfine coupling constants (hccs) used for ESR simulation and DFT-calculated values

hcc / mT	N	H	α-^{13}C	ipso-^{13}C	ortho-^{13}C
Sim.	0.115	0.115	2.75	1.27	1.27
Calcd.	0.113	0.154	3.70	1.18	1.14
		0.148		1.18	1.13
		0.137		1.17	1.09

2-5 DFT calculations and cyclic voltammetry

The electronic structure of PyBTM was estimated by DFT calculation using UB3LYP/6-31G(d) (Figure 2-5-1). The results show that the SOMO is delocalized onto the aromatic rings, and the electronegative N atom in the pyridine moiety lowers the energy of the SOMO. The energy of the α-SOMO of PyBTM (129α, −5.96 eV) was lower than the α-SOMO of TTM (137α, −5.75 eV) by 0.21 eV, and the energy of the β-SOMO of PyBTM (129β, −3.62 eV) was lower than that of TTM (137β, −3.44 eV) by 0.18 eV.

These negative shifts in energy correspond respectively to the positive shifts of the reversible reduction potential $E_{p(ox)}$ and the irreversible oxidation peak $E^{0\prime}_{(red)}$ in the cyclic voltammetry (CV, Figure 2-5-2). The reversible reduction potential $E^{0\prime}_{(red)}$ = −0.74 V vs. ferrocenium/ferrocene (Fc^+/Fc) and the irreversible oxidation peak $E_{p(ox)}$ = 1.04 V were both more positive than those of TTM ($E^{0\prime}_{(red)}$ = −0.99 V and $E_{p(ox)}$ = 0.80 V) by ca. 0.25V. The DFT calculations and cyclic voltammetry confirm that the introduction of the pyridine moiety lowers the energies of the frontier molecular orbitals.

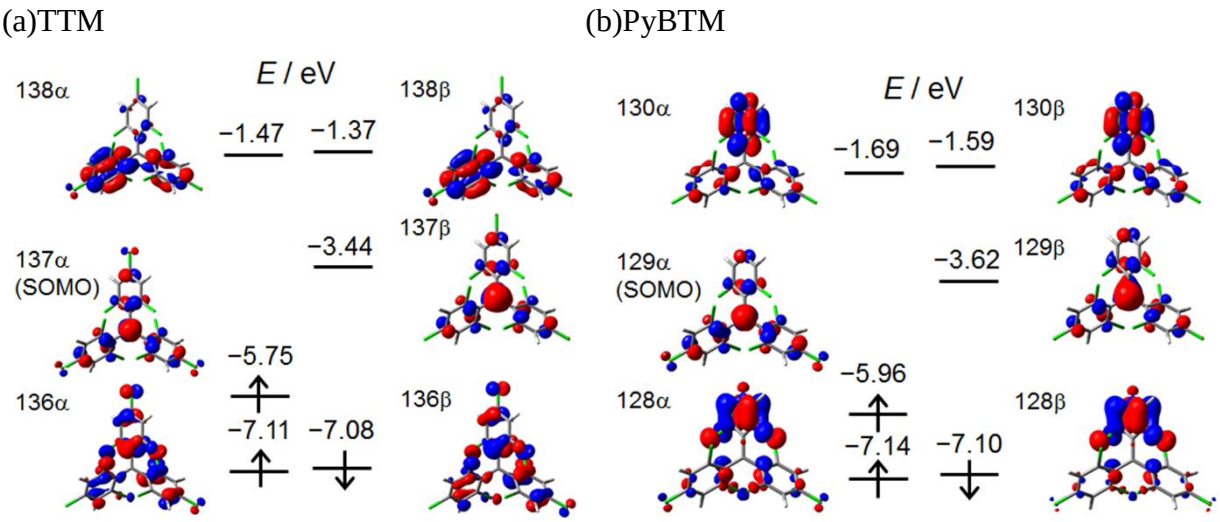

Figure 2-5-1. Frontier orbitals of (a) TTM and (b) PyBTM calculated using DFT methods (UB3LYP/6-31G(d)).

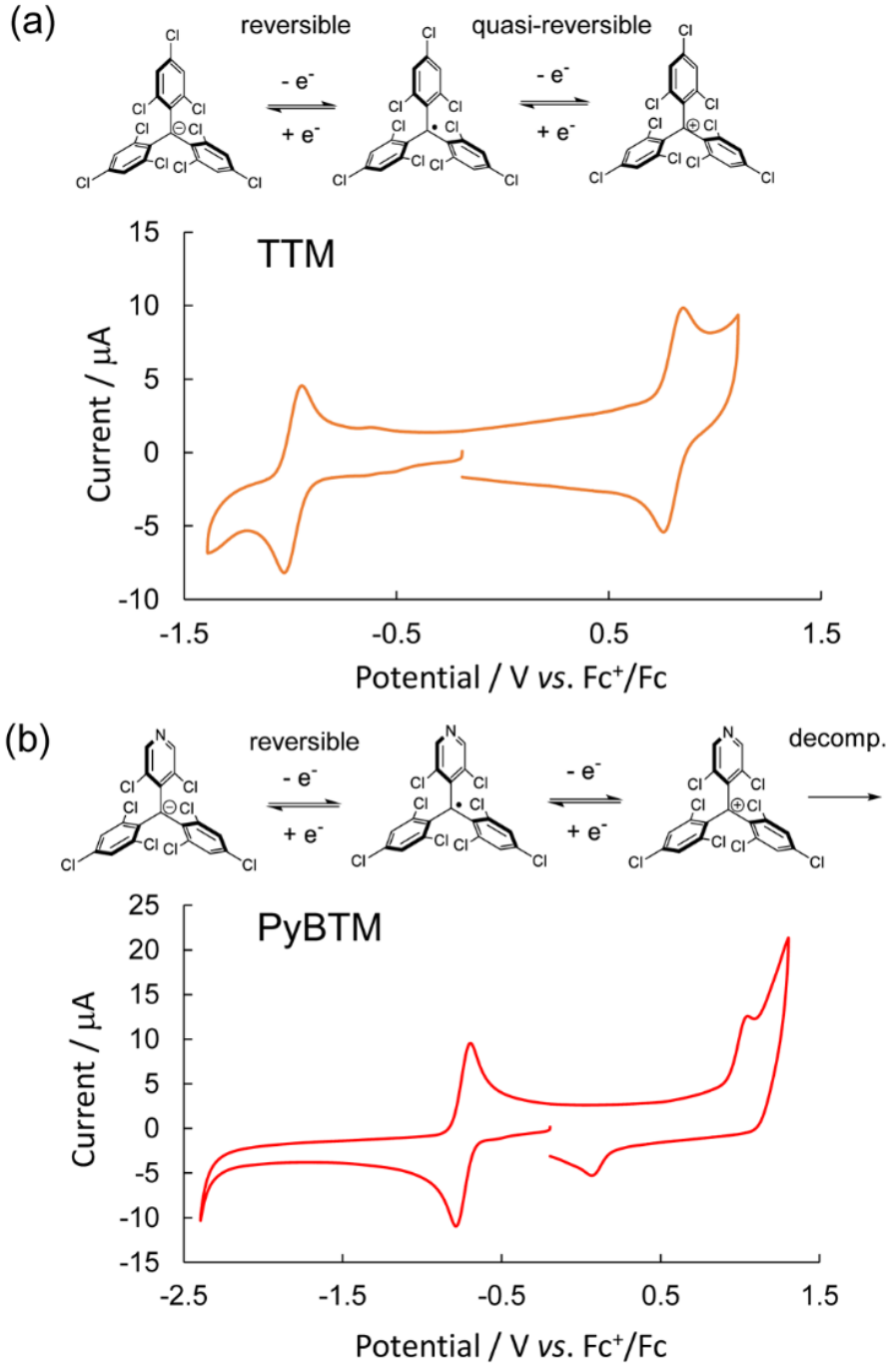

Figure 2-5-2. CVs of (a) TTM (0.5 mM) and (b) PyBTM (0.5 mM) in 0.1 M Bu_4NClO_4–CH_2Cl_2 at a scan rate of 0.1 V s^{-1}.

2-6 Absorption and emission

The UV−Vis absorption spectrum of PyBTM in dichloromethane (Figure 2-6-1) displayed a weak visible absorption band that tails off beyond λ = 600 nm (λ_{max} = 541 nm, ε = 1.01×10^3 M^{-1} cm^{-1}; where ε is the molar extinction coefficient), and a strong near-UV absorption band (λ_{max} = 370 nm, ε = 2.54×10^4 M^{-1} cm^{-1}). Time-dependent DFT (TDDFT) calculations suggested that the band at λ_{max} = 541 nm can be assigned to the transition mainly from 128β (π orbital of pyridine: β-NHOMO) to 129β (the lowest unoccupied spin orbital: β-SOMO; oscillator strength f = 0.019), to form the lowest excited state, whereas the band at λ_{max} = 370 nm was assigned to the transition mainly from 129α (α-SOMO) to 130 α and 131 α (antibonding π* orbitals) with a greater oscillator strength (f = 0.120, 0.151). The agreement of the relative wavelength and oscillator strength with the experimental absorption spectra supports the orbital assignment. A TDDFT calculation of TTM gave similar results.

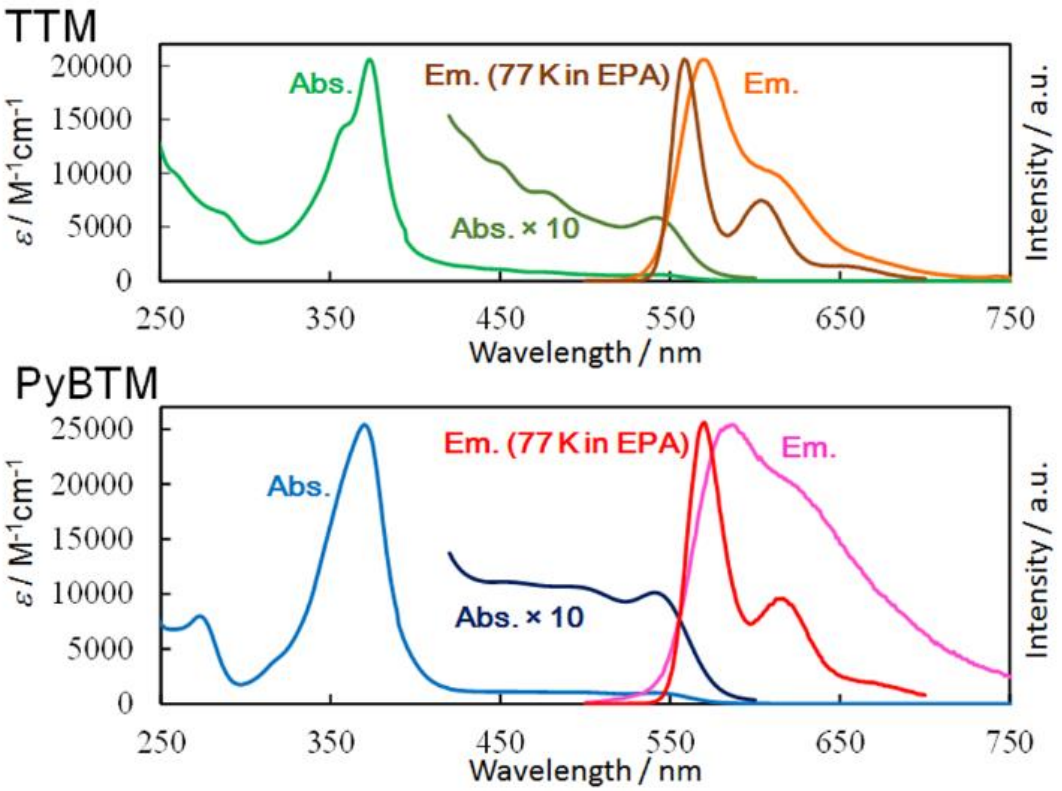

Figure 2-6-1. Absorption, corrected emission spectra in dichloromethane, and corrected emission spectra at 77 K in EPA matrices for TTM and PyBTM. Enlarged portion of absorption spectra (10 fold) are shown from 420 nm to 600 nm.

The fluorescence spectra of PyBTM in dichloromethane upon excitation at λ_{exc} =370 nm (Figure 2-6-1) showed a band with an emission maximum at λ = 585 nm. The shape of the excitation spectrum was similar to that of the absorption spectrum (Figure 2-6-2). The excited-state luminescence lifetime (τ) was 6.4±0.2 ns in dichloromethane with a single-exponential decay, similar to those of TTM (τ = 7.0±0.2 ns) and PTM (τ = 7 ns),[11] supporting the assignment of the emission as fluorescence in nature.

PyBTM displayed similarly shaped absorption and emission bands in cyclohexane, chloroform, dichloromethane, acetone, acetonitrile, ethanol, and methanol. The absolute photoluminescence quantum yields were typically 1–3 % with PyBTM appearing as luminescent as TTM (Table 2-6). The absorption and emission intensities were temperature-dependent (Figures 2-6-3, 2-6-4), and strong luminescence was detected at low temperature in rigid solvents. PyBTM was luminescent at 77 K with excellent absolute photoluminescence quantum yields of 0.81 in EPA (diethyl ether:isopentane:ethanol 5:5:2 v/v) and 0.71 in a mixture of ethanol and methanol (1:1 v/v). The quantum yield of 0.81 is the highest value reported for stable organic radicals. This high quantum yield results from the suppression of the molecular vibrations that promote non-radiative decay.

The results prompted us to disperse the PyBTM molecules in a poly(methyl methacrylate) (PMMA) film (Figure 2-6-5). The rigid polymer chains should suppress the molecular motion of the PyBTM, and a better room-temperature fluorescence quantum yield was expected than that in the solution. The film showed luminescence with ϕ = 0.26 at room temperature under photoirradiation (λ = 370 nm). The encapsulation of PyBTM in a PMMA matrix resulted in a quantum yield that is approximately ten times higher than that in solution.

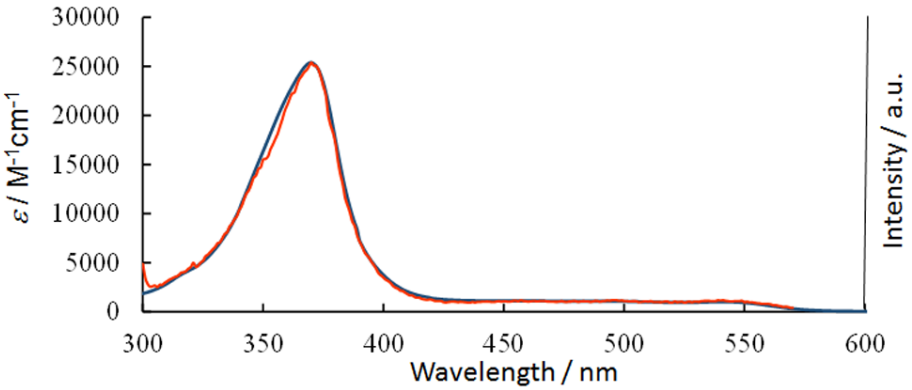

Figure 2-6-2. Excitation spectrum observed for emission wavelength at 585 nm (orange line) and absorption spectrum (blue line) of PyBTM.

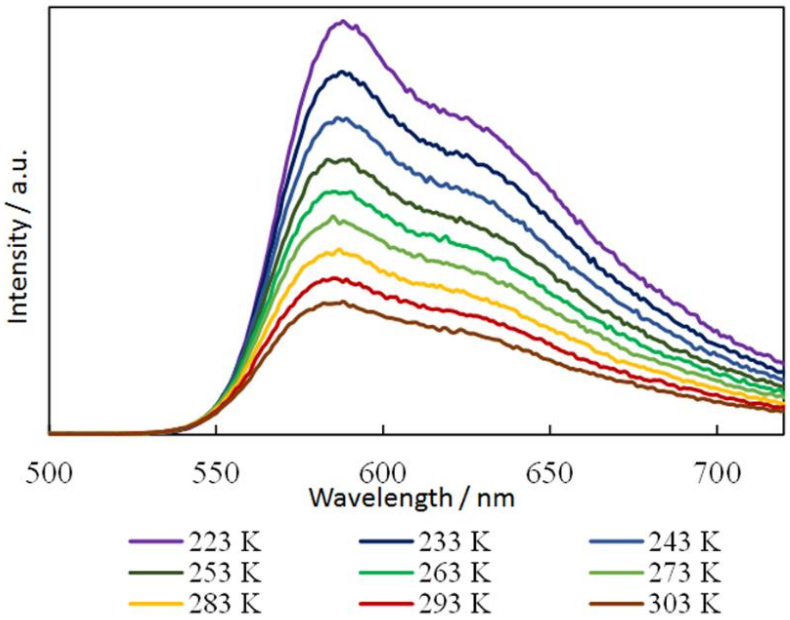

Figure 2-6-3. Temperature-dependent corrected fluorescence spectra of PyBTM in dichloromethane from 303 K to 223 K.

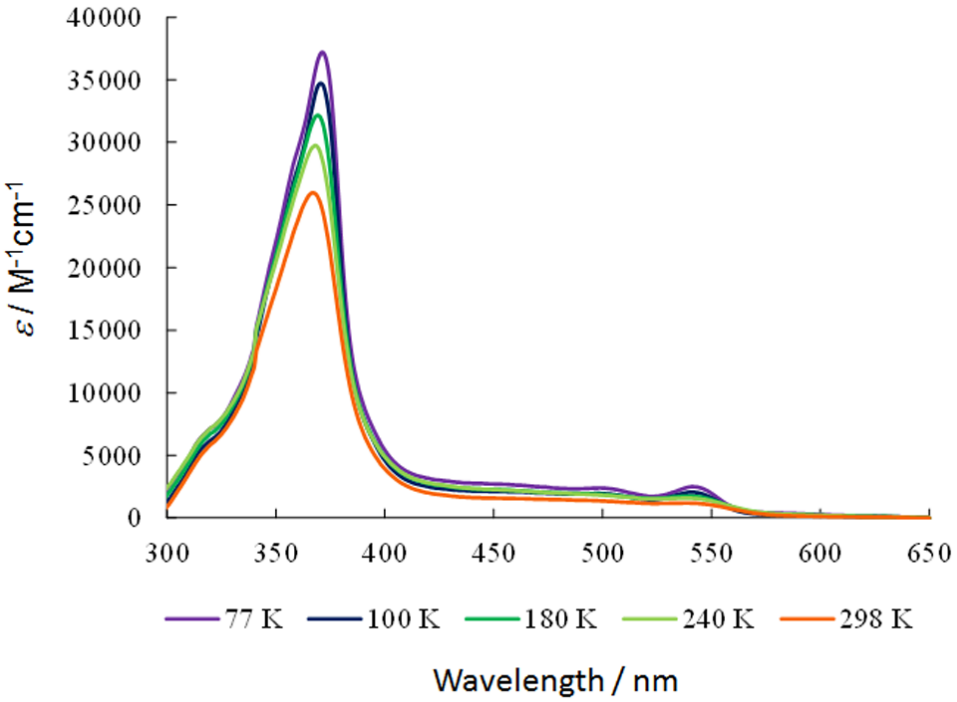

Figure 2-6-4. Temperature-dependent UV-vis absorption spectra of PyBTM in EPA (diethyl ether : isopentane : ethanol = 5:5:2, 2.5×10^{-5} M) from 77 K to 293 K.

(a) (b)

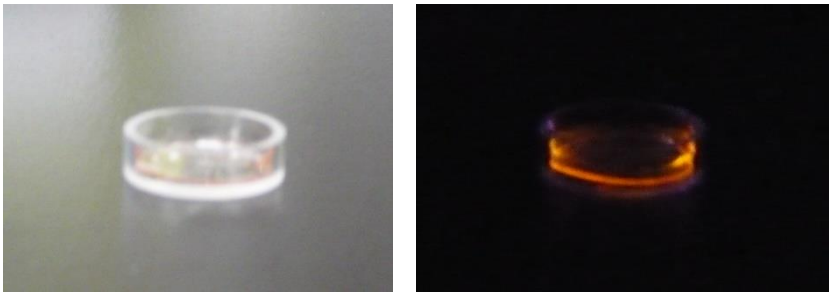

Figure 2-6-5. PyBTM dispersed in PMMA (a) under room light and (b) under UV lamp (λ = 365 nm) in the dark.

Table 2-6. Quantum yield of luminescence of PyBTM and TTM in various solvents

Solvent	ϕ (PyBTM)[a]	ϕ (TTM)[a]
Cyclohexane	2%	2%
Toluene	0.2%	2%
Chloroform	3%	3%
Dichloromethane	2%	2%
Acetone	1%	2%
Acetonitrile	2%	2%
Ethanol	1%	2%
Methanol	2%	2%
EPA[b] (77K)	81%	76%
Ethanol-Methanol (77K)	71%	46%

[a] Excitation wavelength were 370 nm for all samples. Absorption maxima of all samples were around 370 nm and absorbance of the samples at 370 nm were 0.05-0.10.

[b] Diethyl ether : isopentane : ethanol = 5:5:2

2-7 Stability

There was no difference between fluorescence spectrum of a PyBTM solution in chloroform prepared in air and that of a PyBTM solution bubbled with argon. Thus, fluorescence intensity of PyBTM was not affected by oxygen. The stability of PyBTM was examined at ambient condition in air. Solid PyBTM showed no decomposition. Even after heating at 383 K for 48 h, 91% of it was preserved. When PyBTM solution in chloroform was kept at r.t. for 5 days in the dark, no change of absorption and emission spectra and no loss of fluorescence intensity was observed, indicating the high chemical stability of PyBTM.

The improvement of the photostability of luminescent organic radicals is an important issue in the development of luminescent radical materials. PyBTM emitted visibly under UV light irradiation for longer than did TTM. The photostability of PyBTM was evaluated and compared with that of TTM (Figure 2-7-1). When ~1×10^{-5} M acetone solutions of each were irradiated by the 370 nm light source, the decay of the fluorescence intensity of PyBTM ($1/t_{1/2(\mathrm{PyBTM})}$) was 115 times smaller than that of TTM ($1/t_{1/2(\mathrm{TTM})}$; Figure 2-7-2). PyBTM was 45 to 71 times more stable in other aprotic solvents than TTM. The enhanced degradation in alcohols is probably owing to hydrogen bonds to chlorine or nitrogen atoms that promoted the decomposition reaction (Figure 2-7-3). I also observed that TTM undergoes efficient photolysis even under natural light. The introduction of the pyridyl group therefore enables the enhanced photostability of PyBTM. This can be interpreted to be resulted from the lowered energies of the frontier orbitals involved in the luminescent process, as shown by the CV and the DFT calculations. In assumption that the stability of the lowest excited state is attributed to the photostability of the radicals (internal conversion from higher excited states to the lowest excited state is thought to be fast, and decomposition of the radicals are observed under irradiation of visible light), β-SOMO plays the most important role in the frontier orbitals. Lower β-SOMO lowers the energy of the lowest excited state and decreases the reactivity under photoirradiation.

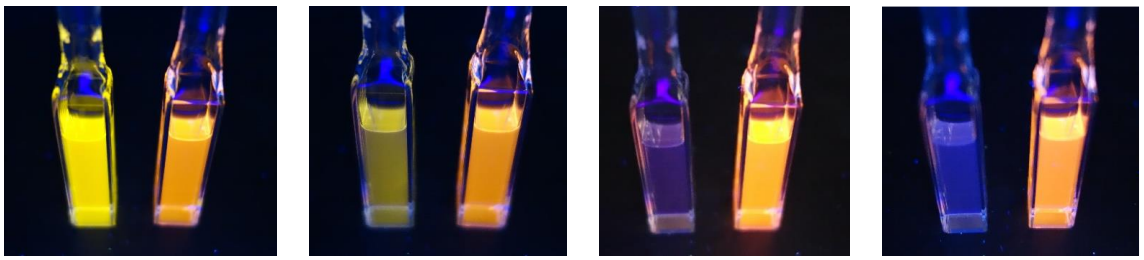

Figure 2-7-1. Photographs of TTM (left cuvette in each image) and PyBTM (right cuvette) solutions (2.5×10^{-4} M) in acetone under irradiation with UV light at λ = 370 nm recorded at different time intervals, showing the emission decay with time.

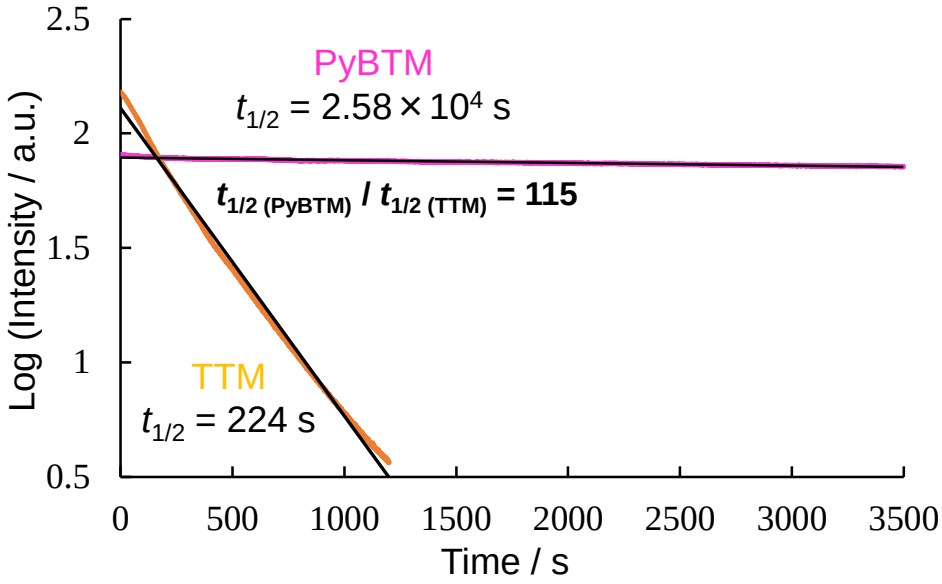

Figure 2-7-2. Plots showing the emission decay of PyBTM and TTM in acetone under continuous excitation with light at λ = 370 nm.

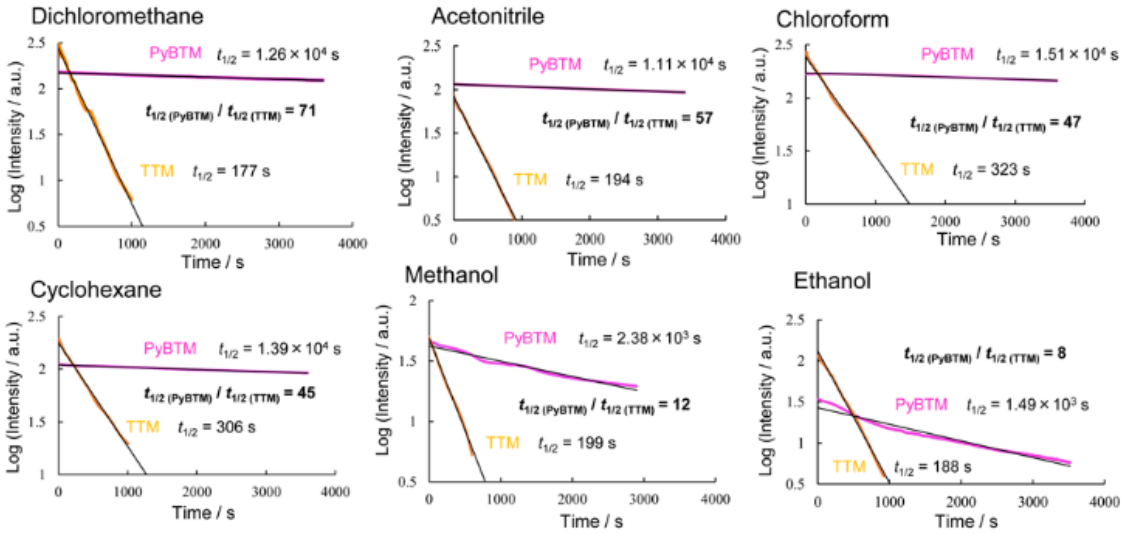

Figure 2-7-3. Comparison of stability of PyBTM and TTM under 370 nm light irradiation in various solvents. $t_{1/2}$ indicates half-life.

2-8 Protonation

Red single crystals of [*NH*-PyBTM]·H_2O·BF_4 were obtained by mixing tetrafluoroboronic acid slowly into an ethanol solution of PyBTM (Figure 2-8-1, Table 2-8, CCDC 1006485). A hydrogen bond was thought to exist between the H atom of pyridinium and the O atom of water.

The redox properties of PyBTM were modulated by protonation and deprotonation. With acid addition, the CVs showed a redox wave attributable to the $[NH\text{-PyBTM}]^+/[NH\text{-PyBTM}]$ couple at $E^{0\prime}_{(red)}$ = +0.05 V vs. Fc^+/Fc in 0.1 M Bu_4NClO_4–CH_2Cl_2 (Figure 2-8-2), which was +0.79 V more positive than that of PyBTM. The successive titration with *p*-toluenesulfonic acid (TsOH) and 1,8-diazabicyclo[5.4.0]undec-7-ene (DBU) demonstrated the reversible response to protons. Given that α*H*-PyBTM was redox inactive, protonation of PyBTM at the α carbon was excluded, and protonation at the nitrogen atom is plausible as was seen from the crystal structure.

Control of the luminescence properties of PyBTM by a protonation-deprotonation reaction on the N atom of the pyridyl group was attempted. By using a method and references developed by Leito et al.,[7] the pK_a of $PyBTMH^+$ (conjugated acid of PyBTM) in acetonitrile was estimated to be 6.9, which was much smaller than that of PyH^+ (conjugated acid of pyridine, pK_a = 12.53). PyBTM is therefore more than five orders of magnitude weaker than pyridine in its basicity, because of the presence of the electron-withdrawing chlorine atoms.

Despite its weakness of basicity, the protonation and deprotonation behavior of PyBTM was confirmed by UV−vis spectroscopy by titration with TsOH and triethylamine in dichloromethane (Figure 2-8-3). In the absorption spectrum of $PyBTMH^+$, the weak visible absorption was bathochromically shifted by ~900 cm^{-1}, another strong absorption peak appeared at 444 nm, and strong near UV absorption was weakened and slightly bathochromically shifted (~700 cm^{-1}). The lower energies of the unoccupied orbitals (129β, 130α, etc.) due to a positive charge on the nitrogen atom explain the bathochromic shift of absorption. The narrower band gaps of $[NH\text{-PyBTM}]^+$ were expected from the DFT calculation. The fluorescence intensity decreased upon addition of the acid, and then recovered when the base was added (Figure 2-8-4). These results show that the luminescence properties are controlled by protons as an external stimulus.

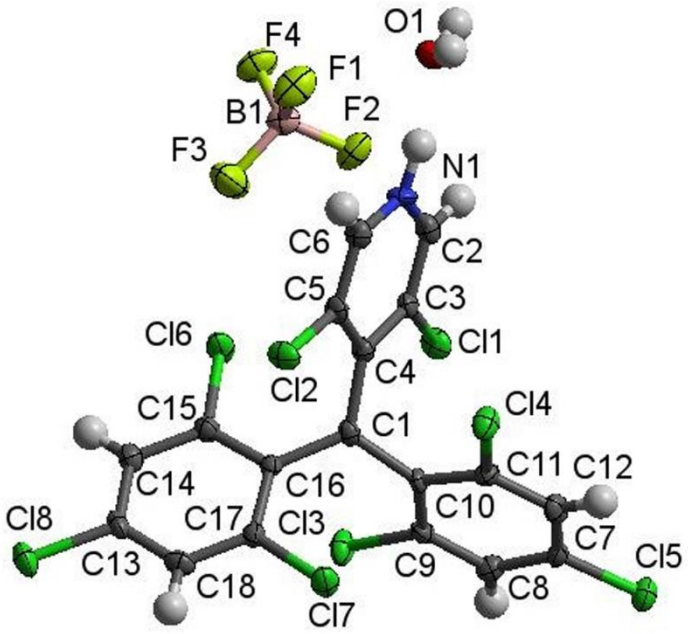

Figure 2-8-1. Molecular structure of crystalline [*NH*-PyBTM]·BF_4·H_2O with thermal ellipsoids at the 50% probability level.

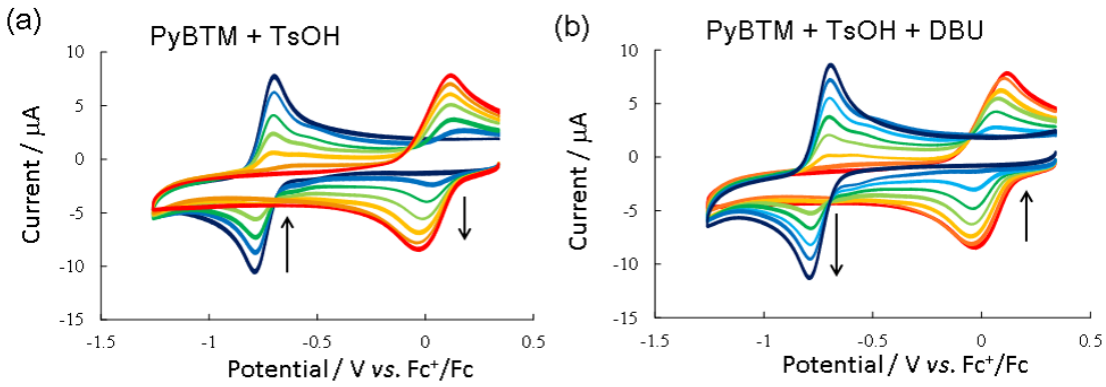

Figure 2-8-2. Proton-response of cyclic voltammograms of PyBTM. (a) To a PyBTM solution (0.5 mM, 5 mL) in 0.1 M Bu_4NClO_4–CH_2Cl_2, *p*-toluenesulfonic acid (TsOH) solution (25 mM in dichloromethane, initial (Indigo), 20 μL (blue), 40 μL (green), 60 μL (pale green), 80 μL (pale orange), 100 μL (orange), 120 μL (red)) was added and CV was measured at a scan rate of 0.1 V s^{-1}. (b) To the solution of (a), diazabicyclo[5.4.0]undec-7-ene (DBU) solution (25 mM in dichloromethane, initial (Indigo), 20 μL (blue), 40 μL (pale blue), 60 μL (green), 80 μL (pale green), 100 μL (pale orange), 120 μL (orange), 140 μL (red)) was added and CV was measured at a scan rate of 0.1 V s^{-1}.

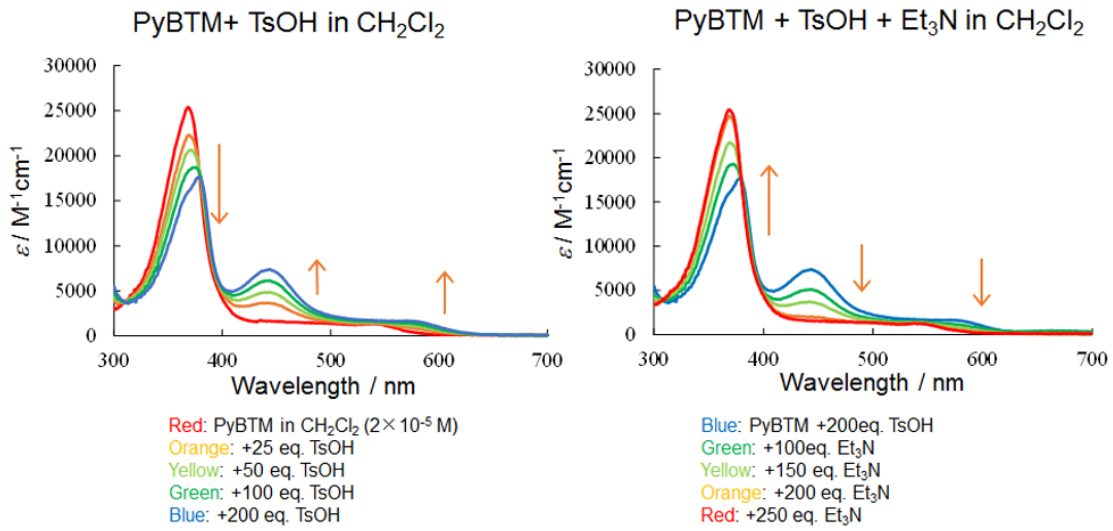

Figure 2-8-3. Protonation (left) and deprotonation (right) of PyBTM by titration with *p*-toluenesulfonic acid (TsOH) and triethylamine (Et_3N) in dichloromethane.

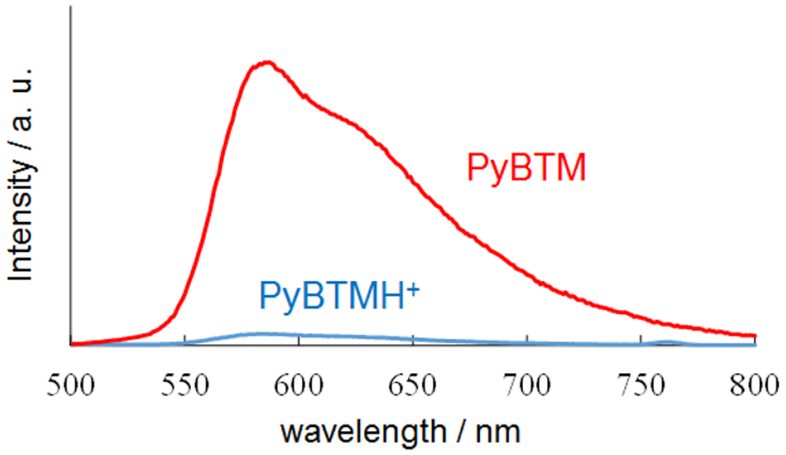

Figure 2-8-4. Corrected fluorescence spectra of PyBTM and $PyBTMH^+$. Fluorescence of $PyBTMH^+$ is almost quenched.

Table 2-8 Crystallographic data of [*NH*-PyBTM]·BF_4·H_2O

	[*NH*-PyBTM]·BF_4·H_2O
Empirical formula	C_{18} H_9 B Cl_8 F_4 N O
Fw / g mol^{-1}	625.70
Crystal system	monoclinic
Space group	$P2_1/c$
Crystal size / mm	0.2×0.2×0.2
Temperature / K	113(2)
a / Å	17.747(6)
b / Å	8.177(3)
c / Å	15.931(6)
α / º	90
β / º	91.343 (4)
γ / º	90
V / $Å^3$	2311.3 (14)
Z	4
ρ_{calced} / g cm^{-3}	1.798
λ / Å	0.7107
μ / mm^{-1}	1.020
Reflections collected	17662
Independent reflections	5287
Parameters	310
R_{int}	0.0741
[a]*R*1	0.0885
[b]*wR*2	0.1884
[c]GoF	1.206
CCDC No.	1006485

[a] $R_1 = \Sigma||F^o|-|F^c||/\Sigma|F^o|$ ($I>2\sigma(I)$). [b] $wR_2 = [\Sigma(w(F^{o2}-F^{c2})^2/\Sigma w(F^{o2})^2]^{1/2}$ ($I>2\sigma(I)$). [c] GoF = $[\Sigma(w(F^{o2}-F^{c2})^2/\Sigma(N^r-N^p)^2]$

2-9 Conclusion

A stable luminescent organic radical PyBTM was newly prepared. PyBTM showed a significantly greater photostability than previously reported for luminescent organic radicals such as TTM. The stability was attributed to the lower energy of the frontier orbitals such as β-SOMO resulting from the introduction of an electronegative nitrogen atom.

Since deactivation of the lowest excited state was attributed to the internal conversion caused by vibronic coupling and vibrational relaxation, conditions to suppress the molecular vibration improved the strength of luminescence. PyBTM exhibited a high luminescence quantum yield in solvent glass at 77 K and a moderate quantum yield in PMMA at room temperature. Efficient luminescence in the solid state is also desirable for some applications.

Reversible protonation at the pyridine N atom can switch the properties of PyBTM. Coordination to other molecules such as metal complexes are also expected to show interesting luminescence properties; a good example will be shown in Chapter 4.

2-10 References

[1] Y. Hattori, T. Kusamoto, H. Nishihara, *Angew. Chem. Int. Ed.* **2014**, *53*, 11845 – 11848; *Angew. Chem.* **2014**, *126*, 12039 – 12042.

[2] O. Armet, J. Veciana, C. Rovira, J. Riera, J. Casteñer, E. Molins, J. Rius, C. Miravitlles, S. Olivella, J. Brichfeus, *J. Phys. Chem.* **1987**, *91*, 5608 – 5616.

[3] D. A. Klumpp, Y. Zhang, P. J. Kindelin, S. Lau, *Tetrahedron* **2006**, *62*, 5915 – 5921.

[4] L. Juliá, M. Ballester, J. Riera, J. Casteñer, J. L. Ortin, C. Onrubia, *J. Org. Chem.* **1988**, *53*, 1267 – 1273.

[5] A. Altomare, G. Cascarano, C. Giacovazzo, A. Guagliardi, M. C. Burla, G. Polidori, M. Camalli, *J. Appl. Cryst.* **1994**, *27*, 435.

[6] G. M. Sheldrick, *Acta Cryst. A* **2008**, *64*, 112 – 122.

[7] I. Kaljurand, A. Kütt, L. Sooväli, T. Rodima, V. Mäemets, I. Leito, I. A. Koppel, *J. Org. Chem.* **2005**, *70*, 1019 – 1028.

[8] M. J. Frisch, G. W. Trucks, H. B. Schlegel, G. E. Scuseria, M. A. Robb, J. R. Cheeseman, G. Scalmani, V. Barone, B. Mennucci, G. A. Petersson, H. Nakatsuji, M. Caricato, X. Li, H. P. Hratchian, A. F. Izmaylov, J. Bloino, G. Zheng, J. L. Sonnenberg, M. Hada, M. Ehara, K. Toyota, R. Fukuda, J. Hasegawa, M. Ishida, T. Nakajima, Y. Honda, O. Kitao, H. Nakai, T. Vreven, J. A. Montgomery, Jr., J. E. Peralta, F. Ogliaro, M. Bearpark, J. J. Heyd, E. Brothers, K. N. Kudin, V. N. Staroverov, R. Kobayashi, J. Normand, K. Raghavachari, A. Rendell, J. C. Burant, S. S. Iyengar, J. Tomasi, M. Cossi, N. Rega, J. M. Millam, M. Klene, J. E. Knox, J. B. Cross, V. Bakken, C. Adamo, J. Jaramillo, R. Gomperts, R. E. Stratmann, O. Yazyev, A. J. Austin, R. Cammi, C. Pomelli, J. W. Ochterski, R. L. Martin, K. Morokuma, V. G. Zakrzewski, G. A. Voth, P. Salvador, J. J. Dannenberg, S. Dapprich, A. D. Daniels, Ö. Farkas, J. B. Foresman, J. V. Ortiz, J. Cioslowski, and D. J. Fox, Gaussian, Inc., Wallingford CT, U. S. A. 2009.

[9] A. D. Becke, *J. Chem. Phys.* **1993**, *98*, 5648 – 5652.

[10] Y. Zhao, D. G. Truhlar, *Theor. Chem. Acc.* **2008**, *120*, 215 – 241.

[11] M. A. Fox, E. Gaillard, C.-C. Chen, *J. Am. Chem. Soc.* **1987**, *109*, 7088 – 7094.

Part of sentences and figures in this chapter is reproduced or adapted from Ref. 1 with permission from John Wiley & Sons, Inc.

Chapter 3

Effects of Halogen Atoms in (3,5-Dihalo-4-pyridyl)bis(2,4,6-trichlorophenyl)methyl Radicals

3-1 Introduction

In stable triarylmethyl radicals including PyBTM, the six *ortho*-chlorine atoms sterically protect the radical center from reactions such as dimerization.[1] Electron-withdrawing effect and electron resonance effect of the chlorine atoms are thought to provide further stability of the radicals. In this study, I aimed to reveal the effects of the choice of the halogen atoms at the *ortho*-position on the pyridine ring in PyBTM on its properties and stabilities in the ground and photoexcited states.

Replacement of the Cl atoms into other halogens is expected to tune not only the stability but also the energy levels of molecular orbitals distributed on the pyridine ring leading to modification of optical properties. No such study has been reported previously probably because of the reduced chemical stability of the radical upon the replacement. Indeed, replacing the Cl atom with a H atom significantly reduces the stability.[1a]

I report herein two new luminescent radicals, (3,5-dibromo-4-pyridyl)bis(2,4,6-trichlorophenyl)methyl radical (Br_2PyBTM) and (3,5-difluluoro-4-pyridyl)bis(2,4,6-trichlorophenyl)methyl radical (F_2PyBTM),[2] which are the first stable luminescent triarylmethyl radicals to have non-chloro halogen atoms at the *ortho*-positions (Figure 3-1). No decomposition of the compounds was observed in air at room temperature. (3,5-Dihalo-4-pyridyl)bis(2,4,6-trichlorophenyl)methyl radical (X_2PyBTM) is the general term for three stable radicals; Br_2PyBTM, PyBTM and F_2PyBTM. Br_2PyBTM (X = Br) and F_2PyBTM (X = F) have two F or Br atoms in place of the Cl atoms in the pyridine ring of PyBTM, and X = Cl indicates PyBTM.

In this chapter, crystal structures, electronic structures, optical characteristics, and photostability of X_2PyBTM are discussed. Bromine atoms are expected to show larger steric effect than chlorine atoms, and fluorine atoms are expected to show smaller steric effect than chlorine atoms. More electronegative fluorine atoms are thought to lower energies of some frontier orbitals, and less electronegative bromine atoms are thought to raise energies of some frontier orbitals compared to those of PyBTM. As a result, superior photostability of Br_2PyBTM is explained by larger steric effect or higher β-NHOMO, and greater fluorescence quantum yield of F_2PyBTM is explained by smaller steric effect or lower β-NHOMO. The nitrogen atom in X_2PyBTM also acts as stimuli-responsive sites. The proton-response of X_2PyBTM is also reported in this chapter, and coordination to gold(I) is described in Chapter 5.

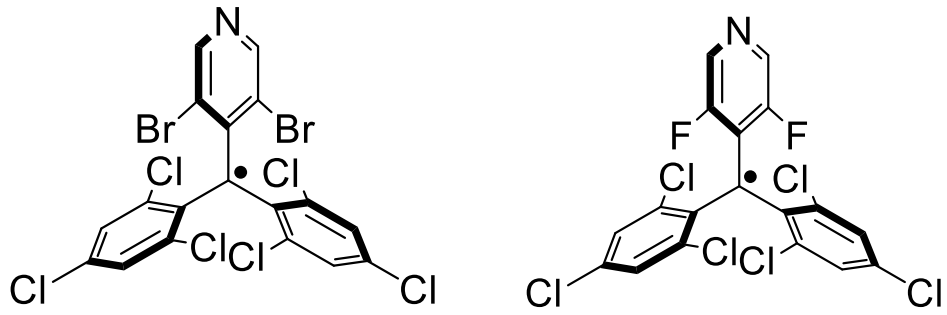

Br_2PyBTM **F_2PyBTM**

Figure 3-1. Structures of Br_2PyBTM and F_2PyBTM radicals.

3-2 Experimental section

Materials

3,5-Dibromo-4-pyridinecarboxaldehyde, 3,5-difluoro-4-formylpyridine, ^{t}BuOK in THF (1 M solution), and 4-hydroxy-TEMPO were purchased from Sigma-Aldrich Co.LLC., 1,3,5-trichlorobenzene was from Wako Pure Chemical Industries, Ltd., trifluoromethanesulfonic acid was from Tokyo Chemical Industry Co., Ltd.

Synthesis of (3,5-dibromo-4-pyridyl)bis(2,4,6-trichlorophenyl)methane (α*H*-Br$_2$PyBTM)

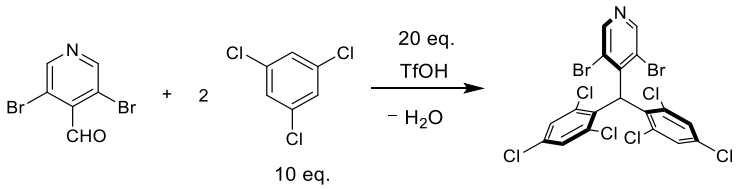

α*H*-Br$_2$PyBTM was synthesized by a similar method to that of α*H*-PyBTM[3] utilizing superacid-catalyzed condensation of pyridine carboxaldehyde with arenes.[4] Under a nitrogen atmosphere, 3,5-dibromo-4-pyridinecarboxaldehyde (532 mg, 2.01 mmol, 1 eq.) and 1,3,5-trichlorobenzene (3.64 g, 20.1 mmol, 10 eq.) were heated to 180 °C. Trifluoromethanesulfonic acid (6.0 g, 40 mmol, 20 eq.) was added, and the reaction mixture was stirred for 9.5 hours at 180 °C. The reaction mixture was cooled to r.t., dissolved in dichloromethane, and added to ice water. The mixture was neutralized using $NaHCO_3$ aq, extracted with dichloromethane (3 × 50 mL), washed with $NaHCO_3$ aq, and dried by $MgSO_4$. The organic layer was purified by SiO_2 column chromatography (dichloromethane : hexane = 1:1), evaporated, and dried in vacuo to afford α*H*-Br$_2$PyBTM (279 mg, 0.458 mmol, 28%) as a white solid. **^{1}H NMR** (500 MHz, $CDCl_3$): δ 8.64 (s, 1H), 8.54 (s, 1H), 7.39 (dd, J = 2.1 Hz, 2.2 Hz, 2H), 7.26 (d, 1H), 7.24 (d, J = 2.3 Hz, 1H), 6.62 (s, 1H). **MS** (positive ion mode FAB) m/z: $[M+H]^+$ Calcd for $C_{18}H_8Br_2Cl_6N$ 609.71; Found 610. **Elem. Anal.** Calcd for $C_{18}H_7NBr_2Cl_6$: C 35.46, H 1.16, N 2.30. Found, C 35.48, H 1.22, N 2.20.

Synthesis of (3,5-dibromo-4-pyridyl)bis(2,4,6-trichlorophenyl)methyl radical (Br$_2$PyBTM)

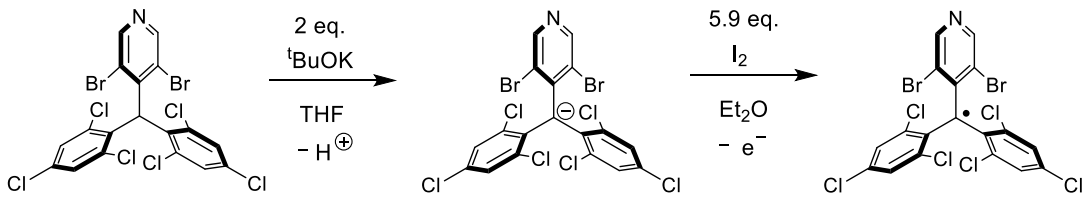

Br_2PyBTM was synthesized by a similar method to that of PyBTM.[3] Under a nitrogen atmosphere, α*H*-Br_2PyBTM (152 mg, 0.249 mmol) was dissolved in dry THF (11 mL). ^{t}BuOK in THF (1M solution, 0.5 mL, 2 eq.) was added dropwise and the color of the solution changed to red. The reaction mixture was stirred overnight in the dark. I_2 (373 mg, 1.47 mmol, 5.9 eq.) in dry diethyl ether (50 mL) was added dropwise and stirred for 2.25 h.[5] Remaining I_2 was reduced by washing with 10 % $Na_2S_2O_3$ aq 3 times, water layer was extracted with diethyl ether, and the combined organic layer was dried with $MgSO_4$. The red solution was filtered, evaporated, purified by Al_2O_3 column chromatography (diethyl ether : hexane = 1:4) and dried in vacuo to afford Br_2PyBTM (70.4 mg, 0.116 mmol, 46%) as a red solid. **IR** (KBr) 3092 (w), 3048 (w), 2955 (w), 2923 (w), 1553 (s), 1527 (s), 1395 (s), 1373 (s), 1292 (m), 1216 (w), 1204 (w), 1182 (m), 1134 (m), 1084 (w), 1071 (w), 1053 (w), 925 (w), 884 (w), 860 (s), 829 (m), 808 (s), 791 (m), 753 (m), 726 (w), 661 (w), 567 (w), 539 (w) **HRMS** (negative ion mode ESI-TOF) m/z: $[M]^-$ Calcd for $C_{18}H_6Br_2Cl_6N$ 607.6948; Found 607.6945. **Elem. Anal.** Calcd for $C_{18}H_6NBr_2Cl_6$: C 35.51, H 0.99, N 2.30. Found, C 35.83, H 1.20, N 2.07. **ESR** Spin concentration of Br_2PyBTM in toluene (1.00×10^{-4} M) was estimated by comparing the value of twice-integration of the signal intensity with that of the reference sample (4-hydroxy-TEMPO in toluene; 9.8×10^{-5} M). The existence of S = 1/2 spin on one Br_2PyBTM molecule was confirmed.

Synthesis of (3,5-difluoro-4-pyridyl)bis(2,4,6-trichlorophenyl)methane (α*H*-F_2PyBTM)

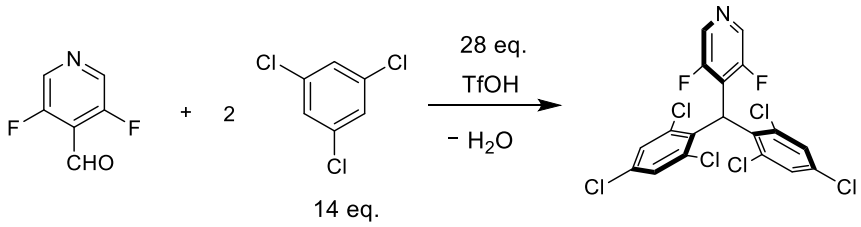

α*H*-F_2PyBTM was synthesized by a similar method to that of α*H*-PyBTM[3] utilizing superacid-catalyzed condensation of pyridine carboxaldehyde with arenes.[4] Under a nitrogen atmosphere, 3,5-difuoro-4-formylpyridin (104 mg, 0.727 mmol, 1 eq.) and 1,3,5-trichlorobenzene (1.81 g, 10.0 mmol, 14 eq.) were heated to 180 °C. Trifluoromethanesulfonic acid (3.0 g, 20 mmol, 28 eq.) was added, and the reaction mixture was stirred for 9 hours at 180 °C. The reaction mixture was cooled to r.t., dissolved in dichloromethane, and added to ice water. The mixture was neutralized to pH 7 using $NaHCO_3$ aq, extracted with dichloromethane (3 × 50 mL), washed with $NaHCO_3$ aq, and dried by $MgSO_4$. The organic layer was purified by SiO_2 column chromatography

(dichloromethane : hexane = 1:1), evaporated, and dried in vacuo to afford α*H*-F_2PyBTM (231 mg, 0.458 mmol, 65%) as a white solid. **^{1}H NMR** (500 MHz, $CDCl_3$): δ8.33 (s, 1H), 8.21 (s, 1H), 7.33 (s, 4H), 6.64 (s, 1H). **MS** (positive ion mode FAB) m/z: $[M\text{-}H]^+$ Calcd for $C_{18}H_8Cl_6F_2N$ 487.87; Found 488. **Elem. Anal.** Calcd for $C_{18}H_7NCl_6F_2$: C 44.31, H 1.45, N 2.87. Found, C 44.45, H 1.67, N 2.78.

Synthesis of (3,5-difluoro-4-pyridyl)bis(2,4,6-trichlorophenyl)methyl radical (F_2PyBTM)

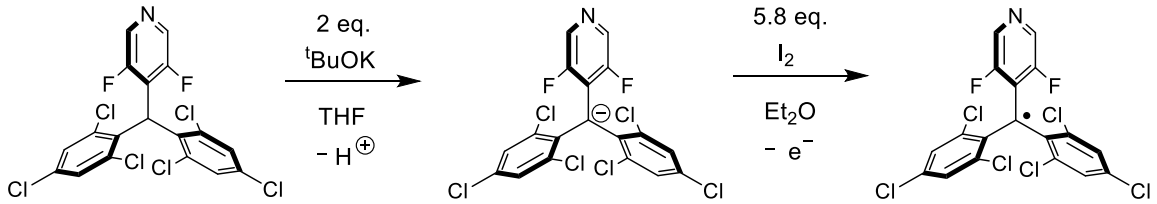

F_2PyBTM was synthesized by a similar method to that of PyBTM.[3] Under a nitrogen atmosphere, α*H*-F_2PyBTM (121 mg, 0.248 mmol) was dissolved in dry THF (13 mL). ^{t}BuOK in THF (1M solution, 0.5 mL, 2 eq.) was added dropwise and the color of the solution changed to reddish orange. The reaction mixture was stirred overnight in the dark. I_2 (367 mg, 1.45 mmol, 5.8 eq.) in dry diethyl ether (43 mL) was added dropwise and stirred for 2.25 h.[5] Remaining I_2 was reduced by washing with 10 % $Na_2S_2O_3$ aq 3 times, water layer was extracted with diethyl ether, and the combined organic layer was dried with $MgSO_4$. The reddish orange solution was filtered, evaporated, purified by Al_2O_3 column chromatography (diethyl ether : hexane = 1:4) and dried in vacuo to afford F_2PyBTM (54.3 mg, 0.112 mmol, 45%) as a red solid. **IR** (KBr) 3049 (w), 2955 (w), 2923 (w), 2851 (w), 1558 (s), 1529 (s), 1423 (s), 1372 (s), 1286 (m), 1257 (m), 1220 (m), 1185 (m), 1142 (m), 1028 (s), 918 (m), 875 (w), 859 (s), 829 (m), 806 (m), 793 (m), 734 (w), 570 (m), 538 (w) **HRMS** (negative ion mode ESI-TOF) m/z: $[M]^-$ Calcd for $C_{18}H_6Cl_6F_2N$ 485.8571; Found 485.8555. **Elem. Anal.** Calcd for $C_{18}H_6NCl_6F_2$: C 44.40, H 1.24, N 2.88. Found, C 44.79, H 1.63, N 2.67. **ESR** Spin concentration of F_2PyBTM in toluene (1.03×10^{-4} M) was estimated by comparing the value of twice-integration of the signal intensity with that of the reference sample (4-hydroxy-TEMPO in toluene; 9.8×10^{-5} M). The existence of S = 1/2 spin on one F_2PyBTM molecule was confirmed.

X-ray structural analysis

Diffraction data for X-ray analysis were collected with an AFC10 diffractometer coupled with a Rigaku Saturn CCD system equipped with a rotating-anode X-ray generator producing graphite-monochromated MoKα radiation (λ = 0.7107 Å). Lorentz

polarization and numerical absorption corrections were performed with the program *Crystal Clear 1.3.6.* Structures were solved by the direct method using SIR 92 software[6] and refined against F2 using SHELXL-97.[7] Br_2PyBTM was refined using ISOR restraints. *Crystal Structure 4.0* software was used to prepare the material for publication. The crystallographic data are listed in Table 3-3-3. CCDC 1058942 and 1058943 contain the supplementary crystallographic data of this paper. These data can be obtained free of charge from The Cambridge Crystallographic Data Centre via www.ccdc.cam.ac.uk/data_request/cif.

Instruments

^{1}H NMR spectra were recorded using a BRUKER US500. The reported chemical shifts of the solvent residual peaks were used for calibration of the ^{1}H NMR spectra in $CDCl_3$ (δ7.26). FAB mass spectra were recorded using a JEOL JMS-700MStation mass spectrometer using 3-nitrobenzyl alcohol as a matrix, and ESI–TOF mass spectra were recorded using an LCT Micromass spectrometer. ESR spectra were recorded with a JEOL JES-FA200 spectrometer with X-band microwave. 4-Hydroxy-TEMPO was used as a spin concentration standard. Deoxygenated sample solutions were charged in a 5mmϕ sample tube. Magnetic field was calibrated with the Mn^{2+}/MgO standard. UV-vis absorption spectra were recorded with a JASCO V-570 spectrometer. Steady-state emission spectra were measured with a HITACHI F-4500 spectrometer. Sample solutions were bubbled with argon before measurement. Absolute photoluminescence quantum yields were measured with a Hamamatsu Photonics C9920-02G. Fluorescence lifetime measurements were performed using a Hamamatsu Photonics Quantaurus-Tau C11367-02. Temperature dependence of fluorescence and UV-vis spectra were measured with a temperature controller (UNISOKU USP-203A). Electrochemical measurements were recorded with an ALS 750D electrochemical analyzer (BAS. Co., Ltd.). The working electrode was a 0.3 mm o.d. glassy carbon electrode; a platinum wire served as auxiliary electrode, and the reference electrode was an Ag^+/Ag electrode (a silver wire immersed in 0.1 M Bu_4NClO_4/0.01 M $AgClO_4$/CH_3CN). Ferrocene was used as an internal standard for calibrating potentials. The solutions were deoxygenated with pure argon prior to the electrochemical measurements.

Evaluation of stability of X_2PyBTM under UV light

A solution (ca. 1×10^{-5} M, 2 mL) in 1-cm-optical-path-length quartz cells was bubbled with argon, sealed, and set at a HITACHI F-4500 spectrometer. Intensity of luminescence at 570 nm was observed exciting at 370 nm light (excitation slit was 5.0

nm, and shutter control was off). Radiation flux of a Xe lamp in the fluorometer was measured using a photon counter (8230E, ADC Corporation). A typical value for this condition was ~70 μW. Logarithm of fluorescence intensity versus time was plotted and a slope of approximate line was estimated to be a rate of photolysis.

Evaluation of pK_a value of X_2PyBTMH$^+$

In an acetonitrile solution, pK_a of X_2PyBTMH$^+$ was evaluated using a method and references developed by Leito et al..[8] Br_2PyBTM solution was titrated with two reference bases, 3-nitroaniline: acid dissociation constant of conjugate acid pK_a = 7.68, 2-chloropyridine: pK_a = 6.79. From UV−Vis absorption spectral simulation of each titration experiment adding trifluoromethanesulfonic acid as a proton source, ΔpK_a (pK_a(PyBTM) − pK_a(reference base)) was calculated using equation ΔpK_a = [PyBTMH$^+$][B] / [BH$^+$][PyBTM]; where B is the reference base. The ΔpK_a values were calculated to be pK_a(3-nitroaniline) − 0.59 ± 0.05, pK_a(2-chloropyridine) + 0.36 ± 0.05 respectively, and pK_a of Br_2PyBTMH$^+$ was decided to be 7.1. F_2PyBTM solution was titrated with two reference bases, 2-chloropyridine: pK_a = 6.79, and 4-nitroaniline: pK_a = 6.22. From spectral simulation of each titration experiment, ΔpK_a (pK_a(PyBTM) − pK_a(reference base)) was calculated to be pK_a(2-chloropyridine) + 0.19 ± 0.05, pK_a(4-nitroaniline) +0.46 ± 0.05 respectively, and pK_a of PyBTMH$^+$ was decided to be 6.8.

Computational details

DFT calculations were executed using the Gaussian09 program package.[9] The geometries of the compounds were optimized without symmetry constraints using the crystal structure coordinate as the starting structure. Calculations were performed using the unrestricted Becke three-parameter hybrid functional with Lee–Yang–Parr correlation functional (B3LYP)[10] or M06 functional[11] with the 6-31G(d) basis set. Cartesian coordinates of all the optimized geometries are listed in the supporting information. Frequency calculations were carried out to ensure that the optimized geometries were minima on the potential energy surface, in which no imaginary frequencies were observed in any of the compounds. TDDFT calculations were performed using UB3LYP to calculate the first 15 doublet transitions.

3-3 Single crystal X-ray diffraction

Red single crystals of Br_2PyBTM and F_2PyBTM were obtained by diffusing water (the lower layer) into an acetone solution of Br_2BTM or F_2PyBTM (the upper layer). The molecular structures of the radicals were revealed by single crystal X-ray diffraction (Figure 3-3, Table 3-3-2, CCDC 1058943 and 1058942). The central methyl carbon atoms are sp^2 hybridized (totals of angles of C4C10C13, C4C13C16, C10C13C16 are both 360°, Table 3-3-1). and shielded sterically by six halogen atoms. The three aryl groups adopt a propeller-like conformation similarly to PyBTM. The C4C10C16 plane was defined as the reference plane, and the dihedral angles between the aryl group planes and the reference plane were measured (Table 3-3-1). Dihedral angle between C4C10C16 and 3,5-dihalopyridyl of F_2PyBTM (33.3°) is smaller than those of PyBTM and Br_2PyBTM (49.3° and 48.1° respectively). This result is not due to packing in crystal structure since similar results were obtained from DFT optimized structures (Table 3-3-2). Because the van der Waals radius of an F atom is smaller than that of either Cl or Br, the pyridyl ring in F_2PyBTM suffers less steric congestion, and can adopt a conformation more closely coplanar to the sp^2 plane of the central carbon.

(a) (b)

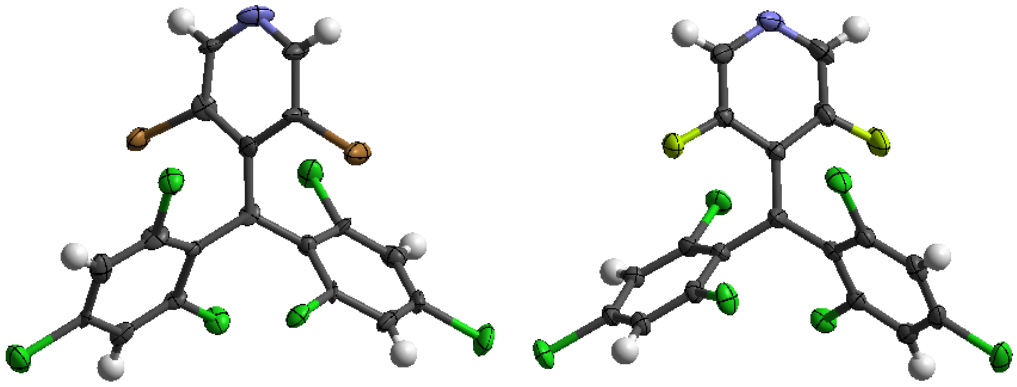

Figure 3-3. Molecular structures of (a) Br_2PyBTM and (b) F_2PyBTM in single crystals.

Table 3-3-1. Selected angles in the crystal of Br_2PyBTM and F_2PyBTM

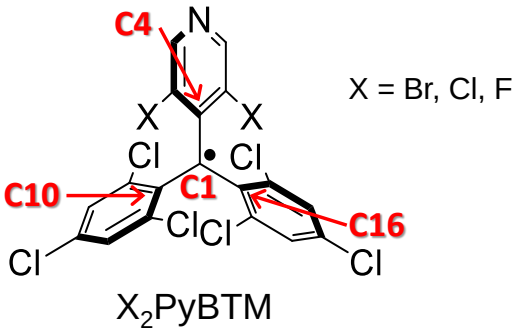

Angles	PyBTM	Br_2PyBTM	F_2PyBTM
C4C1C10	117.5(4)°	118.8(18)°	118.2(2)°
C4C1C16	121.0(4)°	119.6(19)°	122.0(3)°
C10C1C16	121.5(4)°	121.7(18)°	119.6(3)°
Dihedral angle between C4C10C16 plain and			
(3,5-dihalopyridyl)	49.3°	48.1°	33.3°
(2,4,6-trichlorophenyl including C10)	49.5°	42.3°	56.4°
(2,4,6-trichlorophenyl including C16)	42.6°	53.6°	51.7°

Table 3-3-2. Calculated angles of Br_2PyBTM and F_2PyBTM (a) using UB3LYP/6-31G(d)

Angles	PyBTM	Br_2PyBTM	F_2PyBTM
C4C1C10	119.9°	119.5°	120.0°
C4C1C16	119.9°	119.5°	120.0°
C10C1C16	120.2°	121.0°	120.0°
Dihedral angle between C4C10C16 plain and			
(3,5-dihalopyridyl)	47.5°	52.7°	31.3°
(2,4,6-trichlorophenyl including C10)	49.2°	48.5°	52.6°
(2,4,6-trichlorophenyl including C16)	49.2°	48.5°	52.6°

(b) using UM06/6-31G(d)

Angles	PyBTM	Br_2PyBTM	F_2PyBTM
C4C1C10	120.0°	119.2°	120.0°
C4C1C16	120.0°	119.2°	120.0°
C10C1C16	120.1°	121.6°	120.1°
Dihedral angle between C4C10C16 plain and			
(3,5-dihalopyridyl)	47.3°	50.1°	35.1°
(2,4,6-trichlorophenyl including C10)	49.1°	47.1°	50.6°
(2,4,6-trichlorophenyl including C16)	49.1°	47.1°	50.6°

Table 3-3-3. Crystallographic data of Br_2PyBTM and F_2PyBTM

	Br_2PyBTM	F_2PyBTM
Empirical formula	C_{18} H_6 Br_2 Cl_6 N	C_{18} H_6 Cl_6 F_2 N
Fw / g mol^{-1}	608.78	486.97
Crystal system	triclinic	monoclinic
Space group	*P*-1	$P2_1/c$
Crystal size / mm	0.35×0.15×0.10	0.65×0.45×0.25
Temperature / K	113	113
a / Å	7.461(4)	14.5687(14)
b / Å	10.846(6)	8.1370(5)
c / Å	12.660(7)	16.2873(16)
α / º	81.516(11)	90
β / º	88.763(14)	105.775 (4)
γ / º	87.731(14)	90
V / Å^3	1012.4 (9)	1858.1 (3)
Z	2	4
ρ_{calced} / g cm^{-3}	1.997	1.741
λ / Å	0.7107	0.7107
μ / mm^{-1}	4.811	0.946
Reflections collected	6357	12867
Independent reflections	3547	4067
Parameters	245	244
R_{int}	0.0591	0.0225
[a]*R*1	0.1517	0.0434
[b]*wR*2	0.4232	0.1000
[c]GoF	1.173	1.058
CCDC No.	1058943	1058942

[a] $R_1 = \Sigma||F^o|-|F^c||/\Sigma|F^o|$ ($I>2\sigma(I)$). [b] $wR_2 = [\Sigma(w(F^{o2}-F^{c2})^2/\Sigma w(F^{o2})^2]^{1/2}$ ($I>2\sigma(I)$). [c] GoF = $[\Sigma(w(F^{o2}-F^{c2})^2/\Sigma(N^r-N^p)^2]$

3-4 DFT calculations and cyclic voltammetry

DFT calculations were conducted using UB3LYP/6-31G(d). Qualitatively similar results were obtained by DFT calculations using UM06/6-31G(d). The three compounds showed similar electron density distributions in the molecular orbitals (Figure 3-4-1). The energies of the β-SOMO (147β for Br_2PyBTM, 129β for PyBTM, 121β for F_2PyBTM) were calculated to be in the range of −3.59 ± 0.03 eV, thus not affected strongly by the choice of halogen atoms. The energies of the α-SOMO (147α for Br_2PyBTM, 129α for PyBTM, and 121α for F_2PyBTM) were also not different. In contrast, the energies of the filled π-orbitals (NHOMO; 146α, β for Br_2PyBTM, 128α, β for PyBTM, and 120 α, β for F_2PyBTM) distributed on the halogen atoms decreased as the electronegativity of the halogen atom increased. The most electronegative F atoms efficiently withdraw electrons, resulting in the lowest energy of the NHOMO.

Cyclic voltammetry showed that reversible reduction potentials depended little on the halogen atoms on the pyridine ring ($E^{0\prime}_{(red)}$ = −0.75 V vs ferrocenium/ferrocene for X = Br, −0.74 V for X = Cl, −0.75 V for X = F) (Figure 3-4-2). Differences in the irreversible oxidation peaks were also small ($E_{p(ox)}$ = +1.02 V for X = Br, +1.04 V for X = Cl, +1.05 V for X = F). The results are consistent to the DFT calculation results that the halogen atoms negligibly affect the β-SOMO and α-SOMO energies of the radicals.

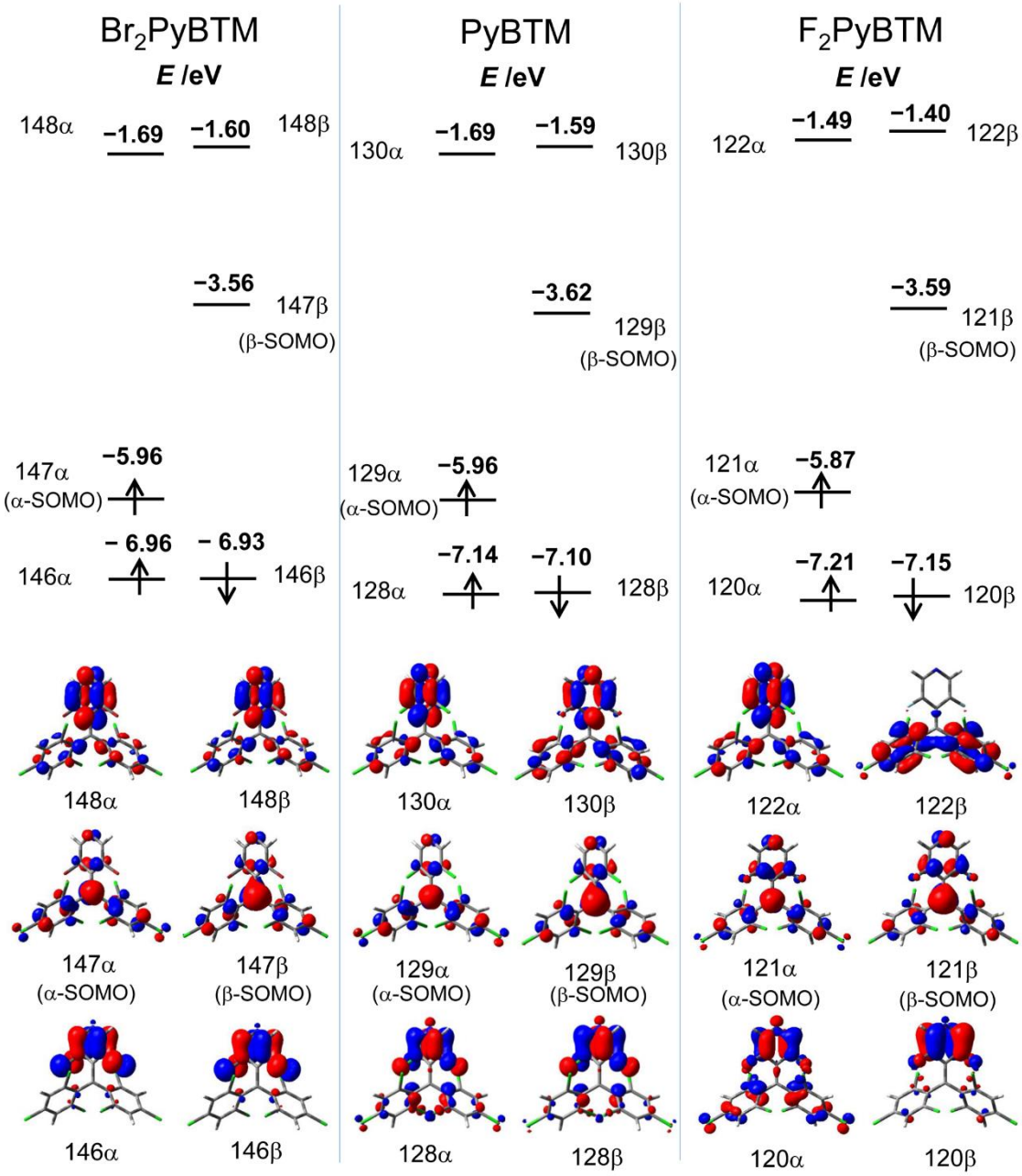

Figure 3-4-1. Molecular orbitals of X_2PyBTM calculated using DFT (UB3LYP/6-31G(d)).

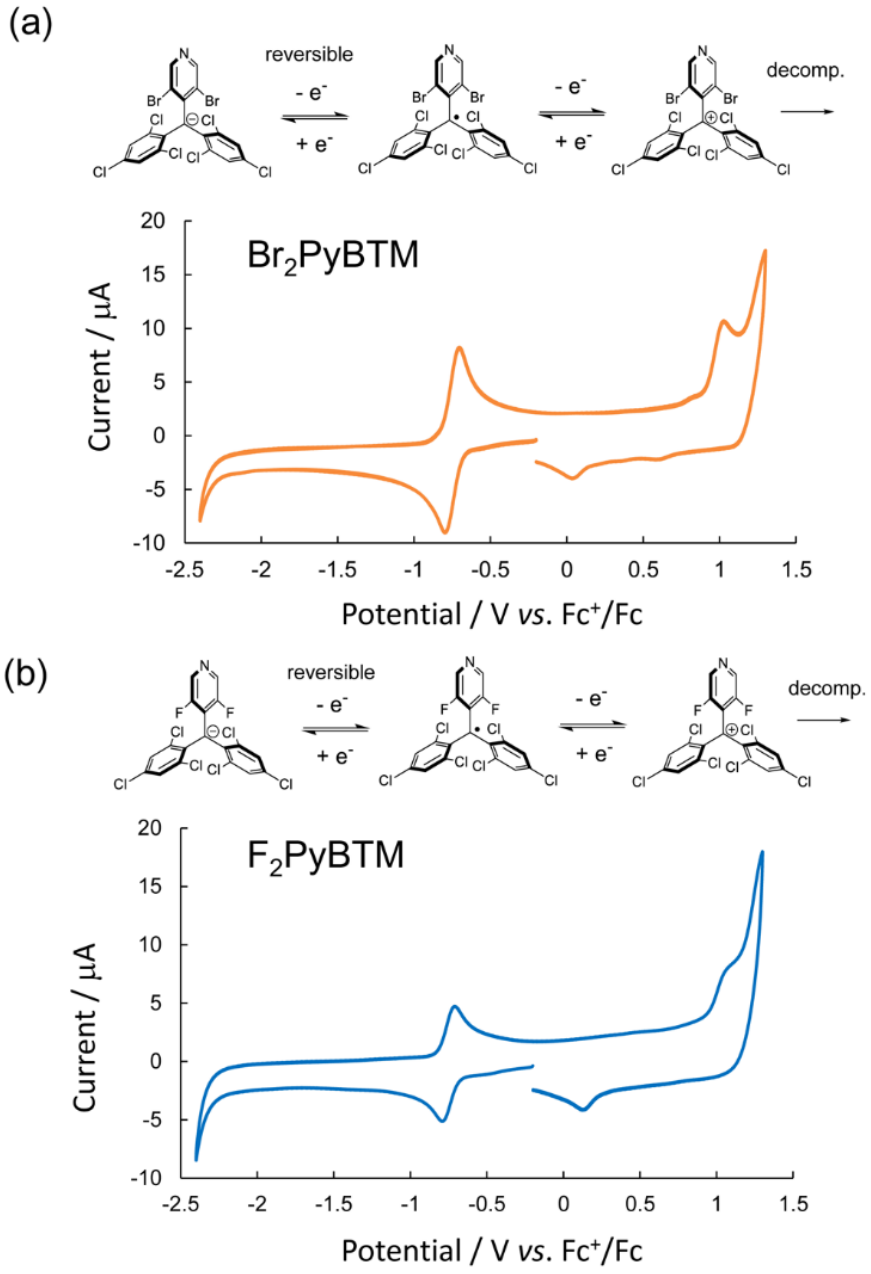

Figure 3-4-2. Cyclic voltammograms of (a) Br_2PyBTM (0.5 mM) and (b) F_2PyBTM (0.5 mM) in 0.1 M Bu_4NClO_4–CH_2Cl_2 at a scan rate of 0.1 V s^{-1}.

3-5 Absorption and emission

UV−vis spectroscopy showed clearly shifted absorption bands after replacement of halogen atoms. Br_2PyBTM, PyBTM, and F_2PyBTM displayed strong near-UV absorption bands at λ_{abs} = 376, 370, and 351 nm, and weak visible absorption bands at λ_{abs} = 548, 541, and 523 nm, respectively (Figure 3-5-1). Fluorescence wavelength shifted in accordance with the shifts of absorption: Br_2PyBTM, PyBTM, and F_2PyBTM displayed fluorescence at λ_{em} = 593, 585, and 566 nm, respectively. These shifts manifest as different visible fluorescence colors (Figures 3-5-1). Fluorescence spectra in EPA (diethyl ether:isopentane:ethanol 5:5:2 v/v) matrices at 77 K displayed identical shifts in the maximum peak wavelengths (Figure 3-5-2).

TDDFT calculations were conducted using UB3LYP/6-31G(d) (qualitatively similar results were obtained by TDDFT calculations using UM06/6-31G(d)). TDDFT calculations showed that the lowest energy visible absorption band mainly resulted from the electronic transitions β-NHOMO→β-SOMO; 146β→147β with a transition energy of 2.51 eV for X = Br, 128β→129β (2.55 eV) for X = Cl, 120β→121β (2.61 eV) for X = F. The order of the calculated transition energies (Br_2PyBTM < PyBTM < F_2PyBTM) results mainly from the order of the energies of the β-NHOMO calculated using DFT (Chapter 3-4). These results rationalize the red-shift of the absorption maxima and emission maxima shown in Figure 3-5-1. The calculations and the spectroscopic results reveal that the halogen atoms affect the energy of the β-NHOMO, thus modulating the lowest excited state.

F_2PyBTM showed an absolute photoluminescence quantum yield (ϕ, Table 3-5) of 6% in chloroform, which is superior to those of PyBTM (ϕ = 3%) and Br_2PyBTM (ϕ = 2%). F_2PyBTM also showed better fluorescence in dichloromethane (ϕ = 4%) than either PyBTM (ϕ = 2%) or Br_2PyBTM (ϕ = 2%). The enhanced fluorescence quantum yields of F_2PyBTM were almost proportional to the decrease of non-radiative decay rate (k_{nr}) estimated from the fluorescence lifetime (τ) measurements and the equations $\phi = k_f/(k_f + k_{nr})$ and $\tau = 1/(k_f + k_{nr})$; where k_f indicates the radiative rate. The reduced k_{nr} in F_2PyBTM is explained by the energy gap law or the enhanced rigidity of the molecular skeleton. The pyridyl ring in F_2PyBTM suffers less steric congestion, and can adopt a conformation more closely coplanar to the sp^2 plane of the central carbon (C4C10C16 plane; Chapter 3-3). This affords stronger π-conjugation between the two moieties. The enhanced π-conjugation suppresses the thermal fluctuation and vibration of molecules that would cause non-radiative decay.

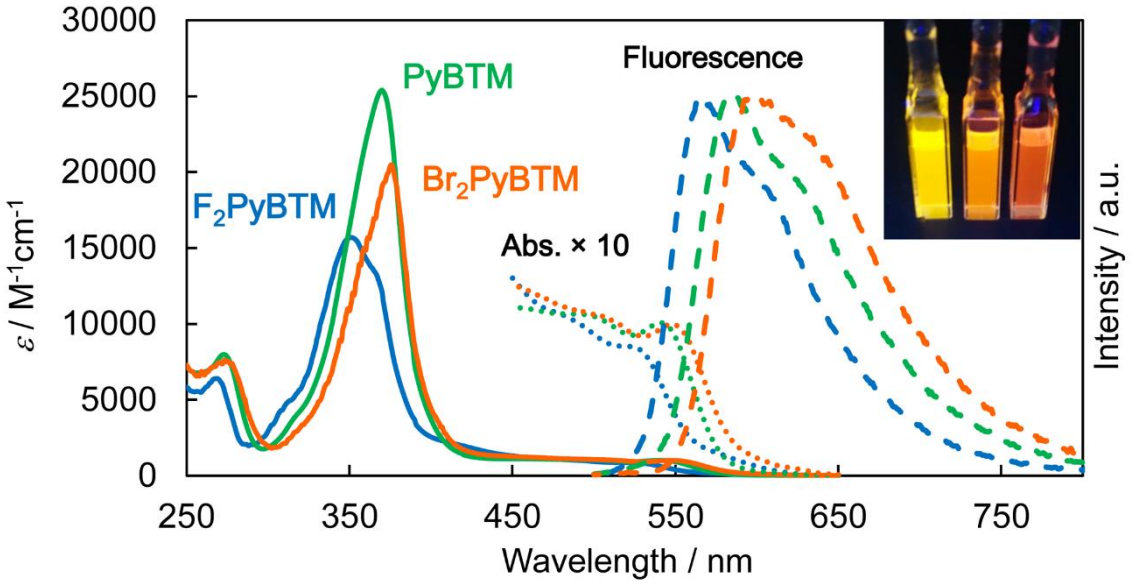

Figure 3-5-1. Absorption (solid lines) and corrected emission spectra (dashed lines) of Br_2PyBTM (orange), PyBTM (green), and F_2PyBTM (blue) in dichloromethane. Enlarged portions of the absorption spectra (10 fold) are shown from λ = 450 to 650 nm (dotted lines). A photograph of fluorescence under UV light at λ = 365 nm (left: F_2PyBTM, center: PyBTM, right: Br_2PyBTM) is in the upper right corner.

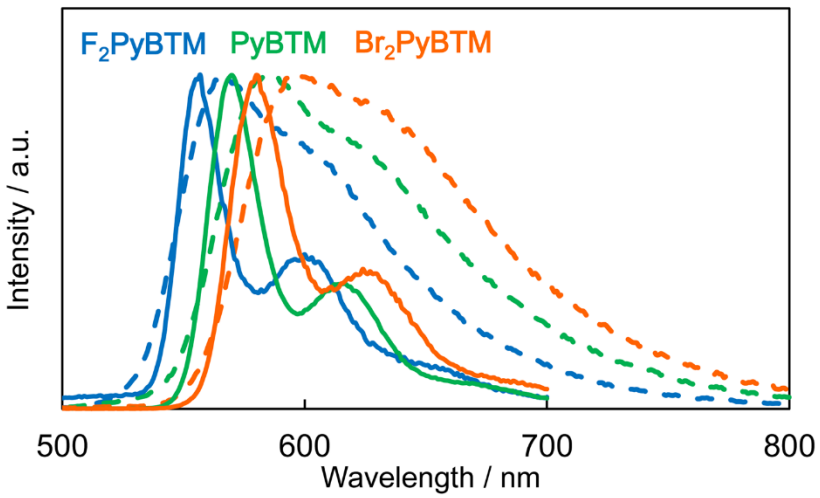

Figure 3-5-2. Corrected emission spectra of Br_2PyBTM (orange), PyBTM (green), and F_2PyBTM (blue) at 77 K in EPA (diethyl ether:isopentane:ethanol 5:5:2 v/v) matrix (solid lines) and at room temperature in CH_2Cl_2 (dashed lines).

Table 3-5. Photophysical properties of X_2PyBTM

X	Solvent	ϕ	τ / ns	k_f / 10^7 s^{-1}	k_{nr} / 10^7 s^{-1}
Br	Chloroform	2%	6.1	0.3	16
Cl	Chloroform	3%	7.6	0.4	13
F	Chloroform	6%	18.1	0.3	5.2
Br	Dichloromethane	2%	5.3	0.4	19
Cl	Dichloromethane	2%	6.4	0.3	15
F	Dichloromethane	4%	12.5	0.3	7.7

3-6 Photostability

Photostability, an important property of luminescent radicals, was investigated by measuring the decay of fluorescence intensity upon continuous photoirradiation (370 nm excitation wavelength) in dichloromethane. The three radicals displayed excellent photostability, and estimated half-life ($t_{1/2}$) was compared to each other (Figure 3-6-1). PyBTM showed 70 times higher photostability than TTM in dichloromethane. F_2PyBTM showed similar photostability ($t_{1/2}$ = (1.3 ± 0.1) × 10^4 s) to PyBTM ($t_{1/2}$ = (1.5 ± 0.2) × 10^4 s), whereas Br_2PyBTM showed superior photostability ($t_{1/2}$ = (3.1 ± 0.6) × 10^4 s; all data are shown in Figure 3-6-2 and Table 3-6). After the continuous excitation for 50 minutes, more than 94% of Br_2PyBTM survived at 298 K (96% at 273 K).

The improved photostability of Br_2PyBTM can be explained from the lower energies for forming the excited states; higher energies of the filled orbitals decrease the energies for forming the excited states, and increase the activation energy for decomposition reaction (Figure 3-6-3). Especially higher β-NHOMO lowers the energy for forming the lowest excited state, which plays the most important role in reactivity in the assumption that the relaxation to the lowest excited state is faster than the decomposition. The photostability might be also related to the enhanced steric hindrance of the Br atoms, which are larger than Cl atoms, and thus more efficiently protect the radical center, and increase the activation energy for decomposition.

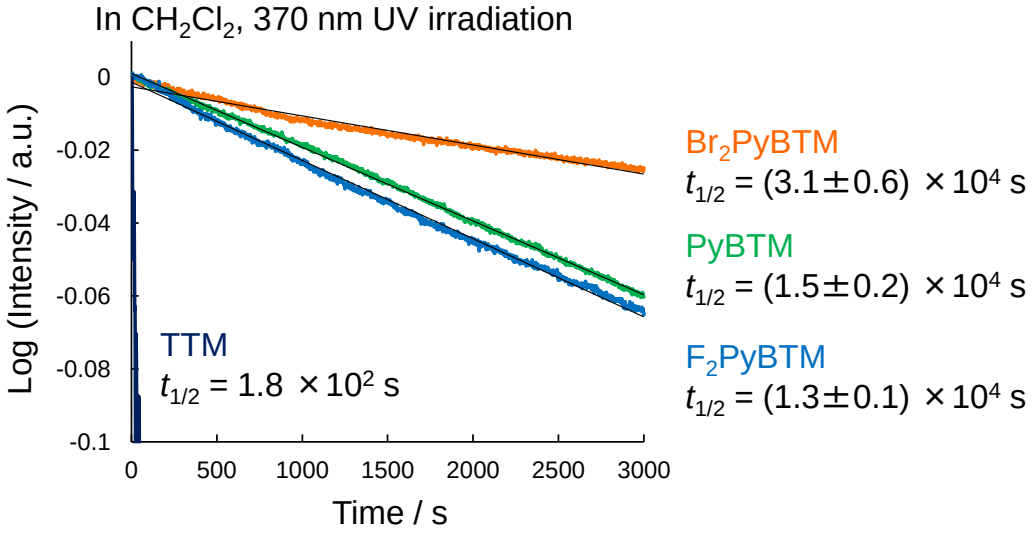

Figure 3-6-1. Plots showing examples of the emission decay of X_2PyBTM and TTM in dichloromethane under continuous excitation with light at λ_{ex} = 370 nm. The half-lives ($t_{1/2(Br2PyBTM)}$ = (3.1 ± 0.6) × 10^4 s, $t_{1/2(PyBTM)}$ = (1.5 ± 0.2) × 10^4 s, $t_{1/2(F2PyBTM)}$ = (1.3 ± 0.1) × 10^4 s) were estimated from repeated experiments (Figure 3-6-2, Table 3-6).

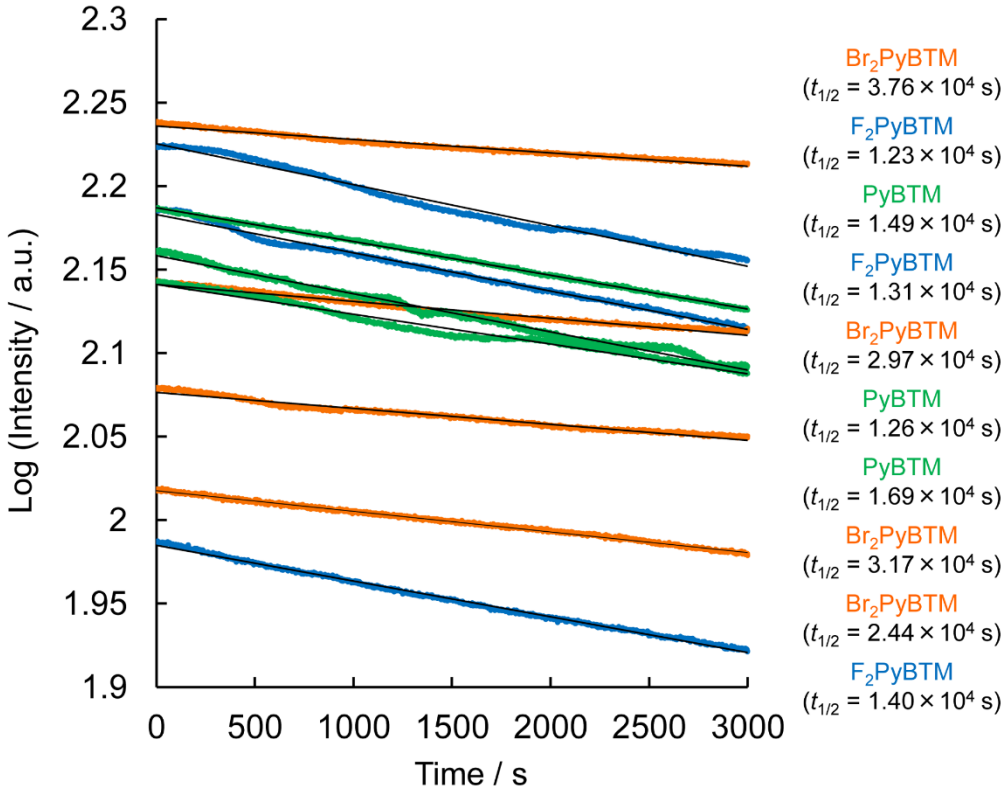

Figure 3-6-2. Plots showing the emission decay of X_2PyBTM in dichloromethane under continuous excitation with light at λ_{ex} = 370 nm. The half-lives ($t_{1/2}$) are given by linear approximation (Table 3-6).

Table 3-6. Stability of X_2PyBTM in dichloromethane under 370 nm UV light irradiation

Exp. no.	$t_{1/2}$(Br_2PyBTM) / 10^4 s	$t_{1/2}$(PyBTM) / 10^4 s	$t_{1/2}$(F_2PyBTM) / 10^4 s
1	2.97	1.26 [a]	1.40
2	3.17	1.49	1.31
3	2.44	1.69	1.23
4	3.76		
Average	3.1	1.5	1.3
Standard Deviation	0.6	0.2	0.1

[a] cited from Chapter 2.

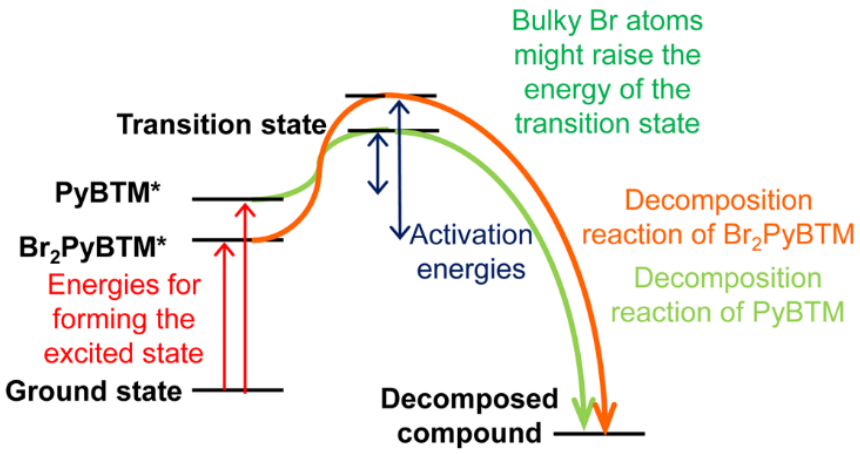

Figure 3-6-3. Energy diagram of the decomposition reaction of PyBTM and Br_2PyBTM. Slower decomposition reaction of Br_2PyBTM under photoirradiation is probably because of higher activation energy due to the lower energy for forming the excited state and the rise of energy of the transition state owing to the larger steric hindrance of Br atoms.

3-7 Protonation

The effect of the halogen atoms in the radicals on protonation was examined (i.e., the pK_a of the conjugate acid). Titration in acetonitrile showed pK_a values of 6.8, 6.9, and 7.1 for F_2PyBTMH$^+$, PyBTMH$^+$ and Br_2PyBTMH$^+$, respectively.[8] As the electron-withdrawing nature of the halogen atom increases, the acidity of these acids increases. The UV−vis absorption bands of Br_2PyBTM and F_2PyBTM bathochromically shifted upon protonation, as observed previously for PyBTM (Figure 3-7-1). The fluorescence was quenched by protonation in all X_2PyBTM (Figure 3-7-2). The reduction potentials of X_2PyBTM were also modulated by protonation and deprotonation (Figure 3-7-3).

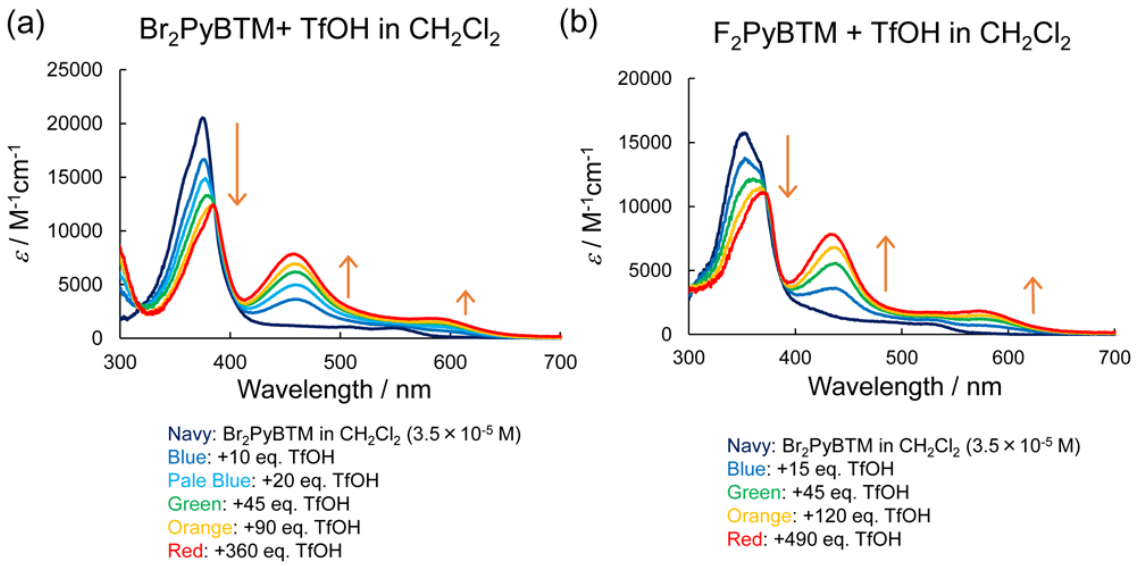

Figure 3-7-1. Protonation of (a) Br_2PyBTM and (b) F_2PyBTM by titration with trifluoromethanesulfonic acid (TfOH) in dichloromethane.

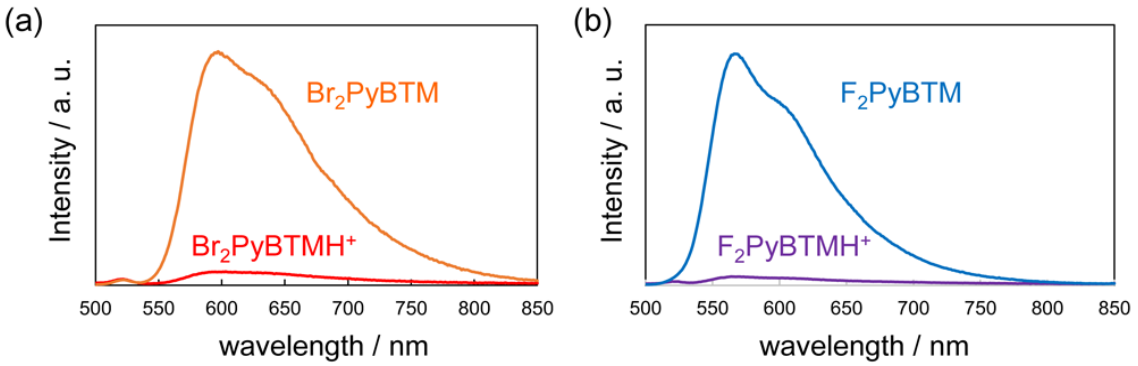

Figure 3-7-2. Corrected fluorescence spectra of (a) Br_2PyBTM and Br_2PyBTMH$^+$, and (b) F_2PyBTM and F_2PyBTMH$^+$. Fluorescence of protonated forms is almost quenched.

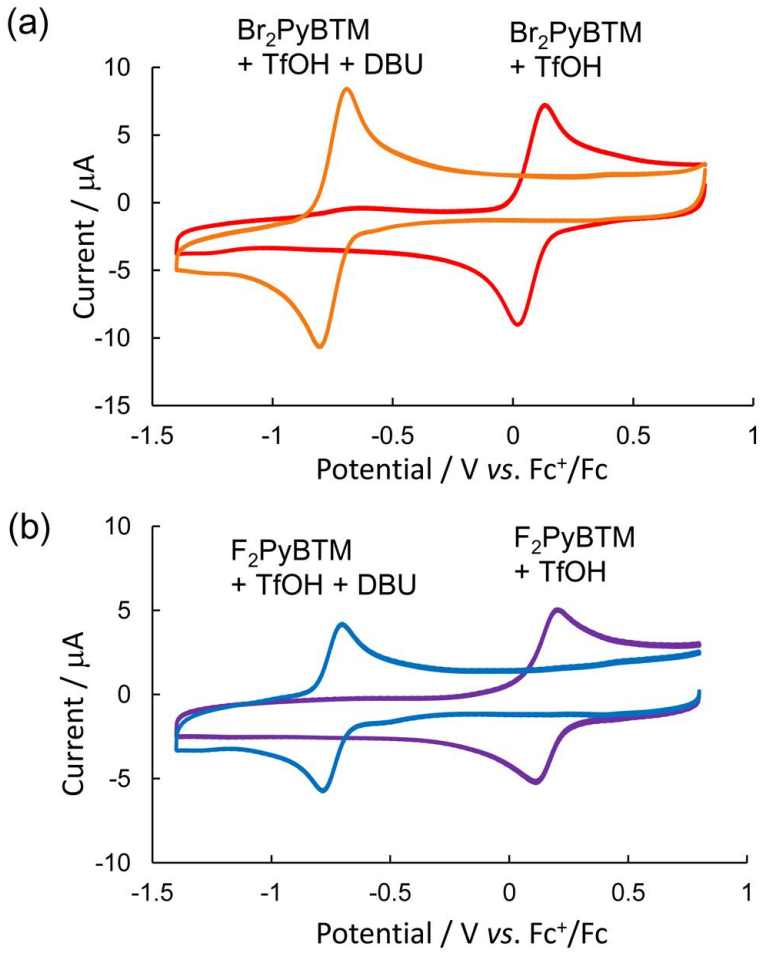

Figure 3-7-3. (a) Proton-response of CVs of Br_2PyBTM solution (0.5 mM, 5 mL) in 0.1 M Bu_4NClO_4–CH_2Cl_2 at a scan rate of 0.1 V s^{-1}. Trifluoromethanesulfonic acid (TfOH, ca. 1 eq.) was added and CV was measured (red line). Diazabicyclo[5.4.0]undec-7-ene (DBU, ca. 1.1 eq.) was added to neutralize the solution and CV was measured (orange line) to observe reversibility of protonation. (b) Proton-response of CVs of F_2PyBTM solution (0.5 mM, 5 mL) in 0.1 M Bu_4NClO_4–CH_2Cl_2 at a scan rate of 0.1 V s^{-1}. TfOH (ca. 1 eq.) was added and CV was measured (blue line). DBU (1.1 eq.) was added to neutralize the solution and CV was measured (purple line) to observe reversibility of protonation.

3-8 Conclusion

New photostable luminescent radicals, Br_2PyBTM and F_2PyBTM, were prepared and compared with PyBTM. The choice of halogen atoms did not affect the energy levels of the SOMO strongly; however, it affected the energy levels of the NHOMO according to the electronegativity of the halogen. The absorption and emission of X_2PyBTM shifted bathochromically in the order of X = F < Cl < Br. The halogen atoms also modulated the structures and stabilities in the ground and excited states.

F_2PyBTM displayed the strongest fluorescence because of the slowest non-radiative decay. The suppression of non-radiative decay can be induced by the energy-gap law (lower β-NHOMO) or enhanced π-conjugation owing to smaller steric effect. Br_2PyBTM showed the highest stability under excitation by 370 nm light. The stabilization can be explained by the least energy of the lowest excited state (higher β-NHOMO) or enhanced steric hindrance of the larger Br atoms, which more efficiently protect the radical center.

This study reveals that atoms at the *ortho*-positions to the radical center affect the properties and stability of the luminescent radicals via both electronic and steric effects. Modulation of β-NHOMO and steric effect around radical center determined the balance of the quantum yield and the photostability. These findings can be used to develop novel luminescent organic radicals with improved luminescent properties and photostability.

3-9 References

[1] a) O. Armet, J. Veciana, C. Rovira, J. Riera, J. Casteñer, E. Molins, J. Rius, C. Miravitlles, S. Olivella, J. Brichfeus, *J. Phys. Chem.* **1987**, *91*, 5608 – 5616; b) J. Veciana, I. Ratera in *Stable Radicals: Fundamentals and Applied Aspects of Odd-Electron Compounds* (Ed.: R. G. Hicks), John Wiley & Sons, Ltd, New York, **2010**.

[2] Y. Hattori, T. Kusamoto, H. Nishihara, *RSC Adv.* **2015**, *5*, 64802 – 64805.

[3] Y. Hattori, T. Kusamoto, H. Nishihara, *Angew. Chem. Int. Ed.* **2014**, *53*, 11845 – 11848; *Angew. Chem.* **2014**, *126*, 12039 – 12042.

[4] D. A. Klumpp, Y. Zhang, P. J. Kindelin, S. Lau, *Tetrahedron* **2006**, *62*, 5915 – 5921.

[5] L. Juliá, M. Ballester, J. Riera, J. Casteñer, J. L. Ortin, C. Onrubia, *J. Org. Chem.* **1988**, *53*, 1267 – 1273.

[6] A. Altomare, G. Cascarano, C. Giacovazzo, A. Guagliardi, M. C. Burla, G. Polidori, M. Camalli, *J. Appl. Cryst.* **1994**, *27*, 435.

[7] G. M. Sheldrick, *Acta Cryst. A* **2008**, *64*, 112 – 122.

[8] I. Kaljurand, A. Kütt, L. Sooväli, T. Rodima, V. Mäemets, I. Leito, I. A. Koppel, *J. Org. Chem.* **2005**, *70*, 1019 – 1028.

[9] M. J. Frisch, G. W. Trucks, H. B. Schlegel, G. E. Scuseria, M. A. Robb, J. R. Cheeseman, G. Scalmani, V. Barone, B. Mennucci, G. A. Petersson, H. Nakatsuji, M. Caricato, X. Li, H. P. Hratchian, A. F. Izmaylov, J. Bloino, G. Zheng, J. L. Sonnenberg, M. Hada, M. Ehara, K. Toyota, R. Fukuda, J. Hasegawa, M. Ishida, T. Nakajima, Y. Honda, O. Kitao, H. Nakai, T. Vreven, J. A. Montgomery, Jr., J. E. Peralta, F. Ogliaro, M. Bearpark, J. J. Heyd, E. Brothers, K. N. Kudin, V. N. Staroverov, R. Kobayashi, J. Normand, K. Raghavachari, A. Rendell, J. C. Burant, S. S. Iyengar, J. Tomasi, M. Cossi, N. Rega, J. M. Millam, M. Klene, J. E. Knox, J. B. Cross, V. Bakken, C. Adamo, J. Jaramillo, R. Gomperts, R. E. Stratmann, O. Yazyev, A. J. Austin, R. Cammi, C. Pomelli, J. W. Ochterski, R. L. Martin, K. Morokuma, V. G. Zakrzewski, G. A. Voth, P. Salvador, J. J. Dannenberg, S. Dapprich, A. D. Daniels, Ö. Farkas, J. B. Foresman, J. V. Ortiz, J. Cioslowski, and D. J. Fox, Gaussian, Inc., Wallingford CT, U. S. A. 2009.

[10] A. D. Becke, *J. Chem. Phys.* **1993**, *98*, 5648 – 5652.

[11] Y. Zhao, D. G. Truhlar, *Theor. Chem. Acc.* **2008**, *120*, 215 – 241.

Part of sentences and figures in this chapter is reproduced or adapted from Ref. 2 with permission from The Royal Society of Chemistry.

Chapter 4

Enhancement of Luminescent Properties of PyBTM by Coordination to Gold

4-1 Introduction

My next aim is to enhance the luminescent properties of the stable luminescent radical, PyBTM,[1] through its coordination to metal. Although the fluorescence properties of PTM and TTM radicals have been enhanced by chemical modification with organic moieties,[2] to our knowledge there are no examples of using coordination chemistry to prepare luminescent open-shell species with superior fluorescence efficiency. This aim is challenging because the luminescence of a radical ligand is usually quenched by coordination to a metal; for example, a carboxylate ligand with luminescent radicals loses its luminescent properties upon coordination to metal ions.[3]

It is also challenging to make a luminescent metal complex with radical character (spin-doublet state) by combining a luminescent closed-shell molecule and a non-luminescent stable radical. The introduction of open-shell radical species into luminescent closed-shell molecules generally quenches their fluorescence. In paramagnetic Cu(II)-porphyrin[4] and Zn-porphyrin with a coordinated nitronyl nitroxide radical,[5] photoexcitation produced the lowest singlet excited state-like electron configuration for porphyrin moiety ($^2S_1$ state); however $^4T_1$ and $^2T_1$ states derived from the lowest triplet excited state of the porphyrin are lower in energy (Figure 4-1-1). Considering spin-multiplicity and the order of energy levels, $^4T_1$ and $^2T_1$ states are the lowest excited quartet (Q_1) and the lowest excited doublet (D_1) state respectively, and $^2S_1$ state is D_2 state. Thus fluorescence from $^2S_1$ (D_2) is quenched via $^2T_1$ (D_1) by spin-allowed process. Spin-labeled luminogens are applied as fluorescent probes; the luminescent off state of the probes is switched to the on state by the loss of its radical character upon the reaction with other radical species such as •OH.[6] In order to display fluorescence from the lowest excited doublet state (D_1) to the ground doublet state (D_0) in luminescent radical complex, using a stable luminescent radical as a ligand seems the best way.

Here I report the synthesis of a Au^I complex with PyBTM as a ligand, $[Au^I(PyBTM)PPh_3]X$ (X = ClO_4, BF_4, Figure 4-1-2),[7] and its photophysical and photochemical properties. I chose Au^I as a metal center because it can form a strong coordination bond with pyridine derivatives (heavy transition metals generally form strong ligand field) and gold complexes often show superior luminescence properties.[8] I have found that $[Au^I(PyBTM)PPh_3]X$ displays fluorescence in solution, and its fluorescence wavelength is longer and its photoluminescence quantum yield is larger than those of free PyBTM. Moreover, the stability of $[Au^I(PyBTM)PPh_3]BF_4$ upon photoirradiation is higher than that of PyBTM. The origin of these effects on the coordination is discussed from the view point of the structure and the molecular orbitals (β-SOMO etc.).

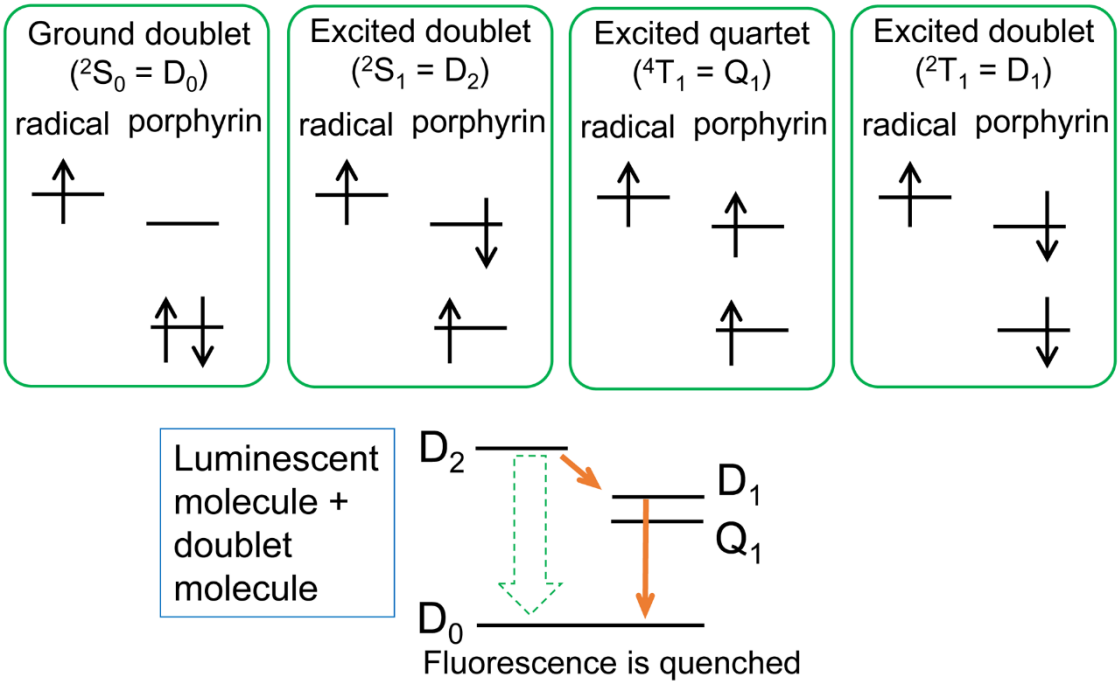

Figure 4-1-1. Scheme of quench of fluorescence by introduction of open-shell radical species into fluorescent closed-shell molecules.

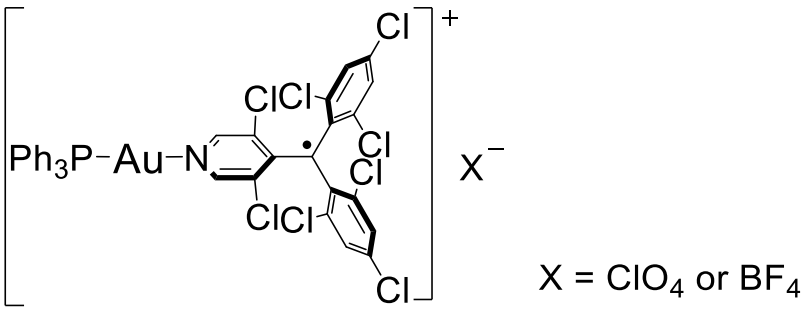

Figure 4-1-2. Structure of [Au^{I}(PyBTM)PPh_3]X.

4-2 Experimental section

Synthesis of $[Au^{I}(PyBTM)PPh_3]ClO_4$

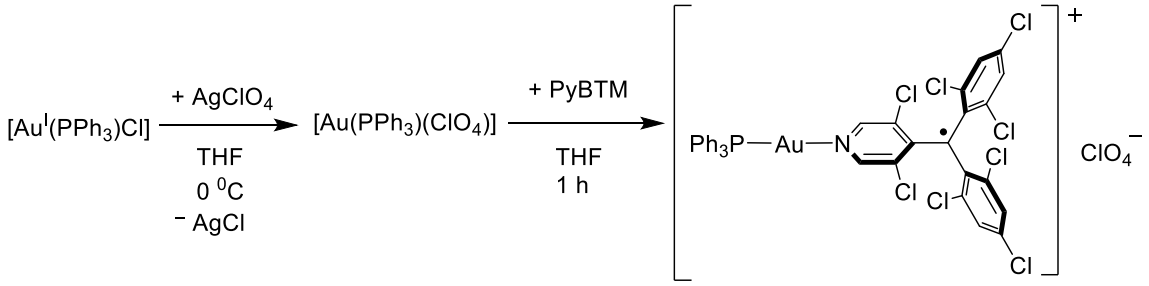

$[Au^{I}(PyBTM)PPh_3]ClO_4$ was prepared according to the literature procedure.[9] Under an argon atmosphere, chloro(triphenylphosphine)gold(I) (49.3 mg, 0.0997 mmol) was dissolved in dry THF (2 mL) and a dry THF (1 mL) solution of silver perchlorate (**Caution**: perchlorate salts are potentially explosive, 24.3 mg, 0.117 mmol) was added at 0°C, stirred for 10 min, and filtered. The filtrate was added to a solution of PyBTM (52.3 mg, 0.101 mmol) in THF (2 mL), and stirred at room temperature for 1 h. Diethyl ether was added to the reaction mixture and stored at 0°C in a refrigerator. The resulting dark red solid was collected to afford crude $[Au^{I}(PyBTM)PPh_3]ClO_4$ (70 mg, 0.065 mmol, 65% yield). Pure $[Au^{I}(PyBTM)PPh_3]ClO_4$ was obtained by recrystallization from dichloromethane-diethyl ether (18.5 mg, 0.017 mmol, 17% yield). **Elemental Analysis** Calcd for $C_{36}H_{21}NAuCl_9O_4P$: C 40.09, H 1.96, N 1.30. Found, C 40.15, H 2.21, N 1.01. **ESI-TOF-MS** m/z: $[Au^{I}(PyBTM)PPh_3]^+$ Calcd for $C_{36}H_{21}NAuCl_8P$ 974.86; Found 974.57.

Synthesis of $[Au^{I}(PyBTM)PPh_3]BF_4$

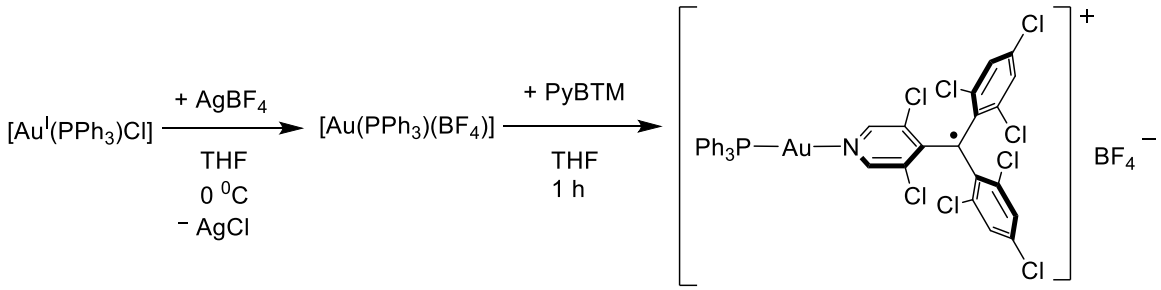

$[Au^{I}(PyBTM)PPh_3]BF_4$ was prepared according to the modified literature procedure.[9] Under an argon atmosphere, chloro(triphenylphosphine)gold(I) (99.3 mg, 0.200 mmol) was dissolved in dry THF (2 mL) and a dry silver tetrafluoroborate (54 mg, 0.277 mmol) was added at 0°C, stirred for 10 min, and filtered. The filtrate was added to a solution of PyBTM (104 mg, 0.200 mmol) in THF (2 mL), and stirred at room temperature for 30 min. Reprecipitation from THF-diethyl ether afforded crude

$[Au^{I}(PyBTM)PPh_3]BF_4$ (69.6 mg, 0.065 mmol, 32% yield). Pure $[Au^{I}(PyBTM)PPh_3]BF_4$ was obtained by recrystallization from dichloromethane-hexane (11.6 mg, 0.0109 mmol, 6% yield). **Elemental Analysis** Calcd for $C_{36}H_{21}NAuBCl_8F_4P$: C 40.57, H 1.99, N 1.31. Found, C 40.75, H 2.36, N 1.09. **ESI-TOF-MS** m/z: $[Au^{I}(PyBTM)PPh_3]^+$ Calcd for $C_{36}H_{21}NAuCl_8P$ 974.86; Found 974.30.

X-ray structural analysis

Diffraction data for X-ray analysis were collected with an AFC10 diffractometer coupled with a Rigaku Saturn CCD system equipped with a rotating-anode X-ray generator producing graphite-monochromated MoKα radiation (λ = 0.7107 Å). Lorentz polarization and numerical absorption corrections were performed with the program *Crystal Clear 1.3.6.* Structures were solved by the direct method using SHELXL-97[10] and refined against F^2 using SHELXL-97. *Crystal Structure 4.0* software was used to prepare the material for publication. The crystallographic data are listed in Table 4-3. Crystal structure data (CIF, CCDC 1034361) can be obtained free of charge via the Internet at http://pubs.acs.org and from The Cambridge Crystallographic Data Centre via www.ccdc.cam.ac.uk/data_request/cif.

Instruments

ESR spectra were recorded with a JEOL JES-RE2X spectrometer with X-band microwave. Deoxygenated sample solutions were charged in a 5mmϕ sample tube. Magnetic field was calibrated with the Mn^{2+}/MgO standard. Isotropic simulation was performed with the program *Isotropic*. UV-vis absorption spectra were recorded with a JASCO V-570 spectrometer. Steady-state emission spectra were measured with a HITACHI F-4500 spectrometer. Sample solutions were bubbled with argon before the measurements. Absolute photoluminescence quantum yields were measured with a Hamamatsu Photonics C9920-02G. Fluorescence lifetime measurements were performed using a Hamamatsu Photonics Quantaurus-Tau C11367-02. Electrochemical measurements were recorded with an ALS 650DT electrochemical analyzer (BAS. Co., Ltd.). The working electrode was a 0.3 mm o.d. glassy carbon electrode; a platinum wire served as auxiliary electrode, and the reference electrode was an Ag^+/Ag electrode (a silver wire immersed in 0.1 M Bu_4NClO_4/0.01 M $AgClO_4$/CH_3CN). Ferrocene was used as an internal standard for calibrating potentials. The solutions were deoxygenated with pure argon prior to the electrochemical measurements.

Evaluation of stability of PyBTM and [Au^{I}(PyBTM)PPh_3]BF_4 under UV light

A dichloromethane solution (ca. 2 mL) in 1-cm-optical-path-length quartz cells was bubbled with argon, sealed, and set at a HITACHI F-4500 spectrometer. Intensity of luminescence was observed exciting at 370 nm light (excitation slit was 5.0 nm, and shutter control was off). Radiation flux of a Xe lamp in the fluorometer was measured using a photon counter (8230E, ADC Corporation). A typical value for this condition was ~70 μW. Record from 600 to 3600 s was used for analysis to eliminate the influence of convection current. Logarithm of fluorescence intensity versus time was plotted and a slope of approximate line was estimated to be a rate of photolysis. Although stability of PyBTM has been previously reported, the more proper value with standard deviation was estimated from additional experiments.

Computational details

DFT calculations were executed using the Gaussian09 program package.[11] The geometries of the compounds were optimized without symmetry constraints using the crystal structure coordinate as the starting structure. Calculations were performed using M06 functional[12] with the SDD basis set (Au) and the 6-31G(d) basis set (H, C, N, P, Cl). Cartesian coordinates of all the optimized geometries are listed in the supporting information. Frequency calculations were carried out to ensure that the optimized geometries were minima on the potential energy surface, in which no imaginary frequencies were observed in any of the compounds. TDDFT calculations were performed using M06 to calculate the first 15 doublet transitions.

4-3 Single crystal X-ray diffraction

Single crystal X-ray diffraction studies revealed the molecular structure of $[Au^{I}(PyBTM)PPh_3]^{+}$ in the crystalline state (Figure 4-3, Table 4-3, CCDC 1034361). Red single crystals of $[Au^{I}(PyBTM)PPh_3]ClO_4$ were obtained by diffusing diethyl ether into a dichloromethane solution. The unit cell contains two sets of crystallographically independent cations and anions in the crystal. The two cations of $[Au^{I}(PyBTM)PPh_3]$ have similar structures: the N−Au−P angles are both 176° and the perchlorate ions do not coordinate to the Au^{I} center, indicating a two-coordinate linear structure. No intermolecular Au−Au contacts (aurophilic bonds) are observed, probably because of the bulkiness of the triphenylphosphine and PyBTM moieties. The central carbon atom of the PyBTM ligand adopts sp^2 hybridized geometry, suggesting that the radical character of PyBTM is maintained.

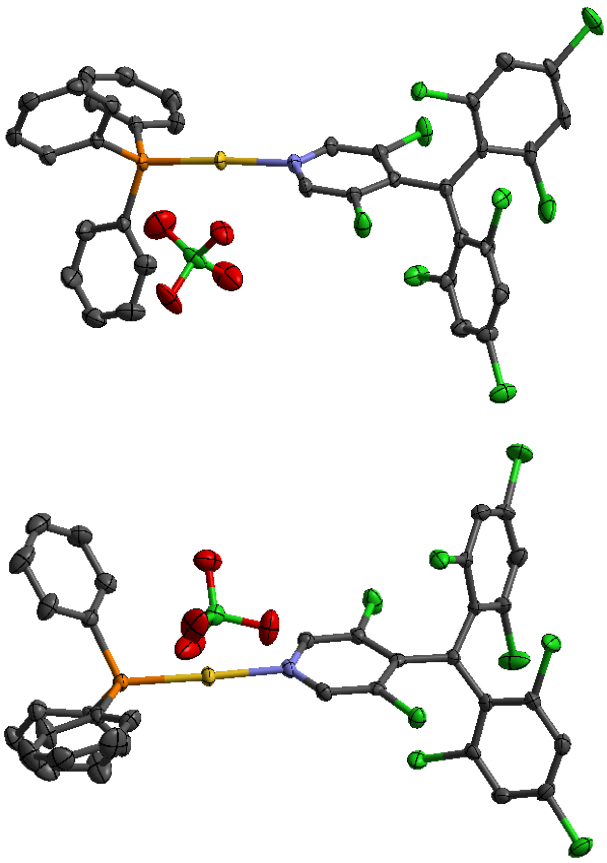

Figure 4-3. Crystal structure of $[Au^{I}(PyBTM)PPh_3]ClO_4$ with thermal ellipsoids at 50% probability level. Two sets of crystallographically independent one cation and one anion are shown. Hydrogen atoms are omitted for clarity.

Table 4-3. Crystallographic data of $[Au^{I}(PyBTM)PPh_3]ClO_4$

	$[Au^{I}(PyBTM)PPh_3]\cdot ClO_4$
Empirical formula	$C_{36}\ H_{21}\ Au\ Cl_9\ N\ O_4\ P$
Fw / g mol^{-1}	1078.58
Crystal system	triclinic
Space group	*P*-1
Crystal size / mm	0.4×0.25×0.15
Temperature / K	113(2)
a / Å	8.9825(11)
b / Å	20.587(3)
c / Å	20.868(3)
α / º	86.568(3)
β / º	79.881(4)
γ / º	84.734(4)
V / Å^3	3779.1(9)
Z	4
ρ_{calced} / g cm^{-3}	1.896
λ / Å	0.7107
μ / mm^{-1}	4.626
Reflections collected	23124
Independent reflections	12577
Parameters	937
R_{int}	0.0434
[a]*R*1	0.0387
[b]*wR*2	0.1060
[c]GoF	1.060
CCDC No.	1034361

[a] $R_1 = \Sigma||F^o|-|F^c||/\Sigma|F^o|$ ($I>2\sigma(I)$). [b] $wR_2 = [\Sigma(w(F^{o2}-F^{c2})^2/\Sigma w(F^{o2})^2]^{1/2}$ ($I>2\sigma(I)$). [c] GOF = $[\Sigma(w(F^{o2}-F^{c2})^2/\Sigma(N^r-N^p)^2]$.

4-4 ESR spectroscopy

An ESR spectrum in dichloromethane was recorded at 180 K to examine the spin density distribution (Figure 4-4-1). The *g* value (2.004) was similar to that of PyBTM. The spectrum showed hyperfine coupling with ^{1}H, ^{14}N, ^{13}C, and ^{31}P atoms, and was fitted by computer simulation. The obtained hyperfine coupling constants (hccs) were qualitatively similar to those calculated using DFT (Table 4-4). The results confirmed that the spin density in $[Au^{I}(PyBTM)PPh_3]^{+}$ is distributed mainly on the PyBTM ligand (Figure 4-4-2). The distribution was different from that in PyBTM, as indicated by the larger hcc of the nitrogen atom and the non-negligible spin density on the phosphorous atoms in $[Au^{I}(PyBTM)PPh_3]^{+}$. In addition, the hccs of hydrogens in the pyridine ring were larger than those in the benzene rings. The biased spin density reflects the lowered symmetry of the MOs, which would affect the optical properties as discussed below.

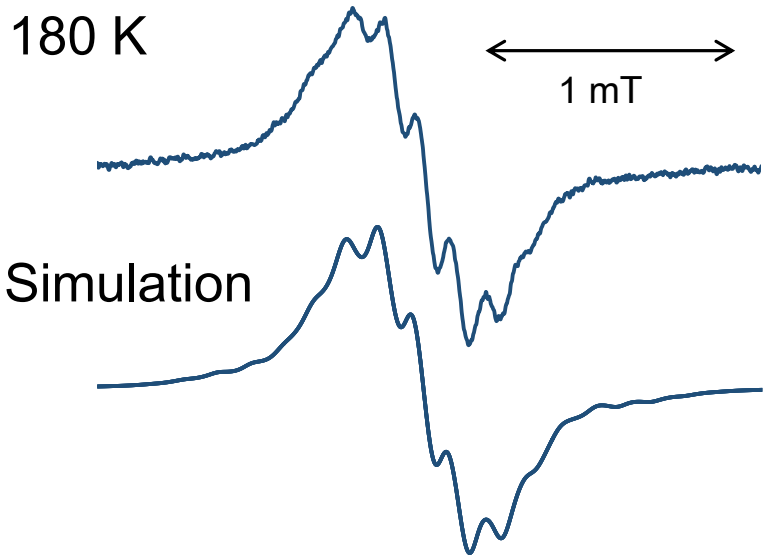

Figure 4-4-1. ESR spectrum of $[Au^{I}(PyBTM)PPh_3]ClO_4$ in dichloromethane at 180 K (top) and computer simulation (bottom).

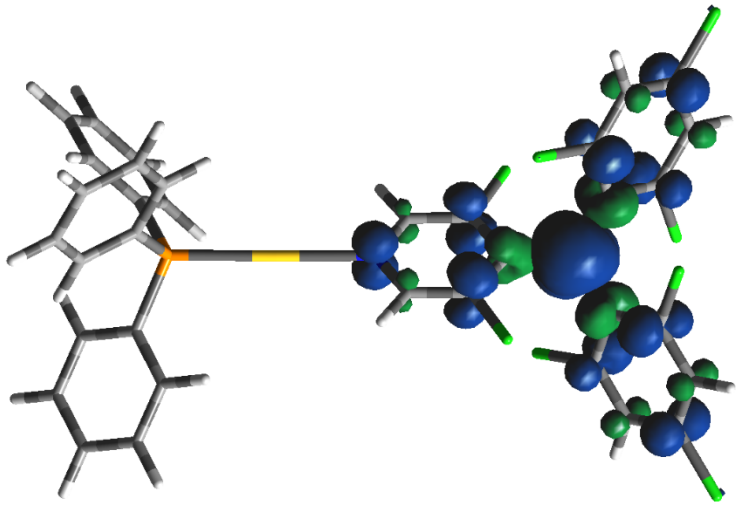

Figure 4-4-2. Calculated spin density distribution of $[Au^{I}(PyBTM)PPh_3]^{+}$.

Table 4-4. Hyperfine coupling constants (hccs) used for ESR simulation and DFT-calculated values

hcc / mT	N	H	P	ipso-^{13}C	ortho-^{13}C
Sim.	0.130	0.125	0.050	1.00	1.00
		0.115			
		0.100			
Calcd.	0.223	0.162	0.088	1.425	1.205
		0.162		1.422	1.204
		0.137		1.358	1.147
		0.136			1.144
		0.092			1.108
		0.090			1.107

4-5 DFT calculations and cyclic voltammetry

MOs of $[Au^{I}(PyBTM)PPh_3]^+$ were calculated using DFT (UM06/SDD(Au), 6-31G(d)(H, C, N, P, Cl)) (Figure 4-5-1). The MOs of $[Au^{I}(PyBTM)PPh_3]^+$ around its frontier orbitals (the MOs 206α, 206β, 207α, 207β, 208α, and 208β) are all distributed mainly on the PyBTM ligand. These results indicate that the PyBTM moiety plays a main role in the electrochemical and optical properties of the complex. PPh_3-centered and Au^{I}-centered orbitals were observed in the lower energy region (201β and 191β, Figure 4-5-2). The electron density distributions of the NHOMO (206α and 206β) were distributed on 1,3,5-trichlorophenyl rings, while NHOMO of X_2PyBTM were centered on the pyridyl rings. The electron density distributions of the SOMO (207α and 207β) were similar to those of PyBTM with small electron densities on the Au(I) atom. The electron density distribution of the NLUMO (208α and 208β) were slightly delocalized on the Au and P atoms.

Coordination to Au(I) lowers the MO energies compared with those of PyBTM. The lower energies of the α-SOMO and β-SOMO (207β and 207α) were confirmed by the cyclic voltammogram in 0.1M Bu_4NClO_4−CH_2Cl_2 (Figure 4-5-3). The reversible reduction potential attributed to the injection of an electron into 207β at $E^{0\prime}_{(red)} = -0.21$ V vs. ferrocenium/ferrocene (Fc^+/Fc) was more positive than that of PyBTM ($E^{0\prime}_{(red)} = -0.74$ V). This means that an electron is more easily accepted in $[Au^{I}(PyBTM)PPh_3]^+$ than in PyBTM owing to the electrostatic effect of the cationic Ph_3PAu^+ moiety. The irreversible oxidation peak of $[Au^{I}(PyBTM)PPh_3]^+$ ($E_{p(ox)}$ = +1.11 V), which reflects the energy of 207α, was slightly more positive than that of PyBTM ($E_{p(ox)}$ = +1.04 V).

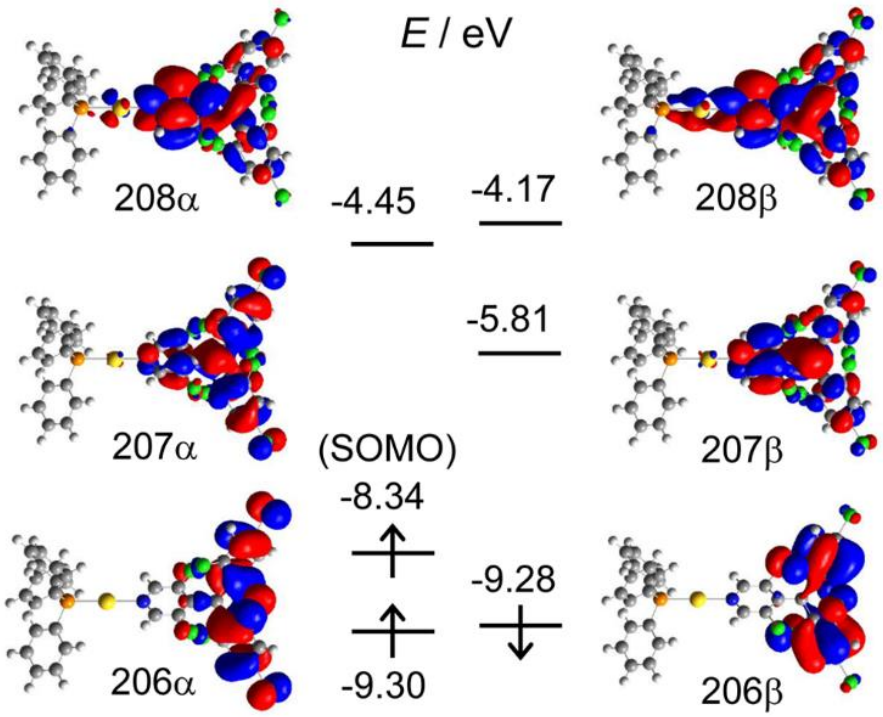

Figure 4-5-1. Molecular orbitals of $[Au^{I}(PyBTM)PPh_3]^{+}$ calculated using DFT (UM06/SDD(Au), 6-31G(d)(H, C, N, P, Cl)).

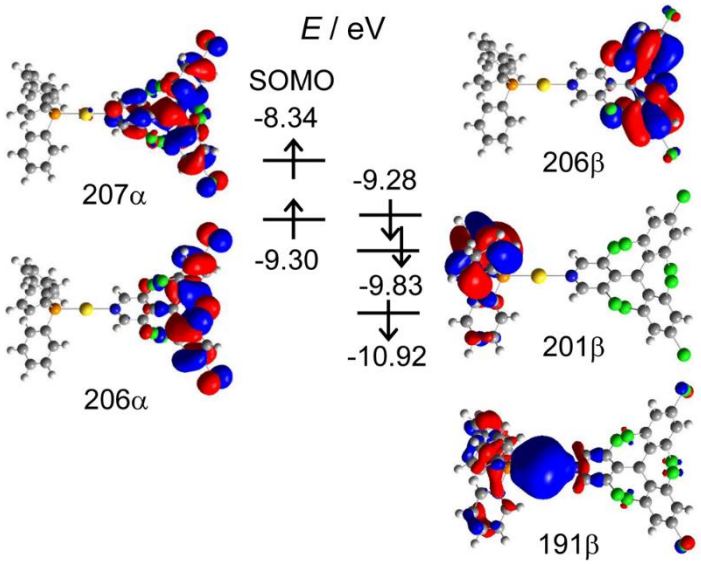

Figure 4-5-2. A PPh_3-centered orbital (201β) and an Au-centered orbital (191β) of $[Au^{I}(PyBTM)PPh_3]^{+}$ calculated using DFT methods (UM06/SDD(Au), 6-31G(d)(H, C, N, P, Cl)). Some frontier orbitals (207α, 206α,β) are shown for comparison of energy levels.

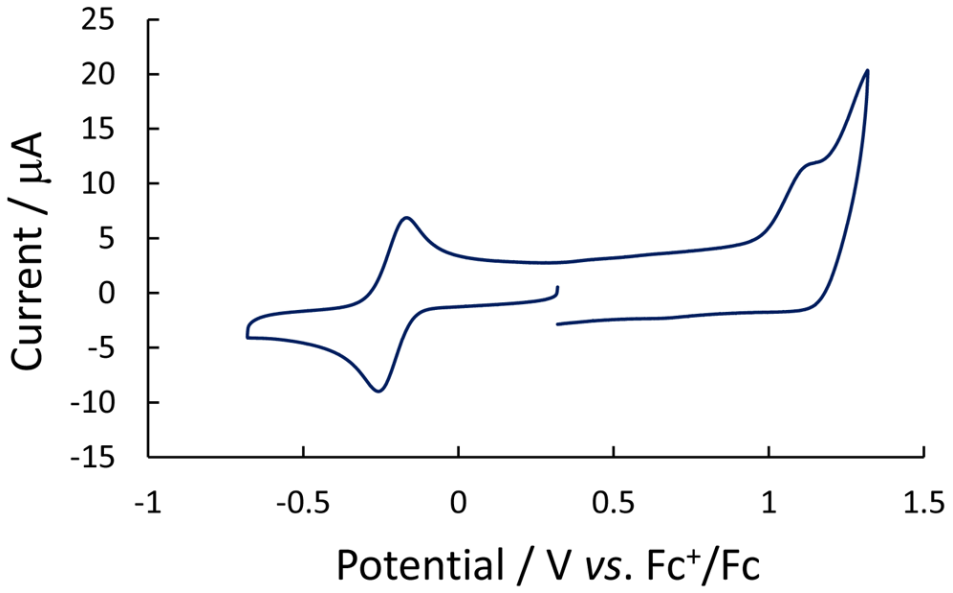

Figure 4-5-3. Cyclic voltammogram of $[Au^{I}(PyBTM)PPh_3]ClO_4$ in 0.1 M Bu_4NClO_4–CH_2Cl_2 at a scan rate of 0.1 V s^{-1}

4-6 Absorption and emission

$[Au^{I}(PyBTM)PPh_3]BF_4$ displayed three characteristic transition bands at λ_{abs} = 566, 434, and 380 nm in the UV-vis absorption spectrum (Figure 4-6-1). Each transition was assigned based on the TDDFT calculations, which confirmed that the transition processes in the visible region were attributed to the PyBTM ligand (Figure 4-6-2). The excitation of the transition band at the longest wavelength, attributed to the 206β→207β transition, forms the D_1 state, from which the fluorescence of $[Au^{I}(PyBTM)PPh_3]BF_4$ arises. The shape of the excitation spectrum was similar to that of the absorption spectrum (Figure 4-6-3). The maximum peak wavelengths of the transition band and the resulting fluorescence band (λ_{em} = 653 nm) were bathochromically shifted compared with those of PyBTM (λ_{em} = 585 nm) owing to the lower energy of the β-SOMO (Figure 4-6-1). It should be noted that $[Au^{I}(PyBTM)PPh_3]X$ is the first example of a luminescent metal complex that contains a luminescent organic radical as a ligand. This result is in contrast with previously reported $Au^{I}PPh_3$ complexes that exhibit luminescent properties with shorter emission wavelengths.[13] The absorption band at 434 nm was assigned as mainly from the 207α→208α transition, which corresponds to the transition at 370 nm for PyBTM; the band was also bathochromically shifted. The band at 380 nm probably originates from transitions such as 207α→213α and 195β→207β.

The coordination of PyBTM to Au^{I} improved the photoluminescence quantum yield in solution. $[Au^{I}(PyBTM)PPh_3]BF_4$ in dichloromethane showed an absolute photoluminescence quantum yield (ϕ) of 8% (Table 4-6). The value was four times that of PyBTM (ϕ = 2%). The fluorescence lifetime measurements revealed that $[Au^{I}(PyBTM)PPh_3]BF_4$ showed a single-component exponential decay with a lifetime (τ) of 13.1 ± 0.2 ns; this value was about twice that of PyBTM (τ = 6.4 ± 0.2 ns). The prolonged lifetime would contribute to enhancing the luminescence quantum yield.

Radiative and non-radiative rate constants, k_f and k_{nr} were estimated by using equations $\phi = k_f/(k_f + k_{nr})$ and $\tau = 1/(k_f + k_{nr})$, to reveal the origin of the improvement in the quantum yield (Table 4-6). The quadrupling of the quantum yield of $[Au^{I}(PyBTM)PPh_3]BF_4$ (from 2% to 8%) originated from two factors: the doubling of the k_f and the halving of the k_{nr}. The increase of k_f was explained by the greater oscillator strength at the lowest excited transition (206β→207β). This transition corresponds to a forbidden transition for a triarylmethyl radical with an ideal three-fold symmetric structure.[14] For PyBTM and $[Au^{I}(PyBTM)PPh_3]^+$, the three-fold symmetries are broken and the transitions are partly allowed. Because of the coordination of PyBTM to the $Au^{I}PPh_3^+$ moiety, the symmetry is lower in $[Au^{I}(PyBTM)PPh_3]^+$ than in PyBTM, resulting in the greater oscillator strength in $[Au^{I}(PyBTM)PPh_3]^+$. The higher oscillator

strength in $[Au^{I}(PyBTM)PPh_3]^+$ was supported by the TDDFT calculations. The greater absorption coefficient in $[Au^{I}(PyBTM)PPh_3]^+$ shown in the absorption spectrum is consistent to the higher oscillator strength.

The decrease of k_{nr} results from suppression of the vibronic coupling, which is a main factor for non-radiative decay in PyBTM. I proposed that the coordination to Au(I), a heavy atom, could decrease the thermal fluctuation and vibration of the molecule. Another explanation is that delocalization of the electron on Au(I) atom in the excited state (β-SOMO) suppresses the vibronic coupling. Difference of the electron density distributions of the β-NHOMO ($[Au^{I}(PyBTM)PPh_3]^+$: the 1,3,5-trichlorophenyl rings, PyBTM: the pyridyl ring) also could be the reason of decrease of the vibronic coupling. Sato et al. has theoretically and experimentally reported that fluorescence of an almost non-fluorescent triphenylamine is much enhanced by carborane substitution because of reduced vibronic coupling.[15] $Au^{I}PPh_3^+$ attached to PyBTM probably plays the role similar to carborane in the substituted triphenylamine.

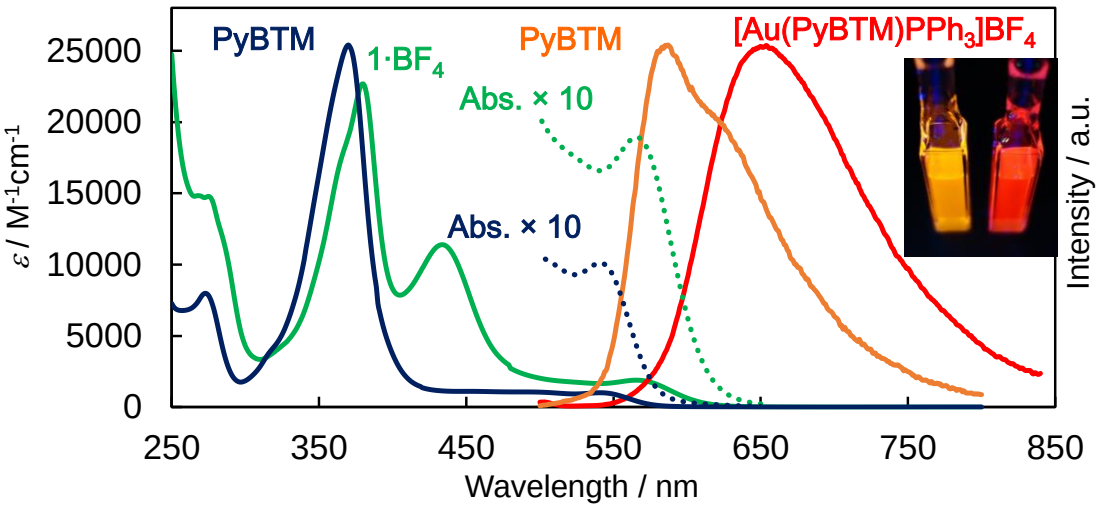

Figure 4-6-1. Absorption spectra of PyBTM (blue line) and $[Au^{I}(PyBTM)PPh_3]BF_4$ (green line) and corrected emission spectra of PyBTM (orange line, λ_{ex} = 370 nm) and $[Au^{I}(PyBTM)PPh_3]BF_4$ (red line, λ_{ex} = 435 nm) in dichloromethane. Enlarged portions of the absorption spectra (10 fold) are shown from λ = 500 to 650 nm (dotted lines). A photograph of fluorescence under UV light at λ = 365 nm (left: PyBTM, right: $[Au^{I}(PyBTM)PPh_3]BF_4$) is in the upper right.

Table 4-6. Photophysical parameters of PyBTM and $[Au^{I}(PyBTM)PPh_3]BF_4$

	ϕ	τ / ns	k_f / 10^7 s^{-1}	k_{nr} / 10^7 s^{-1}
PyBTM	2%	6.4	0.3	15
$[Au^{I}(PyBTM)PPh_3]BF_4$	8%	13.2	0.6	7.0

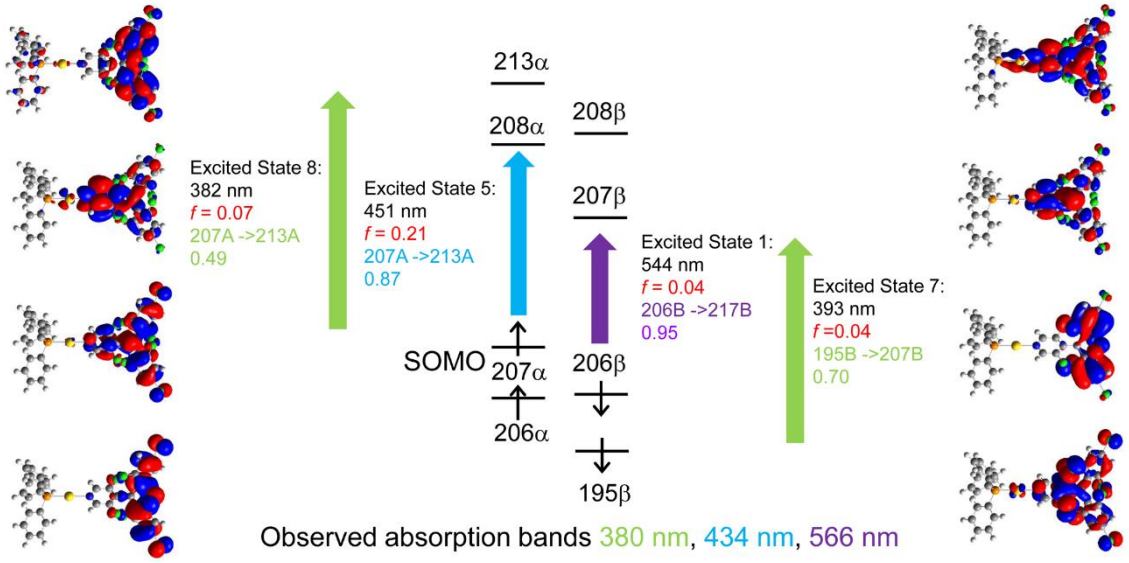

Figure 4-6-2. Summary of TDDFT calculation (UM06/SDD(Au), 6-31G(d)(H, C, N, P, Cl)) of $[Au^{I}(PyBTM)PPh_3]^{+}$ and interpretation of UV-vis absorption bands.

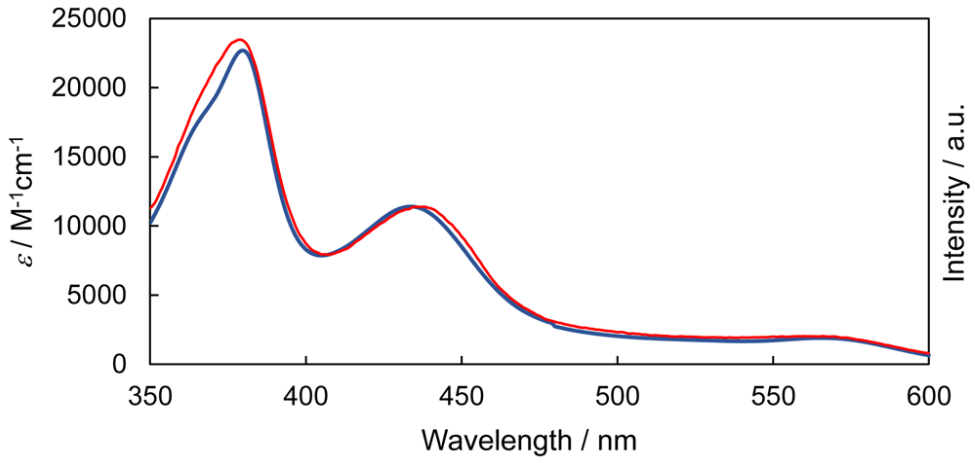

Figure 4-6-3. An excitation spectrum observed for emission wavelength at 650 nm (red line) and an absorption spectrum (blue line) of $[Au^{I}(PyBTM)PPh_3]BF_4$.

4-7 Photostablility

While $[Au^{I}(PyBTM)PPh_3]BF_4$ is a radical complex, it was stable in air at room temperature. Its fluorescence intensity was not affected by oxygen. Solid $[Au^{I}(PyBTM)PPh_3]BF_4$ showed no decomposition. $[Au^{I}(PyBTM)PPh_3]BF_4$ in dichloromethane could be treated in ambient condition with no special care, although the complex seemed a bit unstable in some polar solvents.

Improvement of photostability is an important issue to be overcome for luminescent radicals. The photostability of PyBTM was up to 115 times higher than that of TTM radical as shown in Chapter 2. The decay of the fluorescence intensity was investigated for $[Au^{I}(PyBTM)PPh_3]BF_4$ in dichloromethane upon irradiation with light at λ = 370 nm to elucidate the effect of the coordination to Au^{I} on the photostability of the compound. The estimated half-life ($t_{1/2}$) was $(5.0 \pm 1.1) \times 10^4$ s; this value was three times larger than that of PyBTM ($(1.5 \pm 0.2) \times 10^4$ s) in the same condition, indicating that $[Au^{I}(PyBTM)PPh_3]BF_4$ has superior photostability to PyBTM (Figure 4-7-1 and 4-7-2, Table 4-7). The lower energy levels of the frontier orbital (β-SOMO) involved in the photophysical process, as shown by cyclic voltammetry and DFT, contribute to the enhanced photostability. The results show that the coordination positively affected the photophysical (ϕ) and photochemical ($t_{1/2}$) properties, in comparison with introduction of halogen atoms shown in Chapter 3.

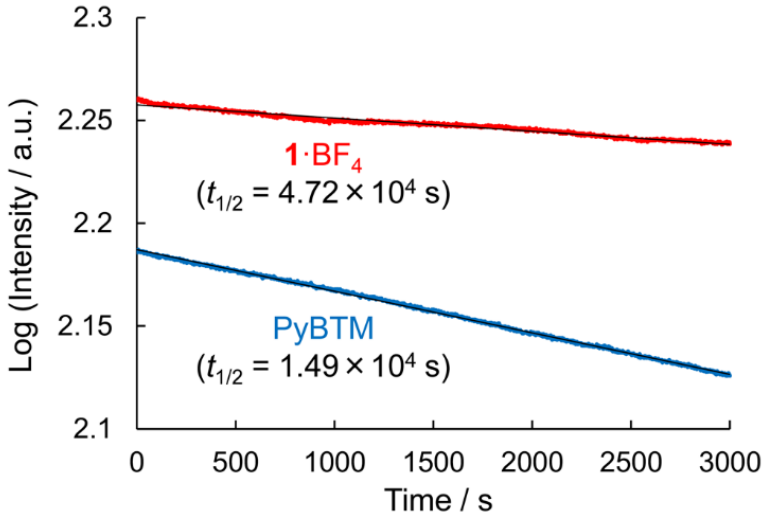

Figure 4-7-1. Plots showing the emission decay of PyBTM and $[Au^{I}(PyBTM)PPh_3]BF_4$ in dichloromethane under continuous excitation with light at λ_{ex} = 370 nm. The half-lives ($t_{1/2(PyBTM)} = (1.5 \pm 0.2) \times 10^4$ s, $t_{1/2([AuI(PyBTM)PPh3]BF4)} = (5.0 \pm 1.1) \times 10^4$ s) were estimated from repeated experiments (Figure 4-7-2, Table 4-7).

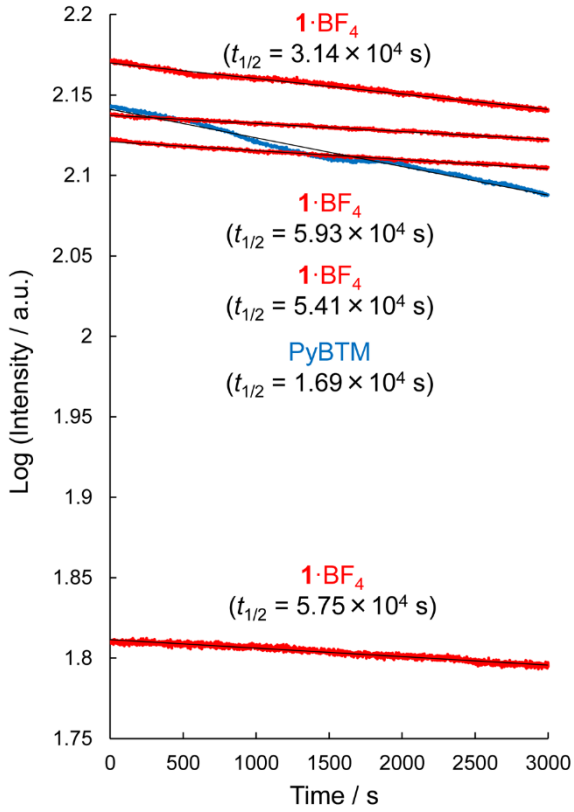

Figure 4-7-2. Plots showing the emission decay of PyBTM (Exp. No. 3 in Table 4-7) and $[Au^{I}(PyBTM)PPh_3]BF_4$ (Exp. No. 1, 2, 3, 5 in Table 4-7) in dichloromethane under continuous excitation with light at λ_{ex} = 370 nm. The half-lives ($t_{1/2}$) are given by linear approximation.

Table 4-7. Stability of PyBTM and $[Au^{I}(PyBTM)PPh_3]BF_4$ in dichloromethane under 370 nm UV light irradiation

Exp. no.	$t_{1/2}$(TTM) / s	$t_{1/2}$(PyBTM) / s	$t_{1/2}([Au^{I}(PyBTM)PPh_3]BF_4)$ / s
1	177 [a]	1.26×10^4 [a]	5.75×10^4 [c]
2		1.49×10^4 [b]	3.14×10^4 [c]
3		1.69×10^4 [c]	5.93×10^4 [c]
4			4.72×10^4 [b]
5			5.41×10^4 [c]
Average	177	1.5×10^4	5.0×10^4
Standard Deviation		0.2×10^4	1.1×10^4

[a] cited from Chapter 2. [b]Figure 4-7-1. [c]Figure 4-7-2

4-8 Conclusion

As far as I know, the first luminescent metal complex with a coordinated luminescent stable radical was prepared. Since the frontier orbitals related to absorption and emission were centered on the PyBTM ligand, the emission was interpreted to be fluorescence from the D_1 state to the D_0 state transition similarly to PyBTM radical.

The coordination of PyBTM to Au^I caused bathochromic shifts of absorption and emission wavelength, because of lowered energy levels of frontier orbitals such as β-SOMO. Fluorescence quantum yield was enhanced in spite of the bathochromic shift, which lowers fluorescence efficiency by the energy-gap law. Higher quantum yield is attributed to (1) the faster fluorescence transition (k_f) and (2) the slower non-radiative decay (k_{nr}). The former is caused by breaking symmetry that forbid $D_1 \rightarrow D_0$ transition, and the latter is the result of suppression of vibronic coupling probably attributable to integration of the gold complex part in the molecule. In addition, the long half-life of PyBTM under photoirradiation became more longer by coordination to Au^I. The enhanced photostability is explained by the lower β-SOMO, which lowers the energy of the lowest excited state. Some structural factors may also affect to the photostability.

In conclusion, coordination of PyBTM to Au^I had a positive effect on the photophysical and photochemical properties by increasing the fluorescence wavelength, quantum yield, and photostability. Further enhancement can be expected by improvement of the ligands on the gold(I) cation. A gold complex with higher quantum yield is shown in Chapter 5 using F_2PyBTM ligand, which showed superior quantum yield to that of PyBTM. Optimization of phosphine ligand (from triphenylphosphine to more electron-donating or electron-withdrawing ligands) will be reported in future.

4-9 References

[1] Y. Hattori, T. Kusamoto, H. Nishihara, *Angew. Chem. Int. Ed.* **2014**, *53*, 11845 – 11848; *Angew. Chem.* **2014**, *126*, 12039 – 12042.

[2] a) V. Gamero, D. Velasco, S. Latorre, F. López-Calahorra, E. Brillas, L. Juliá, *Tetrahedron lett.* **2006**, *47*, 2305 – 2309; b) D. Velasco, S. Castellanos, M. López, F. López-Calahorra, E. Brillas, L. Juliá, *J. Org. Chem.* **2007**, *72*, 7523 – 7532; c) L. Fajalí, R. Papoular, M. Reig, E. Brillas, J. L. Jorda, O. Vallocorba, J. Rius, D. Velasco, L. Juliá, *J. Org. Chem.* **2014**, *79*, 1771 – 1777; d) A. Heckmann, S. Dümmler, J. Pauli, M. Margraf, J. Köhler, D. Stich, C. Lambert, I. Fischer, U. Resch-Genger, *J. Phys. Chem. C* **2009**, *113*, 20958 – 20966.

[3] a) A. Company, N. Roques, M. Güell, V. Mugnaini, L. Gómez, I. Imaz, A. Datcu, M. Solà, J. M. Luis, J. Veciana, X. Ribas, M. Costas, *Dalton Trans.* **2008**, 1679 – 1682; b) A. Datcu, N. Roques, V. Jubera, D. Maspoch, X. Fontrodona, K. Wurst, I. Imaz, G. Mouchaham, J.-P. Sutter, C. Rovira, J. Veciana, *Chem. Eur. J.* **2012**, *18*, 152 – 162.

[4] M. Asano, Y. Kaizu, H. Kobayashi, *J. Chem. Phys.* **1988**, *89*, 6567 – 6576.

[5] a) K. Ishii, J. Fujisawa, Y. Ohba, S. Yamaguchi, *J. Am. Chem. Soc.* **1996**, *118*, 13079 – 13080; b) K. Ishii, J. Fujisawa, A. Adachi, S. Yamauchi, N. Kobayashi, *J. Am. Chem. Soc.* **1998**, *120*, 3152 – 3158.

[6] a) M. V. Encinas, E. A. Lissi, J. Alvarez, *Photochem. Photobiol.* **1994**, *59*, 30 – 34; b) V. Maurel, M. Laferière, P. Billone, R. Godin, J. C. Scaiano, *J. Phys. Chem. B* **2006**, *110*, 16353 – 16358; c) J. Hong, Y. Zhuang, X. Ji, X. Guo, *Analyst* **2011**, *136*, 2464 – 2470.

[7] Y. Hattori, T. Kusamoto, H. Nishihara, *Angew. Chem. Int. Ed.* **2015**, *54*, 3731 – 3734; *Angew. Chem.* **2015**, *127*, 3802 – 3805.

[8] a) A. Barbieri, G. Accorsi, N. Armaroli, *Chem. Commun.* **2008**, 2185 – 2193; b) V. W.-W. Yam, V. K. K.-W. Lo, *Chem. Soc. Rev.* **1999**, *28*, 323 – 334; c) V. W.-W. Yam, E. C.-C. Cheng, *Chem. Soc. Rev.* **2008**, *37*, 1806 – 1813.

[9] M. Munakata, S.-G. Yan, M. Maekawa, M. Akiyama, S. Kitagawa, *J. Chem. Soc. Dalton Trans.* **1997**, 4257 – 4262.

[10] G. M. Sheldrick, *Acta Cryst. A* **2008**, *64*, 112–122.

[11] M. J. Frisch, G. W. Trucks, H. B. Schlegel, G. E. Scuseria, M. A. Robb, J. R. Cheeseman, G. Scalmani, V. Barone, B. Mennucci, G. A. Petersson, H. Nakatsuji, M. Caricato, X. Li, H. P. Hratchian, A. F. Izmaylov, J. Bloino, G. Zheng, J. L. Sonnenberg, M. Hada, M. Ehara, K. Toyota, R. Fukuda, J. Hasegawa, M. Ishida, T. Nakajima, Y. Honda, O. Kitao, H. Nakai, T. Vreven, J. A. Montgomery, Jr., J. E. Peralta, F. Ogliaro, M. Bearpark, J. J. Heyd, E. Brothers, K. N. Kudin, V. N. Staroverov, R. Kobayashi, J.

Normand, K. Raghavachari, A. Rendell, J. C. Burant, S. S. Iyengar, J. Tomasi, M. Cossi, N. Rega, J. M. Millam, M. Klene, J. E. Knox, J. B. Cross, V. Bakken, C. Adamo, J. Jaramillo, R. Gomperts, R. E. Stratmann, O. Yazyev, A. J. Austin, R. Cammi, C. Pomelli, J. W. Ochterski, R. L. Martin, K. Morokuma, V. G. Zakrzewski, G. A. Voth, P. Salvador, J. J. Dannenberg, S. Dapprich, A. D. Daniels, Ö. Farkas, J. B. Foresman, J. V. Ortiz, J. Cioslowski, and D. J. Fox, Gaussian, Inc., Wallingford CT, U. S. A. 2009.
[12] Y. Zhao, D. G. Truhlar, *Theor. Chem. Acc.* **2008**, *120*, 215-241.
[13] a) L. A. Mullice, F. L. Thorp-Greenwood, R. H. Laye, M. P. Coogan, B. M. Kariuki, S. J. A. Pope, *Dalton Trans.* **2009**, 6836 – 6842; b) C.-W. Hsu, C.-C. Lin, M.-W. Chung, Y. Chi, G.-H. Lee, P.-T. Chou, C.-H. Chang, P.-Y. Chen, *J. Am. Chem. Soc.* **2011**, *133*, 12085 – 12099; c) M. Bardají, A. B. Miguel-Coello, P. Espinet, *Inorg. Chim. Acta* **2012**, *392*, 91 – 98.
[14] T. L. Chu, S. I. Weissman, *J. Chem. Phys.* **1954**, *22*, 21 – 25.
[15] a) Y. Kameoka, M. Uebe, A. Ito, T. Sato, K. Tanaka, *Chem. Phys. Lett.* **2014**, *615*, 44 – 49; b) M. Uebe, A. Ito, Y. Kameoka, T. Sato, K. Tanaka, *Chem. Phys. Lett.* **2015**, *633*, 190 – 194.

Part of sentences and figures in this chapter is reproduced or adapted from Ref. 7 with permission from John Wiley & Sons, Inc.

Chapter 5

Combination of (3,5-Difluoro-4-pyridyl)bis(2,4,6-trichlorophenyl)methyl Radical and Coordination to Gold

5-1 Introduction

In Chapter 2, the first reported photostable luminescent radical, PyBTM was prepared. PyBTM displayed excellent photoluminescence quantum yields in conditions which suppress the molecular vibration (in EPA matrix at 77K, or in PMMA polymer at room temperature); however the quantum yield in solution was low (ϕ = 2% in CH_2Cl_2).[1] Substitution of the two chlorine atoms on the pyridine ring to the fluorine atoms decreased the non-radiative decay rate. F_2PyBTM synthesized in Chapter 3 showed the higher quantum yield (ϕ = 4% in CH_2Cl_2), which is two times that of PyBTM.[2] Coordination of PyBTM to Au^I more drastically enhanced the fluorescence efficiency by increasing the radiative rate and decreasing the non-radiative decay rate. In Chapter 4, I described $[Au^I(PyBTM)PPh_3]BF_4$, which displayed the much higher quantum yield (ϕ = 8% in CH_2Cl_2), which is four times that of PyBTM.[3] Although the quantum yield has much improved, it is still less than 10%, and much higher quantum efficiency is desired to convince usefulness of luminescent radicals as luminescent materials.

So far, I have developed two methods to enhance the quantum efficiency of PyBTM. Further greater quantum yield was expected by combining these methods. Thus, I recently prepared another gold complex using F_2PyBTM as a ligand. The prepared complex, $[Au^I(F_2PyBTM)PPh_3]BF_4$ displayed the highest quantum yield as expected. $[Au^I(F_2PyBTM)PPh_3]ClO_4$ was prepared in small scale for single crystal X-ray diffraction. $[Au^I(Br_2PyBTM)PPh_3]BF_4$ was also synthesized using Br_2PyBTM as the ligand in comparison, which displayed a low quantum yield. Coordination to gold(I) lowers the energy levels of unoccupied orbitals on PyBTM such as the β-SOMO, while replacement of halogen atoms changes the energy of the NHOMO. Since the optical properties of the radicals such as fluorescence are mainly controlled by the lowest excited states (β-NHOMO→β-SOMO), the optical properties of $[Au^I(F_2PyBTM)PPh_3]BF_4$ and $[Au^I(Br_2PyBTM)PPh_3]BF_4$ are expected to reflect the effects of both the coordination to gold(I) and the replacement of halogen atoms.

5-2 Experimental section

Synthesis of $[Au^{I}(F_2PyBTM)PPh_3]BF_4$

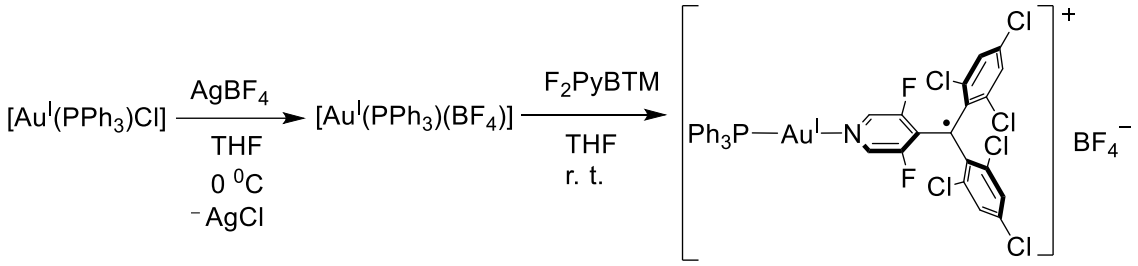

$[Au^{I}(F_2PyBTM)PPh_3]BF_4$ was synthesized by similar method to $[Au^{I}(PyBTM)PPh_3]BF_4$ utilizing modified literature procedure.[4] Under an nitrogen atmosphere, chloro(triphenylphosphine)gold(I) (24.9 mg, 0.0503 mmol) was dissolved in dry THF (2 mL) and silver tetrafluoroborate (ca. 20 mg, 0.1 mmol) was added at 0°C, stirred for 15 min, and filtered. The filtrate was added to a solution of F_2PyBTM (25.0 mg, 0.0513 mmol) in THF (2 mL), and stirred at room temperature for 30 min, and then evaporated. Red powder was precipitated from dichloromethane -diethyl ether (−30 °C), washed with diethyl ether, and dried in vacuo to afford $[Au^{I}(PyBTM)PPh_3]BF_4$ (25.8 mg, 0.0250 mmol, 50% yield). **ESI-TOF-MS** m/z: $[Au^{I}(F_2PyBTM)PPh_3]^+$ Calcd for $C_{36}H_{21}NAuCl_6F_2P$ 974.9177; Found 974.9055.

Synthesis of $[Au^{I}(F_2PyBTM)PPh_3]ClO_4$

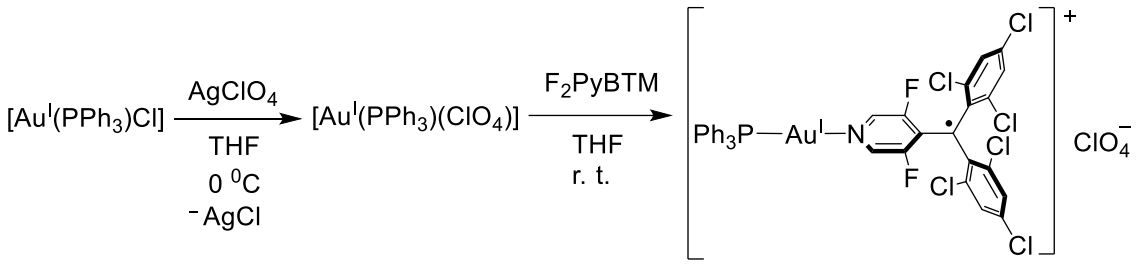

$[Au^{I}(F_2PyBTM)PPh_3]ClO_4$ was synthesized by a similar method to $[Au^{I}(PyBTM)PPh_3]ClO_4$ according to the literature procedure.[4] Under an nitrogen atmosphere, chloro(triphenylphosphine)gold(I) (7.4 mg, 0.015 mmol) was dissolved in dry THF (2 mL) and silver perchlorate (**Caution**: perchlorate salts are potentially explosive, 5 mg, 0.025 mmol) was added at 0°C, stirred for 15 min, and filtered. The filtrate was added to a solution of F_2PyBTM (7.5 mg, 0.015 mmol) in THF (2 mL), and stirred at room temperature for 30 min, and then evaporated. Red powder was precipitated from dichloromethane-hexane to afford $[Au^{I}(PyBTM)PPh_3]ClO_4$ (12.6 mg, 0.012 mmol, 80% yield).

Synthesis of $[Au^{I}(Br_2PyBTM)PPh_3]BF_4$

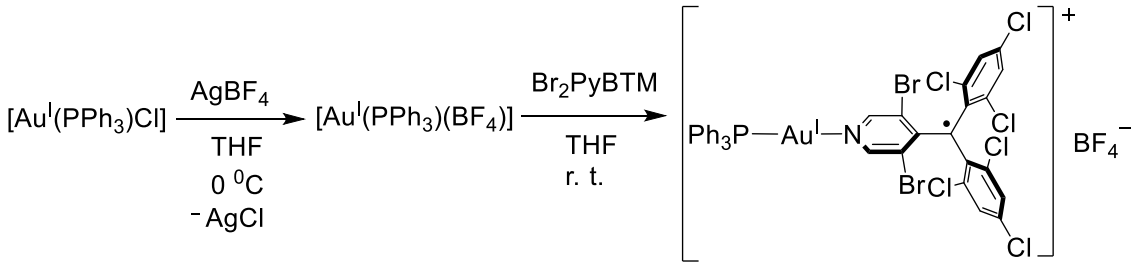

$[Au^{I}(Br_2PyBTM)PPh_3]BF_4$ was synthesized by a similar method to $[Au^{I}(PyBTM)PPh_3]BF_4$ utilizing modified literature procedure.[4] Under an nitrogen atmosphere, chloro(triphenylphosphine)gold(I) (25.5 mg, 0.0515 mmol) was dissolved in dry THF (2 mL) and silver tetrafluoroborate (ca. 20 mg, 0.1 mmol) was added at 0°C, stirred for 15 min, and filtered. The filtrate was added to a solution of Br_2PyBTM (32.5 mg, 0.0534 mmol) in THF (2 mL), and stirred at room temperature for 30 min, and then evaporated. Red powder was precipitated from dichloromethane -diethyl ether (−30 °C), washed with diethyl ether, and dried in vacuo to afford $[Au^{I}(PyBTM)PPh_3]BF_4$ (9.2 mg, 0.00797 mmol, 15% yield). **ESI-TOF-MS** m/z: $[Au^{I}(Br_2PyBTM)PPh_3]^+$ Calcd for $C_{36}H_{21}NAuBr_2Cl_6P$ 1062.7576; Found 1062.7595.

X-ray structural analysis

Diffraction data for X-ray analysis were collected with an AFC10 diffractometer coupled with a Rigaku Saturn CCD system equipped with a rotating-anode X-ray generator producing graphite-monochromated MoKα radiation (λ = 0.7107 Å). Lorentz polarization and numerical absorption corrections were performed with the program *Crystal Clear 1.3.6.* Structures were solved by the direct method using SIR 92 software[5] and refined against F^2 using SHELXL-97.[6] *Crystal Structure 4.0* software was used to prepare the material for publication. The crystallographic data are listed in Table 5-3.

Instruments

ESI–TOF mass spectra were recorded using an LCT Micromass spectrometer. UV-vis absorption spectra were recorded with a JASCO V-570 spectrometer. Steady-state emission spectra were measured with a HITACHI F-4500 spectrometer. Sample solutions were bubbled with argon before the measurements. Absolute photoluminescence quantum yields were measured with a Hamamatsu Photonics C9920-02G. Fluorescence lifetime measurements were performed using a Hamamatsu Photonics Quantaurus-Tau C11367-02.

5-3 Single crystal X-ray diffraction

Single crystal X-ray diffraction studies revealed the molecular structure of $[Au^{I}(F_2PyBTM)PPh_3]^{+}$ in the crystalline state (Figure 5-3, Table 5-3). Red single crystals of $[Au^{I}(F_2PyBTM)PPh_3]ClO_4$ were obtained by diffusing hexane into a dichloromethane solution. The unit cell contained four $[Au^{I}(F_2PyBTM)PPh_3]$, four ClO_4 and two disordered hexane molecules. $[Au^{I}(F_2PyBTM)PPh_3]$ have similar structure to $[Au^{I}(PyBTM)PPh_3]$: the N−Au−P angles is 174° and the perchlorate ions do not coordinate to the Au^{I} center, indicating a two-coordinate linear structure. No aurophilic bonds are observed. The central carbon atom of the F_2PyBTM ligand adopts sp^2 hybridized geometry, suggesting that the radical character of F_2PyBTM is maintained

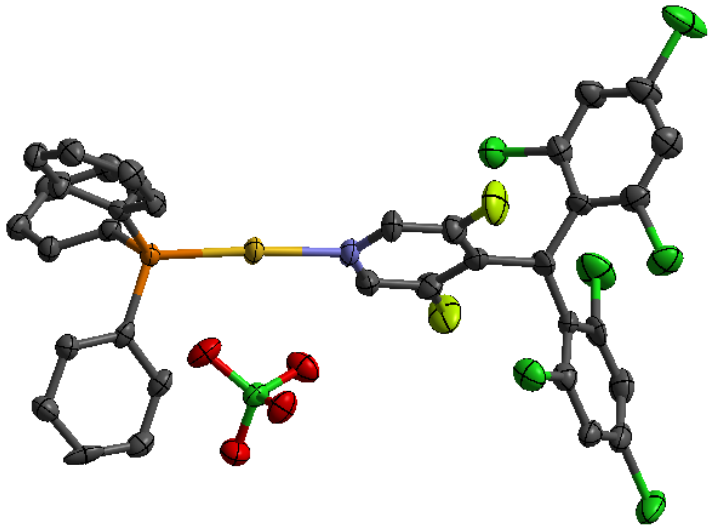

Figure 5-3. Crystal structure of $[Au^{I}(F_2PyBTM)PPh_3]ClO_4$ with thermal ellipsoids at 50% probability level. Hydrogen atoms and a half disordered hexane molecule are omitted for clarity.

Table 5-3. Crystallographic data of $[Au^{I}(F_2PyBTM)PPh_3]ClO_4 \cdot 0.5hexane$

	$[Au^{I}(F_2PyBTM)PPh_3]\cdot ClO_4\cdot 0.5hexane$
Empirical formula	$C_{39}\ H_{21}\ Au\ Cl_9\ F_2\ N\ O_4\ P$
Fw / g mol^{-1}	1081.71
Crystal system	monoclinic
Space group	$P2_1/n$
Crystal size / mm	0.1×0.05×0.05
Temperature / K	113(2)
a / Å	8.7297(6)
b / Å	28.911(2)
c / Å	15.5735(12)
α / º	90
β / º	103.822(4)
γ / º	90
V / Å^3	3816.7(5)
Z	4
ρ_{calced} / g cm^{-3}	1.882
λ / Å	0.7107
μ / mm^{-1}	4.453
Reflections collected	30181
Independent reflections	8723
Parameters	481
R_{int}	0.0471
[a]*R*1	0.0532
[b]*wR*2	0.1221
[c]GoF	1.080

[a] $R_1 = \Sigma||F^o|-|F^c||/\Sigma|F^o|$ ($I>2\sigma(I)$). [b] $wR_2 = [\Sigma(w(F^{o2}-F^{c2})^2/\Sigma w(F^{o2})^2]^{1/2}$ ($I>2\sigma(I)$). [c] GOF = $[\Sigma(w(F^{o2}-F^{c2})^2/\Sigma(N^r-N^p)^2]$.

5-4 Absorption and emission

$[Au^{I}(F_2PyBTM)PPh_3]BF_4$ displayed three characteristic absorption bands at λ_{abs} = 367, 419, and 557 nm and a broad emission band at λ_{em} = 622 nm (Figure 5-4). $[Au^{I}(Br_2PyBTM)PPh_3]BF_4$ displayed absorption bands at λ_{abs} = 381, 438, 571 nm and a broad emission band at λ_{em} = 666 nm. $[Au^{I}(PyBTM)PPh_3]BF_4$ displayed three characteristic absorption bands at λ_{abs} = 380, 434, and 566 nm and a broad emission band at λ_{em} = 653 nm in Chapter 4. The shapes of absorption and emission spectra of $[Au^{I}(F_2PyBTM)PPh_3]BF_4$ and $[Au^{I}(Br_2PyBTM)PPh_3]BF_4$ are similar to those of $[Au^{I}(PyBTM)PPh_3]BF_4$. The shift of absorption and emission of $[Au^{I}(X_2PyBTM)PPh_3]BF_4$ is in the same order as the shift of absorption and emission of X_2PyBTM (F < Cl < Br) in Chapter 3.

$[Au^{I}(F_2PyBTM)PPh_3]BF_4$ showed an absolute photoluminescence quantum yield (ϕ, Table 5-4) of 20% in dichloromethane, which is the best yield in this thesis. The value was 10 times that of PyBTM (ϕ = 2%). $[Au^{I}(PyBTM)PPh_3]BF_4$ showed much better fluorescence quantum yield (ϕ = 8%) than that of PyBTM, due to the doubling of the radiative rate, k_f and the halving of the non-radiative rate, k_{nr}. $[Au^{I}(F_2PyBTM)PPh_3]BF_4$ showed further smaller k_{nr}, which is less than one third that of $[Au^{I}(PyBTM)PPh_3]BF_4$. The reason of the smaller k_{nr} is thought to be similar to the reason of smaller k_{nr} of F_2PyBTM compared to that of PyBTM; the larger energy gap between β-SOMO and β-NHOMO, or the suppression of vibration due to stronger conjugation between the central carbon and the pyridine ring. Since coordination to gold(I) and substitution to fluorine atoms are thought to affect the different molecular orbitals (β-SOMO and β-NHOMO respectively) and the different molecular vibration mechanism, they worked independently to decrease the non-radiative decay. Thus, the enhancement of fluorescence efficiency showed multiplier effect (2%→8%→20%), and the high fluorescence quantum yield of $[Au^{I}(F_2PyBTM)PPh_3]BF_4$ was achieved by combination of coordination to gold(I) and replacement of halogen atoms.

$[Au^{I}(Br_2PyBTM)PPh_3]BF_4$ displayed a lower fluorescence quantum yield (ϕ = 1%) with shorter fluorescence lifetime (τ = 2.4 ns) than those of other radicals due to faster k_{nr}. Since $[Au^{I}(Br_2PyBTM)PPh_3]BF_4$ displayed the longest fluorescence wavelength (the lowest energy for forming the excited state), fast decay of the lowest excited state can be explained by the energy gap law.

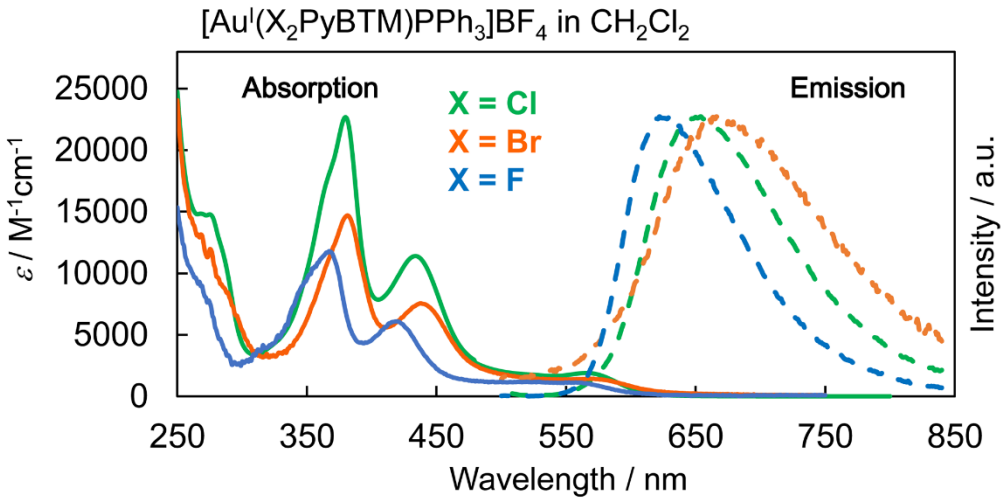

Figure 5-4. Absorption and emission spectra of $[Au^{I}(PyBTM)PPh_3]BF_4$ (green line), $[Au^{I}(Br_2PyBTM)PPh_3]BF_4$ (orange line), and $[Au^{I}(F_2PyBTM)PPh_3]BF_4$ (blue line) in dichloromethane.

Table 5-4. Photophysical parameters of $[Au^{I}(X_2PyBTM)PPh_3]BF_4$ in dichloromethane

	ϕ	τ / ns	k_f / 10^7 s^{-1}	k_{nr} / 10^7 s^{-1}
$[Au^{I}(Br_2PyBTM)PPh_3]BF_4$	1%	2.4	0.4	41
$[Au^{I}(PyBTM)PPh_3]BF_4$	8%	13.2	0.6	7.0
$[Au^{I}(F_2PyBTM)PPh_3]BF_4$	20%	35.7	0.6	2.2

5-5 Conclusion

$[Au^{I}(X_2PyBTM)PPh_3]BF_4$ showed spectrum shifts similar to X_2PyBTM. $[Au^{I}(F_2PyBTM)PPh_3]BF_4$ showed the highest fluorescence quantum yield in the thesis of 20% in dichloromethane. The aim of molecular design; combining two methods to enhance fluorescence quantum yield succeeded.

In conclusion, optical properties of $[Au^{I}(X_2PyBTM)PPh_3]BF_4$ were explained by combination of effects of coordination to gold(I) and replacement of halogen atoms. This supports the discussion in Chapters 3 and 4. The fact that the fluorescence quantum yield was enhanced by multiplication of the effects of metal and that of ligand brought further expectation to enhance fluorescence efficiency of luminescent radicals.

5-6 References

[1] Y. Hattori, T. Kusamoto, H. Nishihara, *Angew. Chem. Int. Ed.* **2014**, *53*, 11845 – 11848; *Angew. Chem.* **2014**, *126*, 12039 – 12042.

[2] Y. Hattori, T. Kusamoto, H. Nishihara, *RSC Adv.* **2015**, *5*, 64802 – 64805.

[3] Y. Hattori, T. Kusamoto, H. Nishihara, *Angew. Chem. Int. Ed.* **2015**, *54*, 3731 – 3734; *Angew. Chem.* **2015**, *127*, 3802 – 3805.

[4] M. Munakata, S.-G. Yan, M. Maekawa, M. Akiyama, S. Kitagawa, *J. Chem. Soc. Dalton Trans.* **1997**, 4257 – 4262.

[5] A. Altomare, G. Cascarano, C. Giacovazzo, A. Guagliardi, M. C. Burla, G. Polidori, M. Camalli, *J. Appl. Cryst.* **1994**, *27*, 435.

[6] G. M. Sheldrick, *Acta Cryst. A* **2008**, *64*, 112 – 122.

Chapter 6

Concluding Remarks

As I described in Chapter 1, luminescent molecules have been developed for extensive applications such as EL devices and fluorescent probes. Spin multiplicity is an important factor for understanding photophysical processes of them. For example in EL devices such as OLED, maximum internal quantum efficiency of usual fluorescent materials are limited to only 25%, and open-shell luminescent molecules are focused as possible candidates as more efficient luminescent materials for EL devices.

In order to make luminescent materials using organic radicals, reactivity of radicals is the first problem to be overcome. Steric protection and π-conjugation are effective methods to stabilize radicals. Several types of stable radicals are easily accessible, but the number of luminescent stable radicals are rather few. As rare examples of fluorescent radicals, perchlorotriphenylmethyl (PTM) radical and tris(1,3,5-trichlorophenyl)methyl (TTM) radical are reported. Photoluminescence quantum yield of PTM and TTM radicals are low. Improvements of the quantum yield of PTM and TTM radicals by incorporation of donor molecules have been reported; however there is another serious problem in PTM and TTM radicals; they decompose upon photoirradiation, and photoluminescent for only short time. No improvement of photostability in PTM and TTM derivatives had been reported so far.

The first aim of studies in my Ph.D. course is to modify the TTM radical to improve the stability under photoirradiation. The second aim is to enhance the photoluminescence quantum yield of photostable luminescent radicals. The structural changes and the frontier orbitals are two important factors for the design of molecules and for the interpretation of optical measurements. Especially, the lowest excited state mainly formed by transition from the β-NHOMO to the β-SOMO are thought to play the most important role in stability and efficiency, since relaxation of higher excited states is very fast by Kasha's rule. Contributions of higher excited states are not excluded but the results were well-descripted by energy levels of the β-SOMO and the β-NHOMO.

In Chapter 2, (3,5-dichloro-4-pyridyl)bis(2,4,6-trichlorophenyl)methyl radical (PyBTM) was designed by incorporated pyridine ring into the TTM skeleton in order to lower the energies of the frontier orbitals owing to the electronegativity of the nitrogen atom. PyBTM showed a significantly greater photostability than that of TTM. Since deactivation of the lowest excited state is mainly attributed to the vibration of the molecule, conditions to suppress the molecular vibration improved the strength of luminescence. The pyridine moiety of PyBTM acted as a proton coordination site, thereby allowing for control of the electronic and optical properties by protonation and deprotonation.

In Chapter 3, (3,5-dibromo-4-pyridyl)bis(2,4,6-trichlorophenyl)methyl radical

(Br_2PyBTM) and (3,5-difluluoro-4-pyridyl)bis(2,4,6-trichlorophenyl)methyl radical (F_2PyBTM) were prepared, and their photophysical and photochemical properties were compared with those of PyBTM. Spectroscopic studies showed the absorption and emission peak maxima shifted bathochromically in the order of F_2PyBTM < PyBTM < Br_2PyBTM. Br_2PyBTM showed the highest photostability of the three X_2PyBTM radicals owing to larger steric effect or higher β-NHOMO, and F_2PyBTM displayed the highest photoluminescence quantum yield owing to smaller steric effect or lower β-NHOMO.

In Chapter 4, the luminescent properties of the stable luminescent radical PyBTM was enhanced through its coordination to metal. The prepared complex, $[Au^I(PyBTM)PPh_3]BF_4$ showed fluorescence centered mainly on the coordinated PyBTM ligand. The coordination of PyBTM to Au^I caused bathochromic shift of absorption and emission wavelength, because of lowered energy levels of frontier orbitals such as β-SOMO. $[Au^I(PyBTM)PPh_3]BF_4$ displayed enhanced fluorescence quantum yield and photostability owing to change of electron density distribution by coordination to gold(I) and the lower β-SOMO.

In Chapter 5, enhancement of fluorescence quantum yield of F_2PyBTM and $[Au^I(PyBTM)PPh_3]BF_4$ was combined to obtain further greater fluorescence quantum yield in photostable luminescent radical. $[Au^I(F_2PyBTM)PPh_3]BF_4$ displayed the highest quantum yield (ϕ = 20% in CH_2Cl_2) in my study.

In conclusion, I have developed novel luminescent radicals. PyBTM obtained photostability, which did not exist in previous luminescent radicals. Br_2PyBTM was more photostable and F_2PyBTM had higher quantum yield. Photostability and quantum yield were further enhanced by coordination to gold. Combining F_2PyBTM and gold complex the highest fluorescence quantum yield of 20% was achieved.

Luminescent radicals will be more photostable and display higher quantum yields by further modification of structures. Coordination compounds using other metals are also expected to be synthesized and to show unique properties. This study developed a chance for basic research of photophysics of doublet molecules in ambient condition, and possibility of application of luminescent radicals to EL devices.

List of Publication

【Publications related to the thesis】

1. “Luminescence, Stability, and Proton Response of an Open-Shell (3,5-Dichloro-4-pyridyl)bis(2,4,6-trichlorophenyl)methyl Radical”
Y. Hattori, T. Kusamoto, H. Nishihara, *Angew. Chem. Int. Ed.* **2014**, *53*, 11845 – 11848; *Angew. Chem.* **2014**, *126*, 12039 – 12042.

2. “Enhanced Luminescent Properties of an Open-Shell (3,5-Dichloro-4-pyridyl)bis(2,4,6-trichlorophenyl)methyl Radical by Coordination to Gold”
Y. Hattori, T. Kusamoto, H. Nishihara, *Angew. Chem. Int. Ed.* **2015**, *54*, 3731 – 3734; *Angew. Chem.* **2015**, *127*, 3802-3805.

3. “Highly photostable luminescent open-shell (3,5-dihalo-4-pyridyl)bis(2,4,6-trichlorophenyl)methyl radicals: significant effects of halogen atoms on their photophysical and photochemical properties”
Y. Hattori, T. Kusamoto, H. Nishihara, *RSC Adv.* **2015**, *5*, 64802 – 64805.

【Publications not related to the thesis】

1. “Structural Modification on Copper(I)-pyridylpyrimidine Complexes for Modulation of Rotational Dynamics, Redox Properties, and Phototriggered Isomerization”
M. Nishikawa, Y. Takara, Y. Hattori, K. Nomoto, T. Kusamoto, S. Kume, H. Nishihara, *Inorg. Chem.* **2013**, *52*, 8692 – 8670.

2. “Regulation of the Rate of Dinucleation of a Monocopper(I) Complex Containing Bipyrimidine Rotary Units by Restricted Double Pyrimidine Rotation”
Y. Hattori, M. Nishikawa, T. Kusamoto, S. Kume, H. Nishihara, *Inorg. Chem.* **2014**, *53*, 2831 – 2840.

3. “Structures and Optical Properties of Tris(trimethylsilyl)silylated Oligothiophene Derivatives”
H. Inubushi, Y. Hattori, Y. Yamanoi, H. Nishihara, *J. Org. Chem.* **2014**, *79*, 2974 – 2979.

4. “Steric Interference on the Redox-conjugated Pyrimidine Ring Rotation of Mono- and Dinuclear Copper Complexes with (4-Methyl-2-pyrimidinyl)imine Ligands”
Y. Hattori, M. Nishikawa, T. Kusamoto, S. Kume, H. Nishihara, *Chem. Lett.* **2014**, *43*, 1037 – 1039.

5. “Geometric and electrochemical properties of complexes consisting of two aminonaphthoquinone-bound Schiff-base ligands and Mn^{II}, Fe^{II}, Ni^{II}, Cu^{II}, or Zn^{II}”
Y. Hasegawa, H. Nakamura, Y. Hattori, K. Hoshiko, T. Kusamoto, M. Murata, S. Kume,

H. Nishihara, *Polyhedron* **2015**, *86*, 111 – 119.

6. “Heteroleptic bis(dipyrrinato)copper(II) and nickel(II) complexes”
R. Toyoda, M. Tsuchiya, R. Sakamoto, R. Matsuoka, K.-H. Wu, Y. Hattori, H. Nishihara, *Dalton Trans.* **2015**, *44*, 15103 – 15106.

7. “Intramolecular Ferromagnetic Radical–Cu^{II} Coupling in a Cu^{II} Complex Ligated with Pyridyl-Substituted Triarylmethyl Radicals”
T. Kusamoto, Y. Hattori, A. Tanushi, H. Nishihara, *Inorg. Chem.* **2015**, *54*, 4186 – 4188.

8. “Synthesis, characterization, and physical properties of oligo(1-(*N*,*N*-dimethylamino)pyrrole)s and their doped forms, precursors of candidates for molecular flat-band ferromagnets”
Y. Yamanoi, K. Takahashi, T. Hamada, N. Ohshima, M. Kurashina, Y. Hattori, T. Kusamoto, R. Sakamoto, M. Miyachi, H. Nishihara, *J. Mater. Chem. C* **2015**, *3*, 4316 – 4320.

9. “Spin-Reconstructed Proton-Coupled Electron Transfer in a Ferrocene-Nickeladithiolene Hybrid”
A. Tanushi, T. Kusamoto, Y. Hattori, K. Takada, H. Nishihara, *J. Am. Chem. Soc.* **2015**, *137*, 6448 – 6451.

Acknowledgement

This work was established by a lot of supports of many people. I would like to express my sincerest gratitude to all of them.

This research was fully supervised by Professor Dr. Hiroshi Nishihara (the University of Tokyo). He gave me a chance to study this interesting research in his lab, favorable research environments, valuable instructions, discussion, suggestion during the course of this work. I would like to express my deep gratitude to Professor Dr. Hiroshi Nishihara.

This research was instructed by Assistant Professor Dr. Tetsuro Kusamoto (the University of Tokyo). He gave me this very interesting research topic, luminescent radicals, a lot of discussion, much guidance, experimental and theoretical advices, revision of writing and encouragement. I would like to express my deep gratitude to Dr. Tetsuro Kusamoto.

I am deeply grateful to Associate Professor Dr. Yoshinori Yamanoi, Assistant Professor Dr. Ryota Sakamoto, Project Assistant Professor Dr. Mariko Miyachi, Project Assistant Professor Dr. Maw-Lin Foo, Project Assistant Professor Dr. Kuo-Hui Wu, and Project Assistant Professor Dr. Hiroaki Maeda (the University of Tokyo) for their helpful suggestion and discussion.

I would like to express my deep gratitude to Associate Professor Dr. Shoko Kume (Hiroshima University) and Assistant Professor Dr. Michihiro Nishikawa (Seikei University) for teaching in my initial research and giving advices.

I thank the all members (students, staffs, secretaries) of Nishihara laboratory (2010.4−2016.3) for their instructions, supports, helpful discussion and enjoyment of research activity.

I would like to deeply acknowledge Chief Scientist Dr. Reizo Kato (RIKEN) for his kind offer of facilities and laboratory equipment while Nishihara Lab was under renovation. I would like to express gratitude to his valuable advices.

I also thank the all members of Kato laboratory (2013.10−2014.7) for their supports, helpful discussion and advices.

I am grateful to Professor Dr. Guido Clever (Georg-August-Universität Göttingen, Technische Universität Dortmund (2015.9-)) for accepting me as an exchange student in his laboratory, helpful guidance, and valuable discussion.

I thank the all members of the Clever laboratory (2015.1−2015.3) for their helpful supports, valuable discussion, and enjoyment of stay in Germany.

I would like to acknowledge Mr. Hideki Waragai (the University of Tokyo) for the measurements of absolute photoluminescence quantum yields in the solid state.

I would like to acknowledge Dr. Aiko Kamitsubo and Ms. Kimiyo Saeki (the Element Analysis Center of the University of Tokyo) for elemental analysis measurements.

I would like to acknowledge Grants-in-Aid from MEXT of Japan, and MERIT (Material Education program for the future leaders in Research, Industry, and Technology) in the MEXT Leading Graduate School for financial support to this research.

I am indebted to a JSPS Research Fellowship for Young Scientists and MERIT for financial support.

I would like to acknowledge John Wiley & Sons, Inc. and The Royal Society of Chemistry for permission to reproduce and adapt the publications related to the thesis.

I thank many chemists and scientists (presentation audience, MERIT students, my personal friends) for valuable discussion and interest in my research. I especially thank Associate Professor Dr. Tohru Sato (Kyoto University) for instruction in vibronic coupling.

I would like to express my hearty gratitude to my family for supporting me mentally and financially.